UNIVERSITÀ DEGLI STUDI DELL'AQUILA

DIPARTIMENTO DI INGEGNERIA
E SCIENZE DELL'INFORMAZIONE E MATEMATICA

DOTTORATO DI RICERCA IN MATEMATICA E MODELLI
XXXIII CICLO

Analysis of entropy solutions to conservation laws with discontinuous flux in space and time

SSD MAT/05

Dottorando
Kwame Atta GYAMFI

Coordinatore del corso
Prof. Davide GABRIELLI

Tutor
Prof. Debora AMADORI

A.A. 2020/2021

Abstract

In this thesis, we consider a first order partial differential equation with coefficient that contains a jump in the space and time variables. The equation is deeply inspired by the one-dimensional model of pedestrian flow introduced by Hughes, commonly referred to as *the Hughes' model* [57]. To be precise, our equation consists in a scalar conservation law whose flux coefficient is a time dependent function that switches sign according to the location of the 'turning curve', $\xi(t)$, given *a priori* in the space domain. The equation writes

$$\partial_t \rho + \partial_x \big(\operatorname{sign}(x - \xi(t)) f(\rho) \big) = 0.$$

The main object of this thesis is to analyse the well-posedness of the above equation via entropy solutions taken in an appropriate sense. In this text, the basic notions of scalar conservation law with continuous and discontinuous flux functions are revisited with a detailed discussion and comparison of existing results regarding entropy admissibility criteria for both classes of equations. Furthermore, the theory of L^1-dissipative germ introduced by Andreianov, Karlsen and Risebro [14] is reviewed and is then extended to our equation with the goal of analysing the entropy solutions for the case of non-classical flux interface coupling at the turning curve.

In a series of steps leading to the existence of solutions to the above equation, we properly define the entropy solutions and construct the exact solution of the Riemann problem that arises at the turning curve. Using the Riemann solver at $\xi(t)$, the total variation in the solution as the slope of ξ changes in time and as ξ interactions with classical waves (i.e. shock and rarefaction) are studied.

Finally, a numerical scheme with a moving mesh adaptation and a modified numerical flux near the turning curve $x = \xi(t)$ is also proposed. In order to be able to prove that the scheme converges to the weak entropy solution, we first establish that it is well-balanced and stable in $\mathbf{L}^\infty$ space. The approximate solution is further analysed in the sense of entropy process solutions. We also present some explicit examples and their approximate solutions to numerically check convergence of the approximate solution provided by the scheme to the weak entropy solutions.

Acknowledgements

The PhD journey would not have been completed without the constant support of several people. Firstly, I would like to express my sincere gratitude to my advisor Prof. Deborah Amadori for the continuous support of my entire Ph.D study and related research, for her patience, motivation, and insight and immense knowledge. Throughout these four years, her guidance helped me in all the time of research as well as during writing of this thesis.

Secondly, I am indebted to Prof. Carlotta Donadello of Laboratoire de Mathematiques de Besancon of the University of Franche-Comté, Besancon, for being a second advisor, and also for allowing me to spend my P.h.D research exchange with her group at Besancon. In fact the main contribution of this work concerning numerical scheme and analysis was acheived after the two visits I made to her lab. I am very grateful for her continuous support and direction throughout this work.

I also express my gratitude to Prof. Massimiliano D. Rosini and and Prof. Maria Laura Delle Monache for accepting to be the reviewers of my manuscript, for the time they devoted to me and their timely advice and suggestions.

And my greatest thanks goes to my family for all the support you have shown me through this research. My second family in L'Aquila, my Christian brothers and sisters, have also been of great help to me, especially during the difficult days that arose due to the covid-19 pandemic. Finally, I thank Jon and the "Calcetto Giovedi 20.30" group, for making me feel like home with soccer play invitations as well as other activities.

May Jehovah God bless all of you.

Contents

List of Figures

DEDICATION

To my mother and family.

Introduction

The main object of this thesis is to analyze the solution of a scalar conservation law with a flux function that has a jump in the space and time variables. Conservation of mass is a naturally occurring phenomenon that has been studied for decades in the physical sciences and continues to enrich an active area of research until the present from both theoretical and application points of view. Typical examples of application problems of mass conservation are macroscopic motion of pedestrian flows [57, 28], flooding models [77], and macroscopic models of traffic flow [74, 69, 78, 66] among others. Nevertheless, the birth of these models have roots deep within some ideas of continuum physics, where fundamental balance equations for mass, momentum, and total energy of fluids are formulated by neglecting the effects of small-scale induced mechanisms. Mostly, such models are proposed by engineers and/or physicists, and then their analytical properties are subsequently studied by mathematicians with the aim of proposing solutions that may serve as the basis for computer simulations and analysis.

The Hughes' model for pedestrian flow [57] is a typical example. It was originally developed by an engineer but used by mathematicians and simulation experts to predict the motion of large crowds as it serves as one of the model equations adapted to run computer simulations of pedestrian flows [19, 79, 40, 48]. Since different application problems lead to different conservation laws, specific assumptions are made when studying the solutions to a conservation law from a theoretical point of view. For instance, macroscopic models of traffic flow on a single lane were first proposed as conservation laws with simple single flux functions resulting from the assumption of a non-increasing speed function [69]. However, incorporating additional conditions on the single road results in further extensions of the simple model (see [74] for the case of traffic flow models), that in turn leads to the derivation of different classes of conservation laws for the single problem.

A class of conservation laws commonly arising in this direction is scalar conservation laws with discontinuous flux functions, herein referred to as *discontinuous flux problems*, which is also the main subject of the work presented in this thesis. In this introductory chapter, we review selected practical problems that motivate this class of equations and then recall basic notions of entropy solutions adapted for them in the chapter that follows.

0.1 Traffic flow models

Traffic flow models given by partial differential equations (PDEs) are based on the well-known continuum formulation initially proposed by Lighthill-Whitham-Richards (LWR) [69, 78]. The models are used to describe the evolution of large volumes of traffic density on an unbounded highway, mostly with a common flux function. That is, they are also based on large scale values of traffic density and flow speed. For this reason, they're commonly referred to as *macroscopic models of traffic flow*.

Consider a one-directional highway parameterized by an interval $I \subseteq \mathbb{R}$, possibly unbounded. The LWR model writes

$$\partial_t \rho + \partial_x [\rho v(\rho)] = 0, \quad (t, x) \in [0, \infty) \times I, \tag{1}$$

where the unknown function $\rho = \rho(t, x) \in [0, \rho_{max}]$, is the mean traffic density at time and position (t, x), $\rho_{max} > 0$ is the maximum density, and the function $v : [0, \rho_{max}] \to [0, v_{max}]$ is the mean traffic velocity given as a non-increasing function with $v_{max} > 0$, being the maximum mean velocity. Setting $f(\rho) := \rho v(\rho)$ to be the flux-density relation, the LWR models stipulates that f satisfies the following:

(H1) $f(0) = f(\rho_{max}) = 0$,

(H2) $f : [0, \rho_{max}] \mapsto [0, +\infty)$ is a $\mathcal{C}^2$ function.

Equation (1) is a first-order order macroscopic model that is closed by a speed-density relation $v = v(\rho)$. Furthermore, it is possible to consider the model on roads with entrances and/or exits by adding a source term to (1) as in [17]; generalization to multi-class traffic population which comprises of fast and slow moving vehicles [20] and traffic models on complex networks [44]. In the theory of traffic flow models, it is mostly convenient to also consider the graph of the speed-density relation as well as of the flux function, called the fundamental diagram. The fundamental diagram corresponding to (2) is shown in figure 1. For a single lane with uniform road conditions, a common choice of the flux function writes

$$f(\rho) = v_{max}\rho \left(1 - \frac{\rho}{\rho_{max}}\right). \tag{2}$$

On a highway stretch, it is common for different segments to have varying speed limits mostly owing to speed control mechanisms such as ramp metering. In modern transportation networks, these meters are equipped with sensors that can be controlled in real time to optimize the free flow of traffic. For these modeling

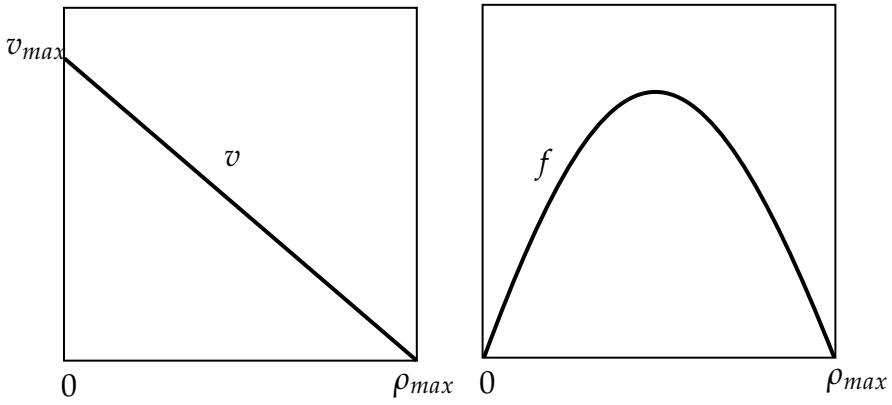

FIGURE 1: The fundamental diagram of the simple LWR traffic flow model.

situations, the LWR model is adjusted to define realistic solutions. This motivates a class of traffic flow model which are scalar conservation laws with time dependent discontinuous flux functions with the velocity function of the form $v(t) \in [v_{min}, v_{max}]$. See [47, 33, 70, 74]. Toward this direction, a common example flux function used are summarized below:

$$\text{Greenshields [51]}: \quad f(t,\rho) = v(t)\rho\left(1 - \frac{\rho}{\rho_{max}}\right),$$

$$\text{Newel-Daganzo type [30]}: \quad f(t,\rho) = \begin{cases} \rho v(t), & \text{if } 0 \le \rho \le \rho_c, \\ \frac{v(t)\rho_c}{\rho_{max}-\rho_c}(\rho_{max} - \rho) & \text{if } 0 \le \rho \le \rho_c, \end{cases}$$

$$\text{where } \rho_c \in (0, \rho_{max})$$

0.2 Pedestrian flow models

Mathematical aspects of pedestrian flow models have received lots of attention in the mathematical modeling research community over the past decade and it has helped to provide deep insights into physical models of pedestrian flow dynamics usually obtained with tools of physics, engineering and social sciences [81]. A basic example is the Hughes' continuum model of pedestrian flow [57] whose original governing equations are born out of fluid dynamic principles with applications derived from the general behavior of the Lighthill and Whitham [69, 78] models of traffic motion. The model is well suited for motions of large crowds in narrow corridors with a common target. However, in [56], it was applied to a two-dimensional walking facility in which a pedestrian chooses a route to minimize the instantaneous travel cost to the destination. In another instance, [89], within a less general setting, powerful resources for computer games and animated movies

was utilized efficiently to provide a real-time simulation of large groups considered as a continuum with common targets. These models provide useful tools for the planning and design of walking facilities as well as aids in the visualization of the movement trajectories of pedestrians and their interactions within such a facility. The motivation to study the qualitative behaviour of pedestrians from an analytical viewpoint is not arbitrary. First, field experiments with human subjects are obviously too expensive and difficult to conduct, and hence analytical studies come only at the cost of computer power [89]. They help architectures and engineers to better plan and design structures such that there will be minimal casualties in case of fire or natural disasters [53]. However, the overarching importance of crowd models are but not limited to estimating migratory flows, traffic forecasting, and urban planning [91].

Mathematical models of crowd motion and dynamics come in two main forms namely, microscopic and macroscopic. The microscopic models are based on the idea that the behavior and interactions of the individual entities (as people are treated as rigid discs) can be determined by physical and social laws subject to constraints imposed by their immediate surroundings. The mathematical equations of these models are generally stated in terms of systems of ordinary differential equations. Some examples of microscopic models include the so-called floor field models, [82, 42] and contact model [72]. For an extensive review on different microscopic approaches we refer to [19, 52]. With respect to macroscopic models, the whole crowd is treated as a single entity but movements of single individuals are ignored. Since they seek to predict the advection of large crowds, the model equations are largely hyperbolic conservation laws with a closure relation expressed as a speed-density function. Included in the list of examples of macroscopic models are those based on optimal transport theory [71], on scalar conservation laws with non-convex flux as in [29] and recently with inspirations from mean field games [22].

The Hughes' model

The Hughes' model of pedestrian flow in the multidimensional setting writes:

$$\partial_t \rho - \operatorname{div}\left(\rho v^2(\rho)\nabla\phi\right) = 0, \quad x \in \Pi_x, \tag{3a}$$

$$\left|\nabla\phi\right| = \frac{1}{v(\rho)}, \quad x \in \Pi_x, \tag{3b}$$

where $x \in \Pi_x$ is the space variable, $\Pi_x \subset \mathbb{R}^d$, a bounded domain for $d \geq 1$, $\rho(t,x)$ represents the crowd density in x at time $t \geq 0$. The density dependent function v plays the role of the speed adapted by the crowd and is usually expressed as a

decreasing function such that over the interval $[0, \rho_{\max})$, where $\rho_{\max}$ is the maximum density, the situation in which $v(\rho_{\max}) = 0$, represents congestion where as there's free flow if $v(0) = v_{\max}$, with $v_{\max} > 0$. The potential function $\phi(t, x)$ in the Eikonal equation (3b) models the common sense strategy adapted by the pedestrians to reach their target (or exit). In most cases it is interpreted as a weighted distance to the exit and so pedestrians take the path down the minimum gradient. That is they avoid congested zones so as to optimize the travel time to the exits.

In the one-dimensional setting, the model writes

$$\partial_t \rho - \partial_x \left(\rho v(\rho) \frac{\varphi_x}{|\varphi_x|} \right) = 0, \tag{4a}$$

$$|\varphi_x| = c(\rho), \tag{4b}$$

in the spatial domain $\Pi_x =]-1, 1[$, coupled with a Dirichlet's boundary conditions:

$$\rho(1, t) = \rho(-1, t) = 0, \quad t > 0, \tag{4c}$$

$$\varphi(1, t) = \varphi(-1, t) = 0, \quad t > 0, \tag{4d}$$

and initial data

$$\rho(x, 0) = \rho_0(x), \tag{4e}$$

where $\rho(t, x) \in [0, 1]$ is the unknown crowd density (normalized); $c(\rho) = 1/v(\rho)$, is the running cost; $v(\rho) = 1 - \rho$ is the mean velocity. A unique viscous solution to the Eikonal equation (4b) with boundary condition (4d) gives rise to a unique turning point $\xi(t) \in \Pi_x$ that satisfies the implicit relation:

$$\int_{-1}^{\xi(t)} c(\rho(t, x))dx = \int_{\xi(t)}^{1} c(\rho(t, x))dx, \quad \forall t \geq 0. \tag{5}$$

The 1D model (4) can be re-written as a scalar conservation law with space-time discontinuous flux:

$$\partial_t \rho + \partial_x \big(\operatorname{sign}(x - \xi(t)) f(\rho) \big) = 0, \tag{6}$$

where, $\rho \mapsto f(\rho)$ is defined by $f(\rho) = \rho v(\rho)$ and $t \mapsto \xi(t)$ satisfies the implicit relation (5) for each $(t, x) \in [0, \infty) \times \Pi_x$.

0.3 Organisation of the thesis

After reviewing the fundamental theoretical tools used to analyse the solution of hyperbolic partial differential equation (PDE), we present the main contribution of the work in two parts beginning from chapters 3 to 4. The thesis is organised as follows:

In Chapter 1, we discuss known results for scalar conservation law with continuous flux and discontinuous flux. Particular emphasis is given to the selection of an appropriate notion of entropy admissible conditions, the new tool of admissibility germ.

In Chapter 2, we then discuss the numerical schemes employed to approximate weak solutions of the equation studied in this work. The first section of this chapter is focused on the standard methods, the so-called Godunov scheme and a brief discussion of its failure to the discontinuous flux problems. We then conclude with an overview of the steps involved to obtain a convergence result for problems without a spatial bound in the total variation.

Chapter 3 begins with the main contribution of the thesis. Here we present our equation and analyse the Riemann solver of the Cauchy problem. We also attempt to lay bare the new tool of admissibility germs and show how it could be useful to prove existence of solutions. Particular emphasis is given to the fact that we do not yet have a bound in the spacial total variation on the solution to the problem, leading to studying the solutions in the framework of the entropy process solutions.

In Chapter 4, we propose a new finite volume scheme with a 'localised' adapt-ed mesh or *moving mesh* near to the space time flux discontinuity. After analysing some key properties of the scheme, we attempt to prove the convergence of the scheme with an $\mathbf{L}^\infty$ stability estimate on the approximation solutions. In the final section, we present some numerical experiments for specific problems and compute the order of convergence of the method.

Finally, in Chapter 5, we draw conclusions and lay a foundation for future works.

Chapter 1

Scalar Conservation laws with discontinuous coefficients

1.1 Introduction

In this chapter, we review the basic theory of scalar conservation laws with discontinuous coefficients. Before discussing the theoretical tools used to study well-posedness, we dedicate the first part of this chapter to scalar conservation laws with continuous flux and then in the second part, present the theoretical tools extended to the discontinuous flux problems.

A scalar conservation law is partial differential equation (PDE) which describes the evolution of a conserved quantity, such as mass, density of cars or concentration of a specie in one dimension in space. The general expression of this PDE appears in the form

$$\partial_t \rho + \partial_x f(t, x, \rho) = 0, \tag{1.1}$$

where ρ represents the conserved quantity and f is a function representing the rate of flux of this quantity through the boundary of the domain and hence referred to as the *flux function*. The work of this thesis is based on scalar conservation laws in which f contains a discontinuity in the space and time variables.

In one dimensional space setting, it can be derived from the basic principle of mass conservation as recalled below. Let $(t, x) \mapsto \rho(t, x) \geq 0$ be a function that represents a conserved quantity (e.g. density, momentum, energy etc.), and $\int_I \rho(t, x)dx$, the total amount of ρ in the interval $I = [x_l, x_r]$ at time t. Suppose that the *total mass* is finite at the time $t = 0$: $\int_{\mathbb{R}} \rho(0, x)\, dx \in \mathbb{R}$, then the conservation principle simply stipulates that:

$$\frac{d}{dt} \int_{\mathbb{R}} \rho(t, x)dx = 0. \tag{1.2}$$

More specifically, assume that the initial mass is finite over the interval I and using the function $f : \mathbb{R}^+ \times \mathbb{R} \mapsto \mathbb{R}$ represent the flux per unit area, then mass conservation principle implies that

$$\frac{d}{dt}\int_{x_l}^{x_r} \rho(t,x)dx = f(t,x_l,\rho(t,x_l)) - f(t,x_r,\rho(t,x_l)). \tag{1.3}$$

In the context of fluid dynamics, ρ is considered to be a fluid density flowing with velocity of $v(t,x)$ and hence the flux function is defined by

$$f(t,x,\rho(t,x)) = v(t,x)\rho(t,x). \tag{1.4}$$

Integrating (1.3) further in time over a finite time interval $I_T = [t_1,t_2]$ and rearranging gives

$$\int_{t_1}^{t_2}\int_{x_l}^{x_r} \partial_t\rho(t,x) + \partial_x f(t,x,\rho)dxdt = 0.$$

The above integral is zero for every choice of $[t_1,t_2]\times[x_l,x_r]$ if the integrand satisfies

$$\partial_t\rho(t,x) + \partial_x f(t,x,\rho) = 0, \tag{1.5}$$

commonly referred to as the *differential form* of a scalar conservation law. It is common to study solutions of a scalar conservation law using its differential form. As this work concerns the existence of solution to scalar conservation law, we shall also adapt to the differential form of the equation. For most problems studied with a scalar conservation law, the velocity relation is a function of the density. Therefore, in such situation, it is convenient to write $v = v(\rho)$, the flux function also becomes a density function given by $f(\rho) = \rho v(\rho)$. The differential form of the conservation law now writes

$$\partial_t\rho + \partial_x f(\rho) = 0. \tag{1.6}$$

For the purpose of our discussion, we shall use the differential form in (1.6) when referring to conservation laws with continuous flux in the next section.

1.1.1 The Cauchy problem and the classical solution

We begin with the Cauchy problem for the PDE (1.6) with a given initial condition

$$\begin{cases} \partial_t\rho + \partial_x F(\rho) = 0, \ (t,x) \in \mathbb{R}_0^+ \times \mathbb{R}, & \text{(1.7a)} \\ \rho(0,x) = \rho_0(x), \ x \in \mathbb{R}. & \text{(1.7b)} \end{cases}$$

As the equation (1.7a) involves first order derivatives in space and time, it makes sense to look for solutions that are continuously differentiable both in space and time.

To illustrate, we parameterize the $x-t$ plane by the *characteristic curve* starting at the point $y \in \mathbb{R}$ as $t \mapsto X(t;y)$ and denote by $\mathfrak{R}(t;y)$ the value of ρ along X, then

$$\begin{aligned}\dot{\mathfrak{R}} &= \partial_t \rho(t, X(t)) + \dot{X} \cdot \partial_x \rho(t, X(t)) \\ &= \partial_t \rho(t, X(t)) + F'(\rho(t, X(t))) \cdot \partial_x \rho(t, X(t)) \\ &= 0.\end{aligned}$$

This implies that the solution is constant along characteristic lines and solving the Cauchy problem (1.7) reduces to finding the characteristic line that also satisfies the ODE

$$\begin{cases} \dot{X} = F'(\mathfrak{R}(t)), \ t > 0, \\ X(0) = y, \ y \in \mathbb{R}, \end{cases}$$

whose solution is given by $X(t;y) = y + tF'(\mathfrak{R}(0))$. Thus given any point (t,x), one only needs to determine the characteristic curve originating from y and that passes through the point x. If $X(t;\cdot)$ is invertible, at least for small $t > 0$, the exact solution to (1.7) can be traced from the initial solution given at y and is implicitly given as:

$$\rho(t,x) = \rho_0\big(x - tF'(\rho(t,x))\big).$$

Such solutions are referred to as *classical solutions* defined below.

Definition 1.1. Let $F \in C^1(\mathbb{R};\mathbb{R})$ and $\rho_0 \in C^1(\mathbb{R};\mathbb{R})$. Let $T > 0$. A classical solution of a Cauchy problem (1.7) is a function $\rho \in C^1([0,T) \times \mathbb{R}, \mathbb{R})$ that satisfies (1.7).

Notice that every characteristic curve $(t, X(t))$ travel with speed, $F'(\rho)$ that is also dependent on the solution itself. This may introduce severe irregularities in the global in time solution and the smoothness property of ρ in general breaks down, even if the initial data is smooth. This severity is a real issue in the study of solutions to hyperbolic conservation laws. For this reason, the concept of weak solution is introduced in order to define global in time solutions of (1.7) where classical solutions do not exist.

1.1.2 Weak solutions

The assertions laid in the previous section merits different notions of solutions when dealing with conservation laws. In this subsection, we describe the notion

of weak or distribution solutions. Indeed, since the PDE (1.7a) is in divergence form, multiplication by a continuous function φ and a formal integration by parts lead to the following definition of solution:

Definition 1.2. (Weak solutions) Let $\Omega = \mathbb{R}_0^+ \times \mathbb{R}$, $\rho_0 \in \mathbf{L}^\infty(\mathbb{R};\mathbb{R})$ and $F \in C^1(\mathbb{R};\mathbb{R})$. A function $\rho \in \mathbf{L}^\infty(\Omega;\mathbb{R})$ is a weak solution of the scalar conservation law (1.7) if it satisfies the integral identity

$$\int_{\mathbb{R}^+}\int_{\mathbb{R}} \rho\varphi_t + F(\rho)\varphi_x dxdt + \int_{\mathbb{R}} \rho_0\varphi(0,x)dx = 0 \tag{1.8}$$

for all test function with compact support $\varphi \in C_c^1(\Omega;\mathbb{R})$.

This definition of solution allows ρ to be discontinuous since the partial derivatives on ρ shift to φ. It can be proved that every classical solution also satisfies the integral condition (1.8) for all φ and hence a weak solution. An important class of functions usually considered in literature is the piecewise smooth functions containing jump discontinuities. The next lemma gives a necessary and sufficient condition to be imposed on such functions in order to be admitted as a weak solution.

Lemma 1.1. ***(Rankine-Hugoniot jump condition)*** *Let Ω be separated into two regions Ω_- and Ω_+ by a Lipschitz curve S parameterized by $S = (t,\sigma(t))$ where $\sigma : \mathbb{R}_0^+ \mapsto \mathbb{R}$. Furthermore, assume that ρ is smooth over Ω_- and Ω_+ occurring in the form*

$$\rho(t,x) = \begin{cases} \rho^-(t,x), & \text{if } x < \sigma(t), \\ \rho^+(t,x), & \text{if } x > \sigma(t), \end{cases} \tag{1.9}$$

where $\rho^\pm : \Omega_\pm \mapsto \mathbb{R}$ are C^1 functions and assume that the limits $\rho(t,\sigma(t)\pm) = \lim_{x\to\sigma(t)\pm} \rho(t,x)$ exist for a.e t. Then, ρ is a weak solution of (1.7) if and only if the following two conditions hold:

i) ρ is a classical solution over Ω_- and Ω_+.

ii) ρ satisfies the jump condition:

$$\sigma'(t) = \frac{F(\rho^+(t,x)) - F(\rho^-(t,x))}{\rho^+(t,x) - \rho^-(t,x)} \quad \text{for a.e. } t. \tag{1.10}$$

If ρ is piecewise constant, (1.9) reduces to

$$\rho(t,x) = \begin{cases} \rho^-, & \text{if } x < st, \\ \rho^+, & \text{if } x > st, \end{cases} \tag{1.11}$$

where $\rho^{\pm}$ are constants and σ is linear with slope $s \in \mathbb{R}$ and the Rankine-Hugoniot relation reads:

$$-s(\rho^- - \rho^+) + F(\rho^-) - F(\rho^+) = 0. \tag{1.12}$$

If $\rho^- \neq \rho^+$ then by lemma 1.1, any weak solution to (1.7) represented by the pair (ρ^-, ρ^+) of the form (1.11) is referred to as the *a shock wave* connecting ρ^- to ρ^+ and travels with speed s, if additional entropy conditions are prescribed to select admissible weak solutions.

1.1.3 Entropy inequalities

In general, the weak solutions in the sense of Definition 1.2 are not uniquely determined by the initial data, ρ_0. Indeed, one can prescribe an entire family of weak solutions to the same Cauchy problem for a given class of initial data. This problem is resolved by the so-called *vanishing viscosity regularization*.

Roughly speaking, a term R^ε is introduced in the PDE (1.7) where ε is a small parameter that approaches 0, and when it does the solution of the Cauchy problem (1.7) is realized as the limit of the regularized (or viscous) equation:

$$\partial_t \rho^\varepsilon + \partial_x F(\rho^\varepsilon) = R^\varepsilon, \quad (t, x) \in \Omega. \tag{1.13}$$

Meaning, ρ^ε is a sequence of solutions of equation (1.13) regularized by R^ε. We may assume that R^ε has a regularizing effect, so that ρ^ε is smooth depend on ρ^ε, $\varepsilon\rho^\varepsilon_x$, $\varepsilon^2\rho^\varepsilon_{xx} \ldots$ that vanishes as $\varepsilon \to 0$. Convergence of ρ^ε to the singular limit ρ holds everywhere in $\mathbb{R}$ if ρ^ε is uniformly bounded in an appropriate sense and the bound is independent of ε. The major drawback in this criteria is that it is very difficult to obtain *a priori* estimates for (1.13) which would allow one to prove the convergence to a weak solution to (1.7) as $\varepsilon \to 0$. This may be overcome by deducing other viscous conditions that can be easily verified according to the physical considerations of the problem. The regularization mechanism applied with R^ε is very crucial as it determines the kind of admissibility condition that allows one to select the unique solution. The most-well known mechanism is the entropy-entropy flux.

Definition 1.3. A pair of functions η, Φ with η convex is called *entropy-entropy* flux pair for (1.7) if

$$\Phi'(\rho) = \eta'(\rho)F'(\rho), \tag{1.14}$$

is satisfied at every ρ where η, Φ, and F are differentiable.

Remark 1.1. If $\rho = \rho(t, x)$ is a classical solution of (1.7) in the sense of Definition 1.1, then the consequence of (1.14) implies that ρ must also satisfy $\eta(\rho)_t + \Phi(\rho)_x = 0$.

The following definitions are needed in order to discuss weak entropy solutions.

Definition 1.4. Let ρ^ε be the smooth solutions of (1.13) such that $\rho = \lim_{\varepsilon\to 0}\rho^\varepsilon$ is a weak solution of (1.7). Then the regularisation term R^ε is said to be a *conservative regularization* in the limit as $\varepsilon \to 0$ if

$$\lim_{\varepsilon\to 0}\iint R^\varepsilon \cdot \varphi dxdt = 0, \quad \forall \varphi \in C_c^\infty(\Omega;\mathbb{R}^+). \tag{1.15}$$

In addition, it is said to be *entropy dissipative regularization* for the entropy $\eta(\rho)$ if

$$\lim_{\varepsilon\to 0}\iint \eta'(\rho^\varepsilon)\cdot R^\varepsilon \cdot \varphi dxdt \le 0, \quad \forall \varphi \in C_c^\infty(\Omega;\mathbb{R}^+). \tag{1.16}$$

If (1.7) is endowed with a convex entropy function, and appropriate limit conditions on the weak solution ρ are derived, then the limit solution is a unique weak solution. The following theorem summarizes the natural conditions on R^ε needed to deduce a unique limit of the weak solution:

Theorem 1.1. *Let ρ^ε be a family of approximate solutions of (1.13) that is bounded in the $\mathbf{L}^\infty$ norm as $\varepsilon \to 0$ and converges a.e to the limit ρ which is a weak solution of (1.7). Suppose also that R^ε is conservative and entropy dissipative for some entropy-entropy flux pair (η,Φ). Then ρ is a weak solution of (1.7) and satisfies the inequality*

$$\int\int \left(\eta(\rho)\partial_t\varphi + \Phi(\rho)\partial_x\varphi\right) dtdx \ge 0, \quad \forall \varphi \in C_c^\infty(\Omega;\mathbb{R}^+). \tag{1.17}$$

For proof of Theorem 1.1, we refer the reader to [65]. In the distributional sense, the inequality (1.17) rewrites as

$$\partial_t\eta(\rho) + \partial_x\Phi(\rho) \le 0 \text{ in } \mathcal{D}'(\Omega). \tag{1.18}$$

This inequality is called the *entropy inequality* for all entropy-entropy flux pair (η,Φ) and any weak solution satisfying (1.18) is an *entropy admissible solution*. A particular class of useful entropy-entropy flux pair is the so-called Kruzkhov entropy pair [63] given by

$$\eta_k(\rho) = |\rho - k|, \quad \Phi_k(\rho) = \text{sign}(\rho - k)\left(F(\rho) - F(k)\right) \tag{1.19}$$

for every fixed $k \in \mathbb{R}$.

Definition 1.5. Let $\rho_0 \in \mathbf{L}^\infty(\mathbb{R})$. A function $\rho \in \mathbf{L}^\infty\big(]0,T[\times\mathbb{R};\mathbb{R}\big)$ with $T > 0$ is a weak entropy solution of (1.7a) if and only if for every $k \in \mathbb{R}$ the following integral

inequality

$$\int_0^T \int_{\mathbb{R}} \left[\eta_k(\rho)\varphi_t(t,x) + \Phi_k(\rho)\varphi_x(t,x)\right] dxdt + \int_{\mathbb{R}} |\rho_0 - k|\varphi(0,x)dx \geq 0 \tag{1.20}$$

holds for all test functions $\varphi \in \mathbf{C_c^1}\left(\mathbb{R}_0^+ \times \mathbb{R}; \mathbb{R}_0^+\right)$.

Remark 1.2. Notice that η_k and Φ_k are convex and Lipschitz continuous functions that satisfy the equality (1.14) at every $\rho \neq k$.

By Remark 1.1, one can conclude that classical solutions are also entropy admissible. However, it is not immediately clear whether or not a given weak solution of the form (1.11) is entropy admissible. On this premise, the following definition gives a simple criterion when a weak solution of the form (1.11) is given.

Proposition 1.1. *A weak solution, (1.11), of (1.7) denoted by the pair (ρ^-, ρ^+) with speed λ satisfying (1.12) and $\rho^- \neq \rho^+$, satisfies the entropy inequality (1.18) if and only if Oleinik entropy inequalities*

$$\frac{F(\rho^*) - F(\rho^-)}{\rho^* - \rho^-} \geq \frac{F(\rho^+) - F(\rho^*)}{\rho^+ - \rho^*}, \quad \forall \rho^* \in [\rho^-,\, \rho^+] \text{ or } \rho^* \in [\rho^+,\, \rho^-]. \tag{1.21}$$

Moreover, the condition (1.21) implies the so-called Lax shock inequalities

$$F'(\rho^-) \geq \lambda \geq F'(\rho^+), \tag{1.22}$$

if F is a strictly concave or convex function.

The inequality (1.21) gives a geometric interpretation of admissible weak solution for a general F, which is the graph of F must be below the secants connecting ρ^- to ρ^+ if $\rho^+ < \rho^-$. On the other hand, if $\rho^+ > \rho^-$ the graph of F must remain above the secants connecting ρ^- to ρ^+. In addition, Lax inequality imply that only solutions in which waves on the left of the characteristic travel faster than waves on the right and impinges on each other to form a discontinuity are admissible.

Proposition 1.2. *A function $\rho(t,x) \in \mathbf{L}^\infty(\Omega; \mathbb{R})$ as in (1.11) is a weak entropy solution of (1.7) in the sense of Definition 1.5 if and only if (1.21) holds.*

The next proposition establishes the uniqueness of the weak entropy solutions.

Proposition 1.3. *(L^1-contraction principle): Suppose that $\rho^1, \rho^2 \in \mathbf{L}^\infty\left(]0, T[\times\mathbb{R}; \mathbb{R}\right)$, with $T > 0$ are two weak entropy solutions of (1.7) with $F \in Lip(\mathbb{R})$ and initial data $\rho_0^1, \rho_0^1 \in \mathbf{L}^\infty(\mathbb{R})$, then the following L^1-contraction property holds:*

$$\left\|\rho^1(t,\cdot) - \rho^2(t,\cdot)\right\|_{L^1} \leq \left\|\rho_0^1 - \rho_0^2\right\|_{L^1}, \tag{1.23}$$

implying the uniqueness of weak entropy solutions.

This proposition can be proved by following the classical idea of the 'doubling of variable' technique introduced by Kruzkhov [63]. Using this technique, one relies on the entropy inequalities of (1.18) with the Kruzkhov entropy-entropy flux pair (1.19) satisfying the integral inequality (1.20) of Definition 1.5. Integrating (1.20) first in (t,x) with the constant $k=\rho^1(s,y)$, if $\rho^2(t,x)$ and then in (s,y) with $k=\rho^2(s,y)$, if $\rho^1(t,x)$, using an appropriate test (or cut off) function, one recovers the Kato inequality

$$\partial_t|\rho^1-\rho^2|+\partial_x\Big(\operatorname{sign}(\rho^1-\rho^2)F(\rho^1)-F(\rho^2)\Big)\leq 0,\qquad \text{in } \mathcal{D}'(\Omega). \tag{1.24}$$

With M being the Lipschitz constant of F and any $P>0$, this inequality is then integrated along the trapezoid, $\Lambda=\big\{(t,x)\in\mathbb{R}_0^+\times\mathbb{R}:|x|\leq P+M(T-t),\ t\in[0,T]\big\}$, to obtain the inequality (1.23). This directly implies that if $\rho^{1,2}$ have the same initial conditions, then clearly $\rho^1=\rho^2$.

1.1.4 The Riemann solvers

From the foregoing, it is clear that shock wave solutions, (1.11) form a special class of weak solutions of (1.7) that merit attention. The most basic form of initial data that gives these forms of solution is the so-called Riemann data.

Definition 1.6. A Riemann's problem is a Cauchy problem with initial datum of the form

$$\rho_0(x)=\begin{cases}\rho_L, & \text{if } x<0,\\ \rho_R, & \text{if } x>0,\end{cases} \tag{1.25}$$

where $\rho_L,\ \rho_R\in[0,R]$. Any function that provides a weak entropy solution to the Riemann problem is referred to as the *the Riemann solver*.

The Riemann problem serves as a building block for developing admissible weak solutions and numerical approximations to the general Cauchy problem. The Riemann solvers allows one to track the solution across a jump discontinuity such that the entropy conditions are satisfied. An important property of Riemann solvers is that they are *self-similar*. Meaning, if $\rho(t,x)$ is a solution to (1.25), then $\rho(\lambda t,\lambda x)$ is also a solution for any scalar $\lambda>0$ and therefore is invariant under the transformation $x\mapsto\lambda x$, and $t\mapsto\lambda t$. For this reason, the Riemann solver is written as a function of x/t: $w(x/t)=\rho(t,x)$. Here we describe the basic types of waves assuming that the flux function is convex, $F''>0$.

1. *Centered Rarefaction:* Set $z = x/t$, then insert $w(x/t)$ into (1.7a), and observing that $w'(x/t) \neq 0$, we obtain
$$z = F'(w). \tag{1.26}$$
With convex F implies that F' is strictly monotone, and so $w = (F')^{-1}(z)$. More precisely, if $\rho_L < \rho_R$, and F' is strictly increasing for $z \in [F'(\rho_L), F'(\rho_R)]$. Then we can define a continuous function of the form
$$\rho(t,x) = \begin{cases} \rho_L, & \text{if } x < F'(\rho_L)t, \\ (F')^{-1}(x/t), & \text{if } x \in [F'(\rho_L)t, F'(\rho_R)t], \\ \rho_R, & \text{if } x > F'(\rho_R)t. \end{cases} \tag{1.27}$$
Solution of this form is referred to as *centered rarefaction wave.*

2. *Shocks:* In the case where $\rho_L > \rho_R$, the weak solution is called *a shock wave* and it is given by:
$$\rho(t,x) = \begin{cases} \rho_L, & \text{if } x < \lambda t, \\ \rho_R, & \text{if } x > \lambda t, \end{cases} \tag{1.28}$$
where $\lambda \in \mathbb{R}$ is the speed of the wave provided by
$$\lambda = \frac{F(\rho_L) - F(\rho_R)}{\rho_L - \rho_R}.$$
Shocks waves are admissible if (1.21) holds.

Remark 1.3. In the case of concave flux (i.e. when $F'' < 0$), the Lax admissible condition (1.22) implies that shocks are admissible if $\rho_L < \rho_R$ whereas for convex flux admissible shocks are due to $\rho_L > \rho_R$.

The concept of entropy solution of scalar conservation laws presented in this section concerns continuous flux problems (i.e., conservation laws in which the flux function depends only on ρ). However, as outlined in the introduction section of this thesis, there are many application problems in which the flux is also a function of the space and, or time variables and is also possibly discontinuous. We refer to such problems as the discontinuous flux problems. The main equation considered in this work is an example of this class of problems. The concepts of entropy solutions presented in this section cannot be extended to characterise a well-defined solution framework for these so-called discontinuous flux problems and hence would require a new set of tools to develop a well-posedness theory. These tools are introduced in the next section.

1.2 The Discontinuous flux problem

In this section, we focus on a specific form of equation (1.1), which is a scalar conservation law with discontinuous flux function written as

$$\begin{cases} \partial_t \rho + \partial_x F(k(t,x),\rho) = 0, \quad \text{on } \Omega, & \text{(1.29a)} \\ \rho(0,x) = \rho_0(x), \ x \in \mathbb{R}, & \text{(1.29b)} \end{cases}$$

where $\rho : \Omega \mapsto \mathbb{R}$ as usual is the unknown conserved variable, $F : \mathbb{R} \times \mathbb{R} \mapsto \mathbb{R}$ is the flux function, and $k : \Omega \mapsto \mathbb{R}$ is a real valued function mostly referred to as the *flux coefficient*. The standard theoretical tools and numerical methods applied to (1.7), some of which are discussed in this work, readily applies to (1.29) as long as k differentiable. However, physical problems modelled by the equation (1.29a) requires that k to belong to certain classes of discontinuous functions, e.g. $\mathbf{L}^\infty(\Omega;\mathbb{R}) \cap BV(\Omega;\mathbb{R})$ [73].

Example 1.1. (*variable speed limit problem*) Consider the flow of traffic on a single lane with speed control mechanism that the maximum speed varies across the road and must be evaluated at discrete points in time. The resulting scalar conservation law has a flux function f with time-dependence discontinuity

$$F(k(t),\rho) = k(t)\rho(1-\rho) \tag{1.30}$$

where $k : [0,T] \to [v_{\min}, v_{\max}]$, representing the maximal (mean) traffic velocity limit belongs to $\mathbf{BV}([0,T];[v_{\min}, v_{\max}])$.

See other examples in [73, 25, 21, 85, 44] and references therein. The study of these equations require the use of novel theoretical tools and design of new numerical methods. In this section, we recall the theoretical tools used to study existence of solutions to equations of the form (1.29a).

1.2.1 The problem

To illustrate the difficulty in studying (1.29a) we suppose that k is constant in time, then the equation can be written as a 2×2 system:

$$\begin{aligned} \partial_t \rho + \partial_x F(k(x),\rho) &= 0, \\ \partial_t k &= 0, \end{aligned} \tag{1.31}$$

where $(\rho, k)^T$ is a vector of the conserved variables and in the matrix representation form, written as

$$\partial_t \begin{bmatrix} \rho \\ k \end{bmatrix} + \begin{bmatrix} \frac{\partial F}{\partial \rho} & \frac{\partial F}{\partial k} \\ 0 & 0 \end{bmatrix} \partial_x \begin{bmatrix} \rho \\ k \end{bmatrix} = \begin{bmatrix} 0 \\ 0 \end{bmatrix}.$$

The Jacobian matrix has eigenvalues $\lambda_1 = 0$ and $\lambda_2 = \frac{\partial F}{\partial \rho}$. Therefore, if $\frac{\partial F}{\partial \rho} = 0$ for some (k, ρ), the system (1.31) fails to be strictly hyperbolic. Indeed the lack of strict hyperbolicity is largely due to the existence of k which presents a major difficulty toward analysis of solutions, since the standard well-posedness theory strictly hyperbolic systems of conservation laws which is well understood, doesn't readily apply to (1.29a). Also, a key ingredient to establish existence of solutions to the general scalar conservation law is to prove that the solution operator is total variation diminishing (TVD). That is, the total variation of the solution does not increase in time. However, for conservation laws with discontinuous flux the total variation in the solution is usually greater than the total variation in the initial data. Moreover, where $\frac{dF}{d\rho}$ vanishes then the two eigenvalues coincide and the system becomes resonant. This problem is even worse in the situation where k also has time dependent variable.

Another delicate issue is the lack of uniqueness for solutions. The framework of entropy solutions proposed for the discontinuous flux problems are based on applying a standard admissibility criterion (such as the Kruzkhov and Lax-Oleinik entropy conditions) over the space domain away from the flux interface and then applying a Rankine-Hugoniot jump relation at each interface. This entropy admissibility condition may not always be enough to select the physically relevant solutions, since for a single problem, it is possible to obtain at least one solution in which both conditions are satisfied. See [3, 10, 73] and references therein. We illustrate this in the following example

Example 1.2. Consider a simple case example of the model of (1.29) with

$$\begin{aligned} F(k(x), \rho) &= k(x)\rho(1-\rho), \\ k(x) &= \begin{cases} 1, & \text{for } x < 0, \\ 2, & \text{for } x > 0, \end{cases} \\ \rho_0(x) &= \bar{\rho} \in [0, 1]. \end{aligned}$$

The using the notation that $f^l(\rho) = \rho(1-\rho)$ and $f^r(\rho) = 2\rho(1-\rho)$, the Lax-Oleinik admissible criterion dictates that the function

$$\rho(t,x) = \begin{cases} \bar{\rho}, & \text{if } x < 0, \\ \theta, & \text{if } 0 < x < \sigma^r t, \\ \bar{\rho}, & \text{if } x \geq \sigma^r t, \end{cases}$$

where $\theta \in [0, \bar{\rho}]$ such that $f^r(\theta) = f^l(\bar{\rho})$ with $\sigma^r = \left(f^r(\theta) - f^r(\bar{\rho})\right)/(\theta - \bar{\rho})$ is a weak entropy solution. However, using the so-called AB type solution introduced in [3], yields yet another weak entropy solution is

$$\rho(t,x) = \begin{cases} \bar{\rho}, & \text{if } x < \sigma^l t, \\ A, & \text{if } \sigma^l t < x < 0, \\ B, & \text{if } 0 < x < \sigma^r t, \\ \bar{\rho}, & \text{if } x > \sigma^r t, \end{cases}$$

where $A, B \in [0,1]$ are chosen such that $f^l(A) = f^r(B)$ with $A \in [1/2, 1]$ and $B \in [0, 1/2]$. The AB type solution also satisfies the Lax-Oleinik conditions as well.

Clearly there's lack of uniqueness and increase in the total variation in the solution. Therefore, there's the need for additional criteria in order to obtain physically relevant solutions.

1.2.2 Entropy weak solutions

As discussed in Section 1.1, classical solutions to scalar conservation laws generally exist up to a finite time even if the initial data is smooth and the flux function is smooth. A considerable amount of work has been done in this direction by several authors some of which are discussed below.

In [46, 45], Gimse and Risebro derived the 'minimal jump condition' for shocks at the interface to supplement the Rankine-Hugoniot jump condition (1.33). This condition consists in requiring that there exist a unique pair (A, B) satisfying (1.33) such that the jump $|A - B|$ across the interface ($x = 0$ in the original paper) is minimum. This minimum jump condition was used in [62] to define unique and stable weak solutions for problems with convex flux $k(x)f(\rho)$, $k(x) \neq 0$, under an additional wave entropy condition. The wave entropy condition has the additional advantage of not requiring that the solution satisfy further regularity conditions. Compare [61, 80]. Later in [35, 36], Diehl coined the $\Gamma-$condition which is a slight modification of the minimum jump condition. In [87], Towers also proved a Kruzkhov-type entropy inequality and for uniqueness, a geometric condition at

the interface using the hypothesis of the minimal jump condition. The geometric condition is a consequence of the standard admissible shock condition (see Section 1.1 and Definition 1.1) which requires that the characteristics on at least one side of the flux discontinuity extends toward the $x-$axis if traced backwards in time. With exception of [87], sign changes in k was ruled out due to some technical difficulties that it introduces in the analysis.

Karlsen, Risebro and Towers in [58] still proposed a modified version of the Kruzkhov-type entropy condition (1.34) for a degenerate equation with flux functions discontinuous in space. These solutions are shown to be L^1 stable and hence unique if traces of the solution at the flux interface satisfy a geometric condition termed "crossing condition". Moreover, Audusse and Perthame proved uniqueness of a Kruzkhov-type entropy solutions to a class of conservation law with spatial flux discontinuity by using the so-called 'adapted entropies' without relying on traces, interface conditions and BV assumptions [16]. The flux crossing condition introduced in [58] was later extended to the case of time dependent coefficients in [59]. Nevertheless, entropy solutions to equations with time-dependent flux discontinuity was also dealt with in [75] by Ostrov, by solving a Hamilton-Jacobi equation associated to the scalar conservation law, with Lipschitz initial data. More recently, Bressan, Guerra and Shen in [21] introduced the concept of *regulated functions* to prove uniqueness of solutions by a vanishing viscosity argument. They obtained comparison estimates for the Hamilton-Jacobi equations corresponding to a parabolic equation and proved that for a family of flux functions whose time-dependent discontinuity is regulated, there exist unique weak limit which is also a solution to the related scalar conservation law.

Since the problem studied in this work satisfies the crossing condition, we largely rely on the entropy framework established in [58] for our analysis. The definition of entropy weak solutions for scalar conservation law with discontinuous flux is recalled in this section.

Definition 1.7. A function $\rho \in \mathbf{L^1_{loc}}(\Omega;\mathbb{R})$, such that $(t,x) \mapsto F(k(t,x),\rho(t,x)) \in \mathbf{L^1_{loc}}(\Omega;\mathbb{R})$ is a weak solution of (1.29) if

$$\int_{-\infty}^{\infty}\int_{0}^{\infty} \left(\rho\partial_t\varphi + F(k(t,x),\rho)\partial_x\varphi\right) dtdx + \int_{-\infty}^{\infty} \varphi(0,x)\rho_0(x)dx = 0 \tag{1.32}$$

for each $\varphi \in C_c^\infty(\Omega;\mathbb{R})$.

Given that the flux function contains a discontinuity, the traces in the solution at the discontinuity need to be well-defined.

Assumption 1.1. Suppose that k is piecewise smooth and has a finite set of discontinuities along the non-overlapping curves $\omega_1, \omega_2, \ldots, \omega_M$ parameterized by

$x = \xi_\nu(t)$ for $t \in \mathbb{R}_0^+$ and $1 \leq \nu \leq M$, then the right and left traces along each ω_ν are denoted $k_\nu^{l,r}(t) = k\left(t, \xi_\nu^{l,r}(t)\right)$ respectively. Furthermore, if the traces in the solution at each $(t, \xi_\nu(t))$ exist for almost every $t \in \mathbb{R}^0$, we denote them by $\gamma^l \rho_\nu(t) = \lim_{x \to \xi_\nu(t)-} \rho(t,x)$ and $\gamma^r \rho_\nu(t) = \lim_{x \to \xi_\nu(t)+} \rho(t,x)$.

Lemma 1.2. *Let ρ be a weak solution to the Cauchy problem (1.29) as in Definition (1.7). If the trace values $k_\nu^{l,r}(t)$ and $\gamma^{l,r}\rho_\nu(t)$, exist they must satisfy the following Rankine-Hugoniot relation*

$$F(k_\nu^r(t), \gamma^r \rho_\nu(t)) - F(k_\nu^l(t)\gamma^l \rho_\nu(t)) = \dot{\xi}_\nu(t)\left[\gamma^l \rho_\nu(t) - \gamma^r \rho_\nu(t)\right], \quad 1 \leq \nu \leq M \tag{1.33}$$

for a.e. $t \in \mathbb{R}^+$.

In the following, we will refer to the case $M = 1$, that is a single discontinuous curve. As was shown in the case of continuous flux problems, weak solutions are generally not the unique solution satisfying the identities (1.32) and (1.33) only. Consequently a notion of entropy solutions is needed to select a physical solution of the problem. We shall adapt to the following notion of entropy weak solution:

Definition 1.8. A function $\rho \in \mathbf{L}^\infty(\Omega; \mathbb{R})$ with traces $\gamma^{l,r}\rho_\nu(t)$ is a weak entropy solution to the Cauchy problem (1.29), if it is a weak solution to (1.29) and for any $c \in \mathbb{R}$, and test function $\varphi \in \mathbf{C}_\mathbf{c}^\infty(\Omega; \mathbb{R}^+)$, the following Kruzkhov-type entropy inequality holds:

$$\begin{aligned}
&\iint_\Omega \left(|\rho - c|\partial_t \varphi + \operatorname{sign}(\rho - c)(F(k(t,x),\rho) - F(k(t,x),c))\partial_x \varphi\right) dxdt \\
&+ \int_{\mathbb{R}} |\rho_0(x) - c|\varphi(0,x)\mathrm{d}x - \int \int_{\Omega \setminus \{\omega_1(t)\}} \operatorname{sign}(\rho - c) F(k(t,x),c)_x \varphi dxdt \\
&+ \int_0^{+\infty} |F(k_\nu^r(t),c) - F(k_\nu^l(t),c)|\varphi(t, \xi_\nu(t))dt \geq 0.
\end{aligned} \tag{1.34}$$

The above integral is a Kruzkhov-type condition presented in [59] and adapted in [58] for a nonlinear degenerate parabolic with spatial discontinuous flux function if Assumption 1.1 holds on k. The adaptation to scalar conservation law is made by ignoring the diffusion terms and assuming that the k is assumed to be piecewise smooth, which is stronger condition. Moreover, integral (1.34) also agrees with the natural requirement that jump discontinuities in the solution satisfy the standard Lax-Oleinik entropy conditions (see section 1.1.3) away from the curves $\{\omega_\nu\}_{\nu=1}^M$.

Remark 1.4. Weak solutions satisfying (1.34) also implies the standard Kruzkhov entropy conditions discussed in Section 1.1 when $x \neq \xi_\nu(t)$. In [73] and other

works, this condition writes

$$\int\int_{\mathbb{R}\times\mathbb{R}^+} (|\rho - c|\partial_t\varphi + \text{sign}(\rho - c)(F(k(t,x),\rho) - F(k(t,x),c))\partial_x\varphi)\, dxdt + \int_{\mathbb{R}} |\rho_0(x) - c|\varphi(0,x)\mathrm{d}x \geq 0, \tag{1.35}$$

for all test functions $\varphi \in \mathbf{C}_{\mathbf{c}}^{\infty}\big(\Omega \setminus \{\omega_1\};\ \mathbb{R}_0^+\big)$, is also referred to as the interior conditions.

It is worth pointing out that even with this notion, the entropy solutions of discontinuous flux problems may not be unique. Even with Riemann's data, the existence of the jump in the flux create waves that may interact with the classical waves and so to obtain entropy solutions, additional conditions at the flux interface and in most cases inspired by the physics of the problem under consideration, must be derived. Noteworthy to see that these entropy frameworks, with the exception of [21, 75], share the common property that a Kruzkhov-type entropy condition is satisfied away from the interface and an interface connection condition satisfying the dissipativity regularization (1.16) is imposed at the jump in the flux function. The following theorem gives the L^1-contraction property of corresponding entropy solution.

Theorem 1.2. *Given $\rho_0^1, \rho_0^2 \in \mathbf{L}^\infty(\mathbb{R};\mathbb{R})$, weak entropy solutions $\rho^1, \rho^2 \in \mathbf{L}^\infty(\Omega;\mathbb{R})$ to (1.29) in the sense of Definition 1.8, satisfy the L^1-contraction property (1.23).*

Generalizing this framework, Andreianov, Karlsen and Risebro introduced a unified approach in [14] that is focused on the admissibility and dissipative behavior in the solution at the interface called *admissible germs*. Compare [10, 11, 13, 15, 9, 12]. As these tools shall be used to prove existence of solutions, we recall this notion in the next section.

1.2.3 Dissipative germs and entropy solutions

In this section, we review the theory of admissibility germs introduced for scalar conservation law in which the flux function has a jump at $x = 0$ as originally defined in [14]. The theory of germs provides a general framework for admissible weak solutions in which one could easily deal with flux interfaces by simply characterizing the dissipative behavior at the interface with a set of piecewise constant pairs. In general, these sets are actually the stationary solutions of the problem at hand. In order to maintain consistency with the literature and also ease the presentation, compare [11, 10], the review of germs in this section is done with the

following equation in view

$$\begin{cases} \partial_t \rho + \partial_x F(k(x), \rho) = 0, \text{on } \Omega, \\ \rho(0, x) = \rho_0(x), \ x \in \mathbb{R}, \end{cases} \tag{1.36}$$
$$\text{with } k(x) = \begin{cases} k_l & \text{if } x < 0, \\ k_r & \text{if } x > 0. \end{cases}$$

Definition 1.9. A subset $\mathcal{G}$ of pairs of $\mathbb{R} \times \mathbb{R}$ is called *admissible germ* (germ for short) if for every $(\rho_l, \rho_r) \in \mathcal{G}$, a Rankine-Hugoniot condition $F(k_l, \rho_l) = F(k_r, \rho_r)$ holds. It is also referred to as L^1-dissipative (L^1D) germ if

$$\Phi_l(k_l, \rho_l, \hat{\rho}_l) - \Phi_r(k_r, \rho_r, \hat{\rho}_r) \geq 0, \tag{1.37}$$

is additionally satisfied for all pairs $(\hat{\rho}_l, \hat{\rho}_l) \in \mathcal{G}$. Here $\Phi_{l,r} : (k, \rho, c) \in \mathbb{R} \times \mathbb{R} \mapsto \text{sign}(\rho - c)(F(k_{l,r}, \rho) - F(k_{l,r}, c))$.

Roughly speaking, $\mathcal{G}$ is the set of peicewise constant pairs encoding the conservation and the entropy dissipativity of the solution at the interface.

Remark 1.5. Admissible germs can also be defined for continuous flux problems. In such cases, the dissipativity condition is recovered at the shockwave discontinuities instead. See Section 1.1.3.

Remark 1.6. Due to the conservation property induced by the Rankine-Hugoniot condition, $\mathcal{G}$ may also be referenced as a conservative germ. However, non- conservative germs has also been used to obtain uniqueness of solution for some models in which case the Rankine-Hugoniot jump condition $F(k_l, \rho_l) = F(k_r, \rho_r)$ is either omitted or takes the form (1.33). Compare [13, 15].

The dissipativity inequality (1.37) is induced by the Kruzkhov entropy flux applied to a centered test function as in Definition 1.8 which essentially derives a Kato inequality and an L^1 contraction principle. This inspires a new notion of admissible solution for the model (1.36).

Definition 1.10. A function $(t, x) \mapsto \rho(t, x) \in \mathbf{L}^\infty(\Omega; \mathbb{R})$ admitting strong traces $\gamma^{l,r}\rho(t)$ at $x = 0$ is a weak entropy solution to the Cauchy problem (1.36), if and only if :

1. For any $c \in \mathbb{R}$, and all test function $\varphi \in C_c^\infty\left(\Omega; \mathbb{R}_0^+\right)$, with $\varphi(t,0) = 0$ for all $t \geq 0$, the following Kruzkhov-type entropy inequality holds

$$\iint_\Omega \left(|\rho - c|\partial_t \varphi(t,x) + \Phi\big(k,\rho,c\big)\partial_x \varphi(t,x)\right) dxdt \tag{1.38}$$
$$+ \int_{\mathbb{R}} |\rho_0(x) - c|\varphi(0,x)dx \geq 0,$$

   where $\Phi\big(k,\rho,c\big)$ is as defined in Definition 1.9.

2. The traces of ρ satisfy

$$\text{for a.e. } t > 0, \left(\gamma^l \rho(t), \gamma^r \rho(t)\right) \in \mathcal{G}.$$

Consider a Riemann data for (1.36) with $(\rho_l, \rho_r) \in \mathbb{R} \times \mathbb{R}$. If $(\rho_l, \rho_r) \in \mathcal{G}$ is an elementary solution of the Riemann problem, then it can be shown that any other elementary solution $(\hat{\rho}_l, \hat{\rho}_r)$ of the same problem also satisfies the dissipative property (1.37). Such pairs are called the dual germ of $\mathcal{G}$ denoted $\mathcal{G}^*$. The following properties of admissible germs derived from [14] that would be of interest to our work:

- Let $\mathcal{G}_1$ and $\mathcal{G}_2$ be two L^1D germs such that $\mathcal{G}_1 \subset \mathcal{G}_2$. Then we say that $\mathcal{G}_2$ is an L^1D extension of $\mathcal{G}_1$.
- An L^1D germ called *maximal*, if it is not a strict subset of some other L^1D germ. This also means that it has no extension that still satisfy the property (1.37).
- An L^1D germ $\mathcal{G}$ is called *definite*, if there exists a unique maximal L^1D germ $\tilde{\mathcal{G}}$ such that $\mathcal{G}$ is a subset of $\tilde{\mathcal{G}}$.
- An L^1D germ $\mathcal{G}$ is called *complete*, if for every Riemann data, there exists a self-similar solution $\rho(t,x)$ to the problem (1.36) such that $\rho_{|\Omega_l}$ and $\rho_{|\Omega_r}$ are the Kruzkhov entropy solutions on domains Ω_l and Ω_r respectively, and in addition admits the one-sided traces $\left(\gamma^l(\rho), \gamma^r(\rho)\right) \in \mathcal{G}$ at the flux interface $\{x = 0\}$.

The general approach which leads to a well-posedness result by the germ admissibility notion is that, given a definite L^1D germ one can define the $\mathcal{G}$-*entropy solutions* and infer their uniqueness. Given a complete L^1D germ, one can establish the well-posedness result and justify convergence of approximate solutions generated by a Godunov finite volume scheme to the weak entropy solution. See [11, 13]. The next definition, also introduced in [14], does not require the use of interface traces

$\gamma^{l,r}\rho(t)$ but is based on the 'adapted Kruzkhov entropies' [16] and a penalization term.

Definition 1.11. $(\mathcal{G}$*-entropy solutions*$)$:
Let $\mathcal{G}$ be L^1D germ. A function $\rho \in \mathbf{L}^\infty(\Omega;\mathbb{R})$ is a $\mathcal{G}$-entropy solution of (1.36) if it admits a Kružhov entropy solution in domains Ω_l and Ω_l it is a weak solution (i.e. the Rankine-Hugoniot condition holds) over the whole domain Ω, and then for a step function,

$$c(x) = c^l \mathbb{1}_{x<0}(x) + c^r \mathbb{1}_{x>0}(x), \text{ s.t. } (c^l, c^r) \in \mathcal{G},$$

the following 'adapted' entropy inequality holds

$$\iint_\Omega \left[|\rho - c(x)|\partial_t\varphi(t,x) + \Phi(k,\rho,c(x))\partial_x\varphi(t,x)\right]dxdt + \int_{\mathbb{R}} |\rho_0(x) - c(x)|\varphi(0,x)dx + \int_0^{+\infty} R_{\mathcal{G}}\big(dist(c^l,c^r),\mathcal{G}\big)\varphi(t,0)dt \geq 0, \tag{1.39}$$

where $R_{\mathcal{G}}$ called a *penalization* remainder term and $dist(\cdot,\cdot)$ is the standard Euclidean distance in $\mathbb{R}^2$.

The definition with (1.39) can be extended to measure-value ($\mathcal{G}$-entropy process) solutions if the solutions of (1.36) are generated by a finite volume approximation scheme possessing only L^∞ bound and compatible entropy inequalities [14]. Indeed, the limit of the finite volume approximation is a $\mathcal{G}-$entropy process solution if an appropriate per cell discrete entropy inequality is obtained in such a way that they 'mimic' a global entropy inequality. However, for the existence of such measure-valued solutions (i.e $\mathcal{G}$-entropy process solution), we need to have established the existence of solution in the framework of $\mathcal{G}$-entropy solution with the additional assumption that $\mathcal{G} = \mathcal{G}^*$.

1.2.4 Measure-valued solutions

As the name suggests, measure-valued solutions is a shift from defining weak solutions as integrable functions to parameterized probability measures, or *Young measures*. A Young measure solution is a function ν that assigns to every point $y \in \mathbb{R}^+ \times \mathbb{R}$ a probability measure ν_y in the probability space over $\mathbb{R}$. When applied to the scalar conservation law (1.7), the generalized problem is to find a Young measure ν_y satisfying the following Cauchy problem:

$$\partial_t\langle\nu_{(x,t)},\rho\rangle + \partial_x\langle\nu_{(x,t)},F(\rho)\rangle = 0, \quad (t,x) \in \mathbb{R}^+ \times \mathbb{R}, \tag{1.40}$$

$$\nu_{(0,x)} = \sigma_0(x), \quad x \in \mathbb{R}, \tag{1.41}$$

where $\langle \nu_{(x,t)}, g(\lambda)\rangle = \int g(\lambda) d\nu_{(x,t)}(\lambda)$ represents the expected value of ν against a continuous function g, σ_0 is a given Young measure on $\mathbb{R}$ and ρ is the unknown density function. Note that we are dealing with weak solutions and so the measure solution that solves (1.40) must be understood in the sense of distributions. We proceed to define measure-valued solutions.

Definition 1.12. *(Measure-valued solution)* A Young measure is a measure-valued solution to (1.40) if the following integral holds:

$$\int_{\mathbb{R}_+}\int_{\mathbb{R}} \partial_t\varphi(t,x)\langle \nu_{(x,t)},\rho\rangle + \partial_x\varphi(t,x)\langle \nu_{(x,t)}, F(\rho)\rangle dxdt + \int_{\mathbb{R}} \varphi(0,x)\langle \sigma_0,\rho\rangle dx = 0, \quad \forall \varphi \in C_c^1(\mathbb{R}_+\times\mathbb{R}).$$

As demonstrated for the case of weak solution, an entropy condition is needed in order to select physically meaningful solutions. This leads to the so-called *entropy measure-valued solutions* which is defined as follows.

Definition 1.13. (*Entropy measure-valued solutions*) A function $\mu \in \mathbf{L}^\infty$ is an entropy measure-valued solution of the problem (1.29) if following integral is satisfied:

$$\begin{aligned}\iint_\Omega \int_0^1 \big(\eta(\mu(x,t,\lambda))\partial_t\varphi(t,x) + \Phi(\mu(x,t,\lambda))\partial_x\varphi(t,x)\big)d\lambda dxdt \\ + \int \eta(\rho_0(x))\varphi(x,0)dx \geq 0, \quad \forall \varphi \in C^1(\mathbb{R}_+\times\mathbb{R}),\end{aligned} \tag{1.42}$$

where convex function $\eta \in C^1$, and $\Phi \in C^1$ a function such that $\Phi' = f'\eta'$.

The characterization of measure-valued solutions can be made as an adaptation of Kruzkhov entropy solution by using the entropy regularization function $\eta(\cdot) = \lambda|\cdot - k|$, $\lambda \in (0,1)$ for all $k \in \mathbb{R}$.

Remark 1.7. In [41], the entropy measure-valued solution is also referred to as *entropy process solutions*.

Definition 1.14. ($\mathcal{G}$-*entropy process solution*): Let $\mathcal{G}$ be an L^1D germ. A function $\mu \in \mathbf{L}^\infty\big(\mathbb{R}_+\times\mathbb{R}\times(0,1);[0,R]\big)$ is called a $\mathcal{G}-$entropy process solution of (1.36) if,

1. (*weak process formulation*):

$$\begin{aligned}\int_{\mathbb{R}}\int_0^{+\infty}\int_0^1 \{\mu(t,x,\lambda)\varphi_t(t,x) + F(x,\mu(x,t,\lambda))\varphi_x(t,x)\}d\lambda dtdx \\ + \int_{\mathbb{R}} \rho_0(x)\varphi(0,x)dx = 0.\end{aligned} \tag{1.43}$$

for all test function $\varphi \in C_c^1(\mathbb{R}_+\times\mathbb{R})$.

2. (*penalized entropy process inequalities*): For all pairs $(c^l, c^r) \in [0,1]^2$, and non-negative test function $\varphi \in \mathcal{D}(\Omega)$

$$\iint_\Omega \int_0^1 \{\mu(t,x,\lambda)\varphi_t(t,x) + \Phi(k,\mu(x,t,\lambda),c(x))\varphi_x(t,x)\}d\lambda dtdx + \int_{\mathbb{R}} |\rho_0(x) - c(x)|\varphi(0,x)dx + \int_0^{+\infty} R_{\mathcal{G}}\left((c^l,c^r)\right)\varphi(t,0) \geq 0, \quad (1.44)$$

where $c(x)$, $R_{\mathcal{G}}\left(dist(a,b),\mathcal{G}\right)$, and Φ are same as given in Definition 1.11.

In general, the convergence result we seek to obtain is based on the notion of nonlinear weak-$\star$ convergence defined [41] and is recapped next.

Definition 1.15. Let Ω be an open subset of $\mathbb{R} \times \mathbb{R}^+$. Given a sequence $\{\rho_n\}_{n\in\mathbb{N}} \subset \mathbf{L}^\infty(\Omega)$, we say that $\{\rho_n\}$ converges towards $\rho \in \mathbf{L}^\infty(\Omega)$ in the "nonlinear weak-$\star$ sense" as $n \to \infty$ if for every test function $\varphi \in L^1(\Omega)$, all $g \in C(\mathbb{R};\mathbb{R})$

$$\int_\Omega g(\rho_n(t,x))\varphi(t,x)dxdt \longrightarrow \int_\Omega \int_0^1 g(\rho(t,x,\lambda))\varphi(t,x)d\lambda dxdt. \quad (1.45)$$

This definition allows for a useful interpretation of convergence of approximate solutions toward a unique Young measure just by relying on the $\mathbf{L}^\infty$ stability bound on the approximate solution by a finite volume method.

Theorem 1.3. *(Convergence of $\mathbf{L}^\infty$ solution [43, Theorem 1.1]) Let Σ be an open subset of $\mathbb{R}$ and $\{\rho_n\}_{n\in\mathbb{N}}$ be a bounded sequence of $\mathbf{L}^\infty$. Then there exists a subsequence of $\{\rho_n\}_{n\in\mathbb{N}}$ still denoted by $\{\rho_n\}_{n\in\mathbb{N}}$, and a function $\rho \in \mathbf{L}^\infty(\Sigma)$ such that the subsequence $\{\rho_n\}_{n\in\mathbb{N}}$ converges towards ρ in the nonlinear weak-$\star$ sense.*

Instead of requiring a strong BV regularity estimate on the approximate solution to establish compactness, a 'weak BV' estimate is only required to prove the convergence of approximate solution in the sense of Definition 1.15. However, it is worth noting that this 'weak BV' estimate does not yield any compactness property for the approximate solution because it is not a necessary condition to have convergence. Applying this method to prove convergence of a scheme, the necessary and sufficient condition is the availability of $\mathbf{L}^\infty-$stability bound on the approximate solution together with the monotonicity of the numerical flux chosen for the scheme.

Chapter 2

Approximation methods for scalar conservation laws

2.1 Introduction

We dedicate this chapter to selected approximation methods used to construct solutions to scalar conservation laws of the Cauchy problem

$$\begin{cases} \partial_t \rho + \partial_x F(k(t,x),\rho) = 0, \ (t,x) \in \mathbb{R}_0^{\pm} \times \mathbb{R}, & \text{(2.1a)} \\ \rho(0,x) = \rho_0(x), \ x \in \mathbb{R}. & \text{(2.1b)} \end{cases}$$

It is standard to approximate solutions to a partial differential equation since for almost all models exact analytical solution may be out of reach. There are numerous approximation methods available to generate numerical solutions, namely, wave front tracking methods, finite volume schemes, finite difference methods and finite element methods. The selection of one method over the other is motivated by physical features of the particular model, the specific properties of solution to be captured and the depth of analysis needed for the study.

For scalar conservation laws, finite volume schemes are highly favored and in some situations wave front tracking methods over finite difference methods since their setup allows one to obtain weak discontinuous solutions. However, each mathematical model needs individual numerical treatment in order to recover their respective physical and analytical features. In the next section, we recall the Finite volume method first for the Cauchy problem with continuous flux function and then in the next section, motivate the selection of an appropriate finite volume method for the discontinuous flux problem of the form that we consider in this work. In the last section, we shall also recall the ideas or tools to be used to prove the convergence of the scheme to weak entropy solutions.

2.2 Finite volume schemes

We begin with finite volume methods for the continuous flux problem

$$\begin{cases} \partial_t \rho + \partial_x F(\rho) = 0, \ (t,x) \in \mathbb{R}_0^{\pm} \times \mathbb{R}, & \text{(2.2a)} \\ \rho(0,x) = \rho_0(x), \ x \in \mathbb{R}. & \text{(2.2b)} \end{cases}$$

To illustrate, the spacial domain is subdivided into smaller intervals or cells over which the conserved quantity is approximated as an average value. Let us first introduce the space step $\Delta x > 0$, and a time step Δt, usually assumed to be constant. We define the mesh interface $x_{j+1/2} = (j+1/2)\Delta x$ for $j \in \mathbb{Z}$ and the times $t^n = n\Delta t$ for $n \in \mathbb{N}$ and set $\nu = \Delta t/\Delta x$. Then the intervals or cells can be denoted $C_j = \left[x_{j-1/2},\ x_{j+1/2}\right)$ with midpoints $x_j = j\Delta x$ for $j \in \mathbb{Z}$. At each time t^n, the goal is to find an approximate solution ρ_j^n of (2.2a) and is written as

$$\rho_j^n = \frac{1}{\Delta x} \int_{x_{j-1/2}}^{x_{j+1/2}} \rho(t^n, x)dx, \ j \in \mathbb{Z}, n \in \mathbb{N}. \tag{2.3}$$

Indeed over each C_j, conservation of mass implies that

$$\frac{d}{dt} \int_{C_j} \rho(t,x)dx = F(\rho(t, x_{j-1/2})) - F(\rho(t, x_{j+1/2})), \text{ for all } t \geq 0.$$

If this relation is integrated from t^n to t^{n+1} and divided through by Δx, we obtain the difference formula:

$$\rho_j^{n+1} = \rho_j^n - \frac{\Delta t}{\Delta x} \left(F_{j+\frac{1}{2}}^n - F_{j-\frac{1}{2}}^n, \right) \tag{2.4}$$

where

$$F_{j\pm 1/2}^n = \frac{1}{\Delta t} \int_{t^n}^{t^{n+1}} F\left(\rho(t, x_{j\pm 1/2})\right) dt, \tag{2.5}$$

is the representation of the flux function and often (and herein) referred to as the numerical flux at point $x_{j\pm 1/2}$ and time $t^n = n\Delta t$. One can immediately observe that the integrand of the numerical is also a function of the unknown function $\rho(t,x)$. This motivates some additional approximation strategies to determine the numerical flux, leading to different Finite volume schemes. A common finite volume scheme known to approximate the weak entropy solutions is the Godunov scheme [50]. We recall the Godunov scheme in the next sub section.

2.2.1 The Godunov scheme

In this section, we recall the Godunov scheme for the Cauchy problem (2.2). One reason why the Godunov scheme is popular is because the numerical flux is chosen based on the exact solution of a local Riemann problem at each interface. It is well-known that the Godunov's scheme consists in two main steps namely: (1) time evolution of a local Riemann problem at each interface at t^n and (2) projection of the piecewise constant solution on each cell at t^{n+1}. We briefly present these below:

Step 1:
For $n \geq 0$, let ρ_j^n be defined by (2.3). At each $x_{j+1/2}$, one solves the local Riemann problem

$$\begin{cases} q_t + F(q)_x = 0, (t,x) \in C_j, \\ q(t^n, x) = \begin{cases} \rho_j^n, & \text{if } x < x_{j+1/2}, \\ \rho_{j+1}^n, & \text{if } x \geq x_{j+1/2}, \end{cases} \end{cases} \tag{2.6}$$

for small $t > t^n$ to obtain the self-similar solution written as

$$q_j(t,x) = q\left(\frac{x - x_{j+1/2}}{t - t^n}; \rho_j^n, \rho_{j+1}^n\right), \text{ for all } (t,x) \in (t^n, t^{n+1}) \times C_j.$$

Since the self-similar solutions are also elementary waves, Δt needs to be chosen so that waves from neighboring cells do not interact at each time step. This means that Δt must satisfy

$$\max_{j \in \mathbb{Z}} \left| F'(\rho_j^n) \right| \frac{\Delta t}{\Delta x} \leq \frac{1}{2}. \tag{2.7}$$

Step 2:
In this step, the new values ρ_j^{n+1} are computed from by the update formula:

$$\rho_j^{n+1} = \frac{1}{\Delta x} \int_{C_j} q(t^{n+1}, x) dx, \quad j \in \mathbb{Z}.$$

This choice of formula is consistent with the conservation of mass in the control volume $[t^n, t^{n+1}) \times C_j$ as demonstrated below by applying the Green's theorem:

$$\begin{aligned} 0 &= \int_{t^n}^{t^{n+1}} \int_{C_j} q_t + F(q)_x dx dt \\ &= \Delta x \rho_j^{n+1} - \Delta x \rho_j^n + \int_{t^n}^{t^{n+1}} F(q(0^-; \rho_j^n, \rho_{j+1}^n)) dt - \int_{t^n}^{t^{n+1}} F(q(0^+; \rho_j^n, \rho_{j+1}^n)) dt, \end{aligned}$$

where $q(0^{\pm};\rho_j^n,\rho_{j+1}^n)$ represents the traces of the Riemann solutions at the interface. This allows the numerical flux for the Godunov's scheme to be written as:

$$F_{j\pm1/2}^n = F(q(0^{\pm};\rho_j^n,\rho_{j+1}^n)), \quad \text{for all } j\in\mathbb{Z},\ n\geq 0. \tag{2.8}$$

It will be convenient to denote the numerical flux by

$$h_{j\pm1/2}^n(\rho_j,\rho_{j+1}) = F(q(0^{\pm};\rho_j^n,\rho_{j+1}^n)).$$

Since the arguments of the numerical flux are the exact solution of the Riemann problem (2.6), it can be shown in a lengthy and case-by-case study that the numerical flux (2.8) becomes:

$$h(a,b) = \begin{cases} \min\limits_{q\in[a,b]} F(q), & \text{if} \quad a<b, \\ \max\limits_{q\in[b,a]} F(q), & \text{if} \quad b\leq a. \end{cases} \tag{2.9}$$

See [67, 54] for detailed presentation.

Remark 2.1. The numerical flux in (2.9) holds for both convex and concave flux. In fact, it is valid for any Lipschitz continuous F.

Therefore with (2.9), the classical Godunov scheme can be expressed in conservative form as

$$\rho_j^{n+1} = \rho_j^n - \frac{\Delta t}{\Delta x}\left(h(\rho_j^n,\rho_{j+1}^n) - h(\rho_{j-1}^n,\rho_j^n)\right). \tag{2.10}$$

Remark 2.2. A key observation in the Godunov scheme is that at the projection step, the traces of the local traces at 0^- and 0^+ obtained from the previous time say t^n, are projected unto the same interface $x_{j+1/2}$ at t^{n+1} via the update formula above. That is the $x_{j+1/2}$ remains unchanged in time and the Rankine-Hugoniot jump condition

$$f(q(0^-;\rho_j^n,\rho_{j+1}^n)) = f(q(0^+;\rho_j^n,\rho_{j+1}^n)), \tag{2.11}$$

holds for all $j\in\mathbb{Z}$ and $n\in\mathbb{N}$ which also ensure mass conservation.

2.3 Finite volume method for discontinuous flux

For a conservation law with smooth function, we have shown how to construct a finite volume scheme to approximate the entropy weak solution. With inspiration from the previous section, we recall the finite volume scheme for the equation (2.1a) in this section. Recall that the Godunov flux uses the explicit solution of

the Riemann problem at each cell interface. The major challenge in adapting a straightforward approach for equations of the form (2.1a) is the presence of additional jump in the flux. Away from the jump, the solution satisfy classical entropy conditions and so the Godunov flux (2.9) holds but may fail to compute the non-classical waves due to the flux interface. Consequentially, the numerical version of the Rankine-Hugoniot jump condition (2.11) at the flux interface would be violated. For this reason, the Godunov numerical flux is modified to accommodate the new Riemann problem arising at the flux interface. Compare [2, 10, 11, 13, 73, 60, 24, 87].
Using the discretization notations of the previous section, the conservative form of the numerical scheme for the equation (2.1a) is

$$\rho_j^{n+1} = \rho_j^n - \frac{\Delta t}{\Delta x}\left(F(k_{j+1/2}^n, \rho_j^n, \rho_{j+1}^n) - F(k_{j-1/2}^n, \rho_{j-1}^n, \rho_j^n)\right), \tag{2.12}$$

where $k_{j+1/2}^n$ is a discretization of the flux coefficient. Since the k is time dependent, some of the cell interface points shall be non-vertical and so an intermediate step are required in most cases before choosing a numerical flux. Finite volume methods for equation (2.1a), how to approximate the flux coefficient is as important as how the numerical flux itself is approximated. Along this line, two main types of numerical schemes emerges from the literature depending on how the flux coefficient is discretized in (2.12), namely: (1) aligned and (2) staggered schemes [73].

2.3.1 Aligned schemes

The central idea in aligned schemes is that the discretization of the unknown, ρ and discontinuous coefficient k in the prescription of the numerical flux are exactly aligned. This alignment is done in the following sense:

$$F(k_{j+1/2}^n, \rho_j^n, \rho_{j+1}^n) = F(k_j^n, \rho_j^n, k_{j+1}^n, \rho_{j+1}^n),$$

where $F(k, \rho, k, \rho) = f(k, \rho)$ satisfy the consistency principle defined earlier and the flux coefficient k is discretized over $C_j = \left[x_{j-1/2}, x_{j+1/2}\right)$

$$k_j^n = \frac{1}{\Delta x}\int_{x_{j-1/2}}^{x_{j+1/2}} k(t^n, x)dx.$$

The numerical flux function F above is usually determined by solving the problem (1.31) with local Riemann data

$$(\rho(0,x),k(0,x)) = \begin{cases} (\rho_l,k_l), & \text{if } x < x_{j+1/2}, \\ (\rho_r,k_r), & \text{if } x > x_{j+1/2}. \end{cases} \tag{2.13}$$

This leads to a Godunov type numerical scheme capable of handling the interface flux conditions, the so-called AB-entropy condition [3, 2].

2.3.2 Staggered schemes

In these types of finite volume scheme, the discretization of the flux coefficient writes

$$k^n_{j+1/2} = \frac{1}{\Delta x}\int_{x_j}^{x_{j+1}} k(t^n,x)dx. \tag{2.14}$$

This implies that the boundaries of the centers of the control volume is actually the boundary of the cell used to discretize the flux coefficient and hence the discretization is *staggered* with respect to that of the ρ^n_j. That is the numerical flux with (2.14) is determined by a local Riemann solver with associated data

$$\rho(0,x) = \begin{cases} \rho^n_j, & \text{if } x < x_{j+1/2}, \\ \rho^n_{j+1}, & \text{if } x > x_{j+1/2}. \end{cases}$$

The main advantage of the staggered schemes is the reduction in complexity as compared to the aligned schemes and ease of implementation. An example of finite volume schemes of this nature has been prescribed in [87, 86, 59].

2.3.3 Approximation of non classical shocks

Small-scale dependent shock waves are fundamental to conservation laws with discontinuous flux. As discussed in section the previous chapter, the problem we consider in this work admits non-classical shocks and therefore in deriving a numerical scheme to approximate the solutions, the non classical behaviour needs to be included. In this section, we briefly recall some of the methods applied to capture classical shocks in the conservation laws.

A moving mesh algorithm

In [93], Zhong, Hou and LeFloch introduced a numerical method for conservation laws capable of computing the dynamic phase boundaries transition in an

exact way. Their strategy leads to a front-tracking that tracks phase boundaries and a shock capturing scheme to capture conventional shocks. They introduced an intermediate step in the Godunov scheme in which exact position of the non stationary phase boundary with speed V^n is computed exactly and then the grid mesh is shifted according to the movement of the phase boundary. To implement the ideas, they used the following algorithm:

1. Compute the speed of propagation of the phase boundary.
2. Shift grid points according to: $x_{j+1/2}^{n+1} = x_{j+1/2}^{n} + V^n \Delta t, \ \forall j$.
3. Compute ρ_j^{n+1}.
4. Repeat steps 1-4.

2.4 A finite volume approach to prove existence

For scalar conservation law, it can be recalled from Section 1.1.3 that the regularization of entropy solutions are based on a the 'regularized' scalar equation (1.13) with a fixed parameter $\varepsilon > 0$, which are studied in the limit as $\varepsilon \to 0$. In this sense, $\{\rho^\varepsilon\}_{\varepsilon>0}$ is considered as a sequence of approximate solutions that can be constructed an approximation scheme like vanishing viscosity method, wave front tracking and finite difference/volume numerical methods. With the availability of corresponding norm estimates, one can then show that these approximate solutions converge to the weak entropy solution as $\varepsilon \to 0$. In most cases, this is equivalent to establishing that the set $\{\rho^\varepsilon\}_{\varepsilon>0}$ is compact, guaranteeing the existence of a subsequence denoted $\{\rho^{\varepsilon_k}\}_{k=1}^{\infty}$ that converges to the weak entropy solution $\rho(t,x)$ as $k \to \infty$. This is referred to as the compactness argument that leads to global entropy solutions and plays a very important role in the study of conservation laws.

However, since most scalar conservation laws with discontinuous flux functions are resonant systems, such bounds on the solution are not readily available making it impossible to establish a compactness arguments for this class of equations. To subvert this problem, alternative methods are sought in order to prove that approximate solutions converges to the entropy solutions so defined. In this section, we describe the alternative approach dubbed entropy process solutions [41], which are essentially measure-valued solutions, introduced by DiPerna in his seminal paper [37].

In order to study the convergence of the scheme to the exact weak entropy solution, it is convenient to introduce the *generic form* of the scheme, the so-called

$2k+1$ point one step (in time) form of the scheme where $k \in \mathbb{N}^*$, written as

$$\rho_j^{n+1} = H\left(\rho_{j-k}^n, \ldots, \rho_{j+k}^n\right), \quad \forall n \geq 0,\ j \in \mathbb{Z}, \tag{2.15}$$

where $H : \mathbb{R}^{2k+1} \to \mathbb{R}$ is a continuous function and ρ_j^n denotes the approximate solution in the cell $C_j = [x_{j-1/2}, x_{j+1/2})$. The set of points $\{\rho_{j-k}^n, \ldots, \rho_{j+k}^n\}$ is referred to as the *stencil* of the scheme and H the *update* function depending on $2k+1$ stencils. The generic form of a numerical scheme makes it easy to deduce some essential features of the scheme that lead to convergence. Since we are studying scalar conservation laws, its natural to deduce whether or not the scheme also satisfies the conservation principle. The discrete version of conservation principle states

$$\sum_{j\in\mathbb{Z}} \rho_j^{n+1} = \sum_{j\in\mathbb{Z}} \rho_j^n, \quad \forall n \geq 0, \tag{2.16}$$

if boundary conditions are ignored. We can deduce that the scheme (2.15) is conservative thanks to the next lemma.

Lemma 2.1. *Assume that $H(0,\ldots,0) = 0$. The numerical scheme (2.15) is conservative if and only if there exist a function $F_{j+1/2}^n = h(\rho_{j-k+1}^n, \ldots, \rho_{j+k}^n)$ such that (2.4) can be written in the conservative form*

$$\rho_j^{n+1} = \rho_j^n - \frac{\Delta t}{\Delta x}\left[h(\rho_{j-k+1}^n, \ldots, \rho_{j+k}^n) - h(\rho_{j-k}^n, \ldots, \rho_{j+k-1}^n)\right]. \tag{2.17}$$

The proof is classical and can be found for example in [67, 49]. Indeed if (2.15) can be written as (2.4), then the conservation property (2.16) follows immediately by using a telescoping sum and cancellation. The sufficiency comes from that $H(0,\ldots,0) = 0$, implies that a continuous function

$$G(\rho_{-k}^n, \ldots, \rho_k^n) := \frac{\Delta x}{\Delta t}\left(\rho_0^n - H(\rho_{-k}^n, \ldots, \rho_k^n)\right)$$

can be defined such that $\sum_{j\in\mathbb{Z}} G\left(\rho_{j-k}^n, \ldots, \rho_{j+k}^n\right) = 0$ using the discrete conservation. There exist therefore $F_{j+1/2}^n = h(\rho_{j-k+1}^n, \ldots, \rho_{j+k}^n)$ such that $F_{j+1/2}^n - F_{j-1/2}^n = G\left(\rho_{j-k}^n, \ldots, \rho_{j+k}^n\right)$.

For the problem considered in this work, it is enough to set $k = 1$. Another important feature of the scheme is consistency,

Definition 2.1. A finite volume scheme is consistent with a scalar conservation law if

$$h(\rho, \rho) = f(\rho). \tag{2.18}$$

Consistency is a natural requirement which ensures that the scheme approximates the correct conservation law.

Remark 2.3. Note that the definition of conservation need to be modified when considering boundary conditions of the problem under consideration.

Remark 2.4. For finite volumes used to approximate a conservation law with discontinuous flux the consistency requirement must be in accordance with the type of scheme, whether *staggered* or *aligned* scheme.

Not all numerical schemes that are conservative and consistent schemes converge to the weak entropy solution. For example, the so-called central schemes and Roe schemes are consistent and conservative but do not converge. This motivates the following definition of monotonicity:

Definition 2.2. A numerical scheme is monotone if H is non-decreasing in each of its arguments.

For a 3-point scheme ($k = 1$), the sufficient condition is,

Lemma 2.2. *($\mathbf{L}^\infty-$bound stability) Consider the conservative and consistent scheme with a locally Lipschitz flux $h(a, b)$. Then the scheme is monotone if and only if,*

$$a \mapsto h(a, b) \text{ is non-decreasing for any fixed } b,$$
$$b \mapsto h(a, b) \text{ is non-decreasing for any fixed } a,$$

and satisfies the CFL-type condition

$$\left|\frac{\partial h}{\partial a}(v, w)\right| + \left|\frac{\partial h}{\partial b}(u, v)\right| \leq \frac{\Delta x}{\Delta t}, \quad \forall u, v, w. \tag{2.19}$$

Combining these conditions leads to a class of finite volume schemes that satisfy all these three important requirements. In [41], this class of schemes is referred to as "Monotone flux schemes" which is collected in the next definition.

Definition 2.3. Under a CLF condition, a finite volume scheme is said to be a " monotone flux scheme" if $k = 1$ and if the numerical flux satisfies,

- $h : \mathbb{R}^2 \to \mathbb{R}$ is locally Lipschitz.
- consistency flux: $h(\rho, \rho) = f(\rho)$ for all $\rho \in [\rho_{\min}, \rho_{\max}]$.

- $(a,b) \mapsto h(a,b)$ is non-decreasing w.r.t. a and non-increasing w.r.t. b.

The monotone flux schemes are useful to consider particularly for problems where no strong BV estimates are readily available or difficult to obtain. Convergence of such schemes follows only with the $\mathbf{L}^\infty-$bound and discrete entropy inequalities which are easy to obtain. Then passing to the limit as $\Delta t, \Delta x \to 0$, can be achieved using the so-called "weak BV" estimate. We derive this estimate for a general monotone flux in the next lemma.

Lemma 2.3. *(Weak BV estimate) Assume that ρ_j^n for all $j \in \mathbb{Z}, n \in \mathbb{N}$ is the approximate solution of (3.1) defined by the scheme (2.10) with the CFL condition (2.7) and a flux satisfying (2.3). Then, for all $T > 0$, there exists $C > 0$ such that*

$$\sum_{n\in\mathbb{N}, n\Delta t<T} \sum_{j\in\mathbb{Z}} \left| h(\rho_j^n, \rho_{j+1}^n) - h(\rho_{j-1}^n, \rho_j^n) \right| \leq C/\sqrt{\Delta x}. \tag{2.20}$$

Proof. Multiply (2.10) by $\Delta t \rho_j^n$ and sum over n, j to obtain $A + B = 0$, where

$$A = \sum_{n=0}^{N} \sum_{j=J_0}^{J_1} \Delta x \rho_j^n (\rho^{n+1} - \rho_j^n)$$

and

$$B = \sum_{n=0}^{N} \Delta t \sum_{j=J_0}^{J_1} \left[h(\rho_j^n, \rho_{j+1}^n) - h(\rho_{j-1}^n, \rho_j^n) \right] \rho_j^n$$

The term A, by the same algebraic rearrangements from [41], re-writes as

$$\begin{aligned} A &= -\frac{1}{2} \sum_{n=0}^{N} \sum_{j=J_0}^{J_1} \Delta x (\rho^{n+1} - \rho_j^n)^2 + \frac{\Delta x}{2} \left[\sum_{j=J_0}^{J_1} (\rho_j^{N+1})^2 - \sum_{j=J_0}^{J_1} (\rho_j^0)^2 \right] \\ &\geq -\frac{C_1}{2} \sum_{n=0}^{N} \Delta t \sum_{j=J_0}^{J_1} \left[h(\rho_j^n, \rho_{j+1}^n) - h(\rho_{j-1}^n, \rho_j^n) \right]^2 - \frac{\|\rho^0\|_\infty}{2} \int_I \rho_0 dx, \end{aligned}$$

where C_1 is chosen to satisfy the CLF condition (4.14). For the B term, we have

$$\begin{aligned} B = B_1 + B_2 = &\sum_{n=0}^{N} \Delta t \sum_{j=J_0}^{J_1} \left[h(\rho_j^n, \rho_{j+1}^n) - h(\rho_j^n, \rho_j^n) \right] \rho_j^n \\ &+ \sum_{n=0}^{N} \Delta t \sum_{j=J_0}^{J_1} \left[h(\rho_j^n, \rho_j^n) - h(\rho_{j-1}^n, \rho_j^n) \right] \rho_j^n. \end{aligned}$$

Let's introduce a function $\phi(a) = \int_0^a s\partial_a h(s,b)ds$, for any $a \in \mathbb{R}$ if b is fixed. Then it can be deduced that

$$\phi(b) - \phi(a) = b\left[f(b) - h(a,b)\right] - a\left[f(a) - h(a,b)\right] - \int_a^b \left[f(s) - h(a,b)\right] ds. \quad (2.21)$$

An application of Lemma 18.5 of [41] to $s \mapsto h(s,b) + h(a,b)$ in the above equation leads to

$$\int_a^b \left[g(s,b) - g(a,b)\right] \geq \frac{1}{2\mathbf{L}_h^1}\left(h(b,b) + h(a,b)\right)^2, \ \forall (a,b),$$

where $\mathbf{L}_h^1$ is the Lipschitz constant of h w.r.t. the first variable. If we set $a = \rho_{j-1}^n, b = \rho_j^n$, the B_2 term gives

$$\begin{aligned} B_2 &\geq \frac{\Delta t}{2L_h^1} \sum_{n=0}^{N} \sum_{j=J_0}^{J_1} \left[f(\rho_j^n) - h(\rho_{j-1}^n, \rho_j^n)\right]^2 - \Delta t \sum_{n=0}^{N} \sum_{j=J_0}^{J_1} \left[\phi(\rho_j^n) - \rho_{j-1}^n\right] \\ &= \frac{\Delta t}{2L_h^1} \sum_{n=0}^{N} \sum_{j=J_0}^{J_1} \left[f(\rho_j^n) - h(\rho_{j-1}^n, \rho_j^n)\right]^2 - \Delta t \sum_{n=0}^{N} \left[\phi(\rho_{J_1}^n) - \phi(\rho_{J_0-1}^n)\right] \\ &\geq \frac{\Delta t}{2L_h^1} \sum_{n=0}^{N} \sum_{j=J_0}^{J_1} \left[f(\rho_j^n) - h(\rho_{j-1}^n, \rho_j^n)\right]^2 - C_2 \cdot N, \quad C_2 > 0. \end{aligned}$$

Similarly, defining the function $\phi(a) = -\int_0^a s\partial_b h(b,s)ds$, and proceeding as earlier leads to

$$\begin{aligned} B_1 &\geq \frac{\Delta t}{2\mathbf{L}_h^2} \sum_{n=0}^{N} \sum_{j=J_0}^{J_1} \left[f(\rho_j^n) - h(\rho_j^n, \rho_{j+1}^n)\right]^2 - \Delta t \sum_{n} \left[\phi(\rho_{J_1+1}^n - \rho_{J_0}^n\right] \\ &\geq \frac{\Delta t}{2\mathbf{L}_h^2} \sum_{n=0}^{N} \sum_{j=J_0}^{J_1} \left[f(\rho_j^n) - h(\rho_j^n, \rho_{j+1}^n)\right]^2 - C_3 \cdot N, \quad C_3 > 0. \end{aligned}$$

This implies that there exists $C_4, C_5 > 0$ independent of $n, j, \Delta t, \Delta x$, such that

$$B_1 + B_2 \geq C_4 \Delta t \sum_{n=0}^{N} \sum_{j=J_0}^{J_1} \left[h(\rho_j^n, \rho_{j+1}^n) - h(\rho_{j-1}^n, \rho_j^n)\right]^2 + \mathcal{O}(T).$$

Now,

$$0 = A + B \geq \left(C_4 - \frac{C_2}{2}\right) \Delta t \sum_{n=0}^{N} \sum_{j=J_0}^{J_1} \left[h(\rho_j^n, \rho_{j+1}^n) - h(\rho_{j-1}^n, \rho_j^n)\right]^2 - \frac{\left\|\rho^0\right\|_\infty}{2} \int_I \rho_0 dx + \mathcal{O}(T).$$

This also implies that if $\widetilde{C} = C_4 - \frac{C_2}{2}$, then

$$\widetilde{C} \Delta t \sum_{n=0}^{N} \sum_{j=J_0}^{J_1} \left[h(\rho_j^n, \rho_{j+1}^n) - h(\rho_{j-1}^n, \rho_j^n)\right]^2 \leq \frac{\left\|\rho^0\right\|_\infty}{2} \int_I \rho_0 dx,$$

which gives the existence of a constant $\widetilde{C}_1 > 0$, only depending on ρ_0, Δt, T, and the flux h such that

$$\sum_{n=0}^{N} \sum_{j=J_0}^{J_1} \Delta t \left[h(\rho_j^n, \rho_{j+1}^n) - h(\rho_{j-1}^n, \rho_j^n)\right]^2 \leq \widetilde{C}_1.$$

Now, applying the Cauchy-Schwartz inequality further we have

$$\sum_{n=0}^{N} \sum_{j=J_0}^{J_1} \Delta t \left|h(\rho_j^n, \rho_{j+1}^n) - h(\rho_{j-1}^n, \rho_j^n)\right| \leq \sqrt{\widetilde{C}_1 \sum_{j=J_0}^{J_1} \sum_{n=0}^{N} \Delta t} \tag{2.22}$$

from which (2.20) can be deduced by noting that $T = \sum_{n=0}^{N} \Delta t$, and $\sum_{j=J_0}^{J_1} j \leq \frac{4R}{\nu \Delta x}$, where $R > 0$ and $\nu \in (0, 1)$ completing the proof. □

Chapter 3

An existence result for conservation law with discontinuous flux

3.1 Introduction

In this and the following chapters, we present the main results of this thesis which concerns a scalar conservation law with discontinuous coefficients consisting of a sign (switch) function in both space and time variables. Though the equation we consider here has some inspirations from the Hughes' model [57] of pedestrian flow, it is not exactly similar to it. The Hughes' model is a conservation law strongly coupled to an eikonal equation whose viscous solution leads to the appearance of the so-called *turning curve* function, which is interpreted as the point at which pedestrians are bound to alter their speed so as to reach the boundary (or exit) as fast as possible. See the introduction sections of this thesis for more details. The existence of solutions together with numerical approximations of the Hughes' model has been studied by several authors. See [5, 48, 40, 7, 34]. Granted that the time-dependent flux discontinuity in our equation is also referred to as the turning curve and is also assumed to be Lipschitz continuous, ours has the simplification that the curve is given *a priori*. Put simply, the turning curve does not need to satisfy the non-local integral identity.

Scalar conservation law with discontinuous flux has received lots of attention by several authors due its extensive applications. See the following partial list and references therein [2, 14, 21, 3, 73, 45, 24, 22, 59, 58, 60, 75, 86, 87, 88] for well-posedness results of these equations. However, almost all these studies are focused on space dependent discontinuous coefficient problems out of which only a selected few even allows for a change in sign of the coefficients for simplicity. See [75, 21, 59, 27, 88] for time dependent problems with [59] using the hypothesis that the coefficients may change sign even in time.

The classical approach to a well-posedness result is to approximate the solution and prove convergence of the approximate scheme using a compactness argument. The shortage of well-posedness results for space-time dependent problems can be attributed to lack of a straightforward compactness argument needed to prove convergence of approximate solution to the weak entropy solution. In [59] and [88] the authors used the compensated compactness and one-sided Lipschitz continuity methods respectively both of which did not require a bound on total variation to prove convergence with $\mathbf{L}^\infty$ data. The problem we consider in this work also suffers from a similar severity. We begin this chapter by studying the weak entropy solution of the Cauchy problem in this section, construct entropy solutions for the Riemann problem at the interface ξ in Section 3.1.3, analyse the changes in time of total variation when the slope of the interface function changes and when it is likely to interact with classical waves in 3.2. In order to prove the convergence of a Godunov-type scheme, we explore the tool of admissibility germs [14] and derive some of their useful properties in Section 3.4. In the final part of this chapter, we state the uniqueness and stability result for our problem.

3.1.1 The Cauchy problem

Consider the initial value problem of the form:

$$\partial_t \rho + \partial_x F(t,x,\rho) = 0, \quad (t,x) \in \Omega = (0,+\infty) \times (-\infty,+\infty), \tag{3.1a}$$

$$\rho(0,x) = \rho_0(x), \quad x \in \mathbb{R}, \tag{3.1b}$$

where,

- $t \in \mathbb{R}^+$ and $x \in \mathbb{R}$ are the usual time and space variable, $(t,x) \mapsto \rho(t,x)$ is the unknown density function, $\rho \in \mathbf{L}^\infty(\Omega;[0,R])$;
- the flux function is

  $$(t,x,\rho) \mapsto F(t,x,\rho) := \text{sign}(x-\xi(t))f(\rho)$$

  where
  - $\rho \mapsto f(\rho)$ is a bell-shaped (uni-modal) function, $f \in \mathbf{Lip}([0,R];\mathbb{R}^+)$. Here we will consider the special case $f(\rho) = \rho v(\rho)$, where $v(\rho)$ is a non-increasing function, but in general f could be any function satisfying the following condition:

    $$\begin{cases} f \in \mathbf{Lip}([0,R];\mathbb{R}^+), \text{ with } \|f'\|_\infty \leq L\,,\ f(0) = 0 = f(R); \\ \exists\, \bar{\rho} \in]0,R[\text{ such that } f'(\rho)\ (\bar{\rho} - \rho) > 0 \text{ for a.e. } \rho \in [0,R]; \end{cases} \tag{3.2}$$

– ξ is here referred to as the *turning curve* such that

$$\xi : \mathbb{R}^+ \to \Omega \text{ is Lipschitz continuous,} \qquad \xi(t) \to 0 \text{ as } t \to \infty. \tag{3.3}$$

Recall from the discussions of Chapter 1 that classical (or smooth) solutions of scalar conservation laws breaks down even with smooth initial data and/or flux function for which reason weak solutions are sought. Without additional entropy conditions, these weak solutions are not unique. If the flux contains a discontinuity, like the equation considered in this work, there are additional issues like the loss of strict hyperbolicity. This severity becomes complicated if the discontinuity in the flux is also time-dependent. Worse yet if the discontinuous coefficient changes sign as is the case of the problem considered in this work.

To simplify the presentation, if (3.1a) is written as hyperbolic partial differential equation with discontinuous space-time discontinuous flux function

$$\begin{cases} \partial_t \rho + \partial_x (k(t,x) f(\rho)) = 0, \\ k(t,x) = \text{sign}(x - \xi(t)), \end{cases} \tag{3.4}$$

it is immediately clear that k has the effect of changing the shape of the continuous flux function, f at every $t \in \mathbb{R}^+$. This is also due to the presence of the turning curve that divides Ω into two sub domains $\Omega_l := \{(t,x) : x < \xi(t)\}$ and $\Omega_r := \{(t,x) : x > \xi(t)\}$ each with its corresponding conservation equation

$$\begin{aligned} \partial_t \rho - \partial_x f(\rho) = 0, \quad (t,x) \in \Omega_l, \\ \partial_t \rho + \partial_x f(\rho) = 0, \quad (t,x) \in \Omega_r. \end{aligned}$$

The following assumptions are made on $t \mapsto \xi(t)$:

S1: Piecewise Lipschitz continuous on $[0, +\infty)$ with constant L_ξ defined:

$$L_\xi = \sup_{0 \le t_1 < t_2} \left| \frac{\xi(t_1) - \xi(t_2)}{t_1 - t_2} \right| < \infty$$

for any $t_1, t_2 \in [0, \infty)$.

3.1.2 The entropy weak solution

In this section, we characterize the solution of the Cauchy problem (3.1) with an $\mathbf{L}^\infty-$data. Following the general entropy inequality of [59], the entropy weak solution of the Cauchy problem (3.1) should be understood in the following sense also used in [7]:

Definition 3.1. A weak solution $(t,x) \mapsto \rho(t,x)$ is an entropy solution to the Cauchy problem (3.1), if ρ is in $\mathbf{L}^{\infty}\left([0,+\infty[;\ \mathbf{L}^{\mathbf{1}}\left(\Omega;\ [0,R]\right)\right)$ and for any $c \in [0,R]$, and any test function $\varphi \in \mathbf{C}_{\mathbf{c}}^{\infty}\left(\mathbb{R}^2;\ [0,+\infty[\right)$, the following Kružkov-type entropy inequality holds:

$$\int\int_{\Omega}\left(|\rho-c|\partial_t\varphi+\mathcal{F}(t,x,\rho,c)\partial_x\varphi\right)dxdt-\int\int_{\Omega\setminus\xi}\operatorname{sign}(\rho-c)F(t,x,c)_x\varphi dxdt$$
$$+\int_{\mathbb{R}}|\rho_0(x)-c|\varphi(0,x)\mathrm{d}x+2\int_0^{+\infty}f(c)\varphi(t,\xi(t))dt\geq 0, \tag{3.5}$$

where $\mathcal{F}(t,x,\rho,c)=\operatorname{sign}(\rho-c)\left[F(t,x,\rho)-F(t,x,c)\right]$.

The first line and the first terms of the second line are the Kružkov definition of entropy weak solution of a Cauchy problem, [63] whereas the second term of the second line are due to the contribution of the non stationary jump at $x=\xi(t)$. As will be shown in section 3.3, this condition satisfy the interior condition and the Rankine-Hugoniot jump condition of lemma (3.1).

Remark 3.1. By choosing $c=0$ and $c=R$, in (3.5), we recover the integral formulation of the weak solution

$$\iint_{\Omega}\left(\rho\partial_t\varphi+F(k(t,x),\rho)\partial_x\varphi\right)dtdx+\int_{-\infty}^{\infty}\varphi(0,x)\rho_0(x)dx=0.$$

Remark 3.2. This integral can also be interpreted that ρ admits the Kružkov entropy conditions away from the discontinuity, ξ and an additional interface flux condition in order to 'connect' the left and right states or traces, the so-called *interior conditions* [73].

Remark 3.3. By the assumption **(S1)**, there exist traces of ρ, denoted $\gamma^l\rho(t),\gamma^r\rho(t)$. Since the flux function f is non-linearly degeneracy these traces are indeed strong traces, thanks to the result of Panov [76] and Vasseur [90].

The next lemma yields the condition across $\xi(t)$ that need to be satisfied for the entropy solution defined above.

Lemma 3.1. *Assume **(S1)**. Let ρ be a weak solution of the Cauchy problem (3.1) containing a jump at $x=\xi(t)$ and admits the left and right traces $\gamma^l\rho(t),\gamma^r\rho(t)$, then the following jump condition holds a.e $t>0$*

$$f(\gamma^r\rho(t))+f(\gamma^l\rho(t))=\alpha\left[\gamma^r\rho(t)-\gamma^l\rho(t)\right], \tag{3.6}$$

where α is the slope of $\xi(t)$.

3.1.3 The Riemann problem

We devote this section, for the Riemann problem, which is the Cauchy problem (3.1) coupled with the initial data

$$\rho_0(x) = \begin{cases} \rho_L, & \text{if } x < 0, \\ \rho_R, & \text{if } x > 0. \end{cases} \tag{3.7}$$

The interior condition, see remark 3.2 implies that the solution shall admit the Lax admissible criterion, where downward jumps are admissible shocks on Ω_l whereas on Ω_r admissible shocks are upward jumps to select the unique entropy solution. Furthermore, the presence of $\xi(t)$ shall introduces non-classical waves which need to be explicitly defined. The following notations are used to represent the Riemann solvers:

- $\mathcal{R}^{\alpha}(\rho_L, \rho_R)(t, x)$, for the non standard Riemann solver at the turning point;
- $\mathcal{R}^{\pm}(\rho_L, \rho_R)(t, x)$, for the classical Standard Riemann solver (SRS) by Lax with $\pm f$ depending on which side of the discontinuity the solution is provided.

We will define Riemann solvers which are self-similar, and hence we shall write $\mathcal{R}^{\alpha}(\rho_L, \rho_R)(x/t)$, $\mathcal{R}^{\pm}(\rho_L, \rho_R)(x/t)$ instead of $\mathcal{R}^{\alpha}(\rho_L, \rho_R)(t, x)$, $\mathcal{R}^{\pm}(\rho_L, \rho_R)(t, x)$ respectively. Our construction of the Riemann solvers can be distinguished into two main cases of $\alpha = 0$ or $\alpha \neq 0$.

Case $\alpha = 0$***:*** Here $\xi(t) = 0$, $\forall t \geq 0$, and so the Riemann problem is standard. That is for any couple $(\rho_L, \rho_R) \in [0, R]^2$ in (3.7), the solution takes the form

$$\mathcal{R}^{\alpha}(\rho_L, \rho_R)(x/t) = \begin{cases} \mathcal{R}^{-}(\rho_L, 0)(x/t), & \text{for } x/t < 0, \\ \mathcal{R}^{+}(0, \rho_R)(x/t), & \text{for } x/t > 0. \end{cases} \tag{3.8}$$

If $(\rho_L, \rho_R) \in [0, R)$, the solution actually experiences a non-classical undercompressive shock at $x = 0$ joining vacuum states. This means that the solution is continuous but characteristics emanate from the vertical line $\xi(t) = 0$ from both sides and $\gamma_l(\rho) = \gamma_r(\rho) = 0$. Furthermore, if ρ_L or $\rho_R = R$, then the solution has the same structure, but the discontinuity at $x(t) = 0$ is only a one-side undercompressive wave. In the special case $\rho_L = \rho_R = R$ the solution is continuous and characteristics lines run into the line $x = 0$ from both sides. The geometry of the flux function allows us to say that the solution can be rewritten as

$$\mathcal{R}^{\alpha}(\rho_L, \rho_R)(x/t) = \begin{cases} \rho_L, & \text{if } x/t < -v(\rho_L), \\ 0, & \text{if } -v(\rho_L) \leq x/t \leq v(\rho_R), \\ \rho_R, & \text{if } x/t > v(\rho_R), \end{cases} \tag{3.9}$$

because the waves joining ρ_L to $\gamma_l(\rho) = 0$ and $\gamma_r(\rho) = 0$ to ρ_R are necessarily shock discontinuities.

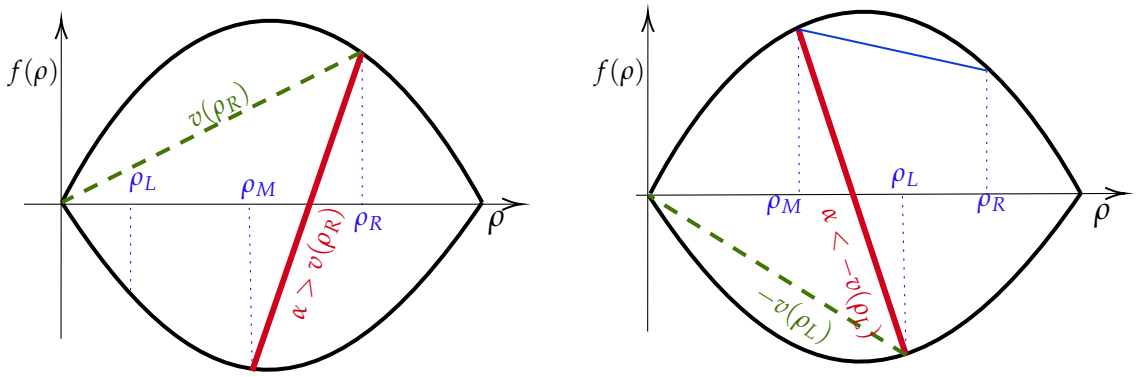

FIGURE 3.1: Non classical Riemann solvers at turning curve with $\alpha > v(\rho_R)$ (left) and $\alpha < -v(\rho_L)$ (right) given *a priori* and data (3.7) where $\rho_L, \rho_R \in (0, R)^2$.

Case $\alpha \neq 0$***:*** This case can be discussed under two subcases, namely $\alpha > 0$ and $\alpha < 0$.

1. Suppose $\alpha > 0$, then if $\alpha \in [0, v(\rho_R)]$ the Riemann solver will be composed of double sided shocks given by the pairs $(0, \rho_R)$ with speed $v(\rho_R)$ and $(\rho_L, 0)$ also with speed $-v(\rho_L)$ emanating from $\xi(t) = \alpha t$. This description is exactly the same as the Riemann solver defined in (3.9).

2. If $\alpha > v(\rho_R)$, two shocks emanates from $x = 0$ as in the previous cases. But since $\alpha > v(\rho_R) > 0$, the discontinuity ξ impinges on the right side shock and so to satisfy the Rankine Hugoniot relation (3.6), an intermediate state in $[0, \rho_R)$ needs to be added. See figure 3.1. The Riemann solver writes:

$$\mathcal{R}^\alpha(\rho_L, \rho_R)(x/t) = \begin{cases} \mathcal{R}^-(\rho_L, \rho_M)(x/t), & \text{for } x/t < \alpha, \\ \rho_R, & \text{for } x/t > \alpha, \end{cases} \tag{3.10}$$

where ρ_M is the intermediate value in $[0, \rho_R)$ such that the jump condition across $\xi(t) = \alpha t$,

$$\alpha = \frac{f(\rho_R) + f(\rho_M)}{\rho_R - \rho_M}, \tag{3.11}$$

is satisfied with $\gamma_l(\rho) = \rho_M$ and $\gamma_r(\rho) = \rho_R$. Therefore the Riemann solver is composed of a classical shock (ρ_L, ρ_M) in Ω_L and a non-classical shock (ρ_M, ρ_R) at $x = \xi$.

On the other hand, if $\alpha < 0$, we have:

3. If $\alpha \in [-v(\rho_L), 0)$, the Riemann solver is same as in case $\alpha = 0$ above.
4. If $\alpha < -v(\rho_L)$, the Riemann solver is similarly written

$$\mathcal{R}^{\alpha}(\rho_L, \rho_R)(x/t) = \begin{cases} \rho_L, & \text{for } x/t < \alpha, \\ \mathcal{R}^{+}(\rho_M, \rho_R)(x/t), & \text{for } x/t > \alpha, \end{cases} \tag{3.12}$$

where the intermediate state value, $\rho_M \in [0, \rho_L)$ satisfies

$$\alpha = \frac{f(\rho_M) + f(\rho_L)}{\rho_M - \rho_L}. \tag{3.13}$$

See the figure 3.1 above. The following lemma proved in [6] shows that the intermediate state value is unique.

Lemma 3.2. *Let f be a concave function. Then for any given $\rho_R \in (0, R)$ and $\alpha > v(\rho_R)$ there exists a unique $\rho_M \in (0, \rho_R)$ which satisfies (3.11).*

To ensure that the Riemann solver in (3.10) is well defined, a necessary condition is that for any couple (ρ_L, ρ_R) and $\alpha > v(\rho_R)$ the speed of waves in $\mathcal{R}^{-}(\rho_L, \rho_M)$ is lower than α. This condition is easily verified, thanks to the convexity of $-f$. From the foregoing, the Riemann solver $\mathcal{R}$ can be summarized in the following proposition.

Definition 3.2. The Riemann solver $\mathcal{R} : [0, R]^2 \to \mathbf{L}^{\infty}(\Omega; [0, R])$ of the associated Cauchy problem of (3.1a) with the Riemann data (3.7), is defined as follows:

1. If $\alpha \in \big[-v(\rho_L),\ v(\rho_R)\big]$, then

$$\mathcal{R}[\rho_L, \rho_R](x/t) := \begin{cases} \mathcal{R}^{-}[\rho_L, 0](x/t), & \text{if } x/t < 0, \\ \mathcal{R}^{+}[0, \rho_R](x/t), & \text{if } x/t > 0. \end{cases}$$

2. If $\alpha > v(\rho_R)$, then

$$\mathcal{R}[\rho_L, \rho_R](x/t) := \begin{cases} \mathcal{R}^{-}[\rho_L, \rho_M](x/t), & \text{if } x/t < \alpha, \\ \mathcal{R}^{\alpha}[\rho_M, \rho_R](x/t), & \text{if } x/t \geq \alpha. \end{cases}$$

where $\rho_M \in [0, \rho_R)$ s.t $\alpha = \frac{f(\rho_R) + f(\rho_M)}{\rho_R - \rho_M}$.

3. If $\alpha < -v(\rho_L)$, then

$$\mathcal{R}[\rho_L, \rho_R](x/t) := \begin{cases} \mathcal{R}^{\alpha}[\rho_L, \rho_M](x/t), & \text{if } x/t \leq \alpha, \\ \mathcal{R}^{+}[\rho_M, \rho_R](x/t), & \text{if } x/t > \alpha. \end{cases}$$

where $\rho_M \in [0, \rho_L)$ s.t. $\alpha = \frac{f(\rho_L)+f(\rho_M)}{\rho_M - \rho_L}$.

3.2 Analysis of the total variation

In this section, we analyze the spatial total variation in the solution, which is denoted $\mathrm{TV}\rho(t,\cdot)$. Estimating the bounds on the $\mathrm{TV}\rho(t,\cdot)$, which implies that the solution has a bounded variation, is a crucial step to prove the compactness of approximate solutions of a scalar conservation laws. See [32, 68]. In our case, it turns out that the total variation in the solution is higher than the total variation in the initial data if the turning curve changes slope or interacts with a shock or rarefaction wave. These situations make it difficult to prove that the solution has a bounded variation. We illustrate this difficulty with the following set of examples using the Riemann solvers constructed in Section 3.1.3.

3.2.1 Changes in slope of turning curve

Fix $T > 0$ and let $\xi : [0,\ T] \to \mathbb{R}$ be a polygonal line with

$$\xi'(t) = \begin{cases} \alpha, & \text{if } 0 \leq t < \tau, \\ \beta, & \text{if } \tau \geq t < T. \end{cases}$$

We take $\rho_L < \rho_R$ and also assume that there are interactions between shocks and/or rarefaction waves in the domains $\Omega_{l,r}$. Since the Lax admissible conditions are satisfied in $\Omega_{l,r}$ this assumption allows us to focus the analysis $x = \xi(t)$.

Consider case studies in which $\alpha \in [-v(\rho_L), v(\rho_R)]$ and $\beta \in \mathbb{R}$. If $\beta \in [-v(\rho_L), v(\rho_R)]$, then $\mathrm{TV}\rho(t,\cdot) = \mathrm{TV}\rho(0,\cdot),\ \ \forall t \in (0,T)$. On the other hand, if $\beta \in (v(\rho_R), +\infty)$ (or $\beta \in (-\infty, -v(\rho_L))$), then $\mathrm{TV}\rho(t,\cdot) = \mathrm{TV}\rho(0,\cdot),\ \ \forall t \in (0,\tau^*)$, where $\tau^* \in [\tau, T)$ is the time at which ξ interacts with the one-sided shock $(0, \rho_R)$ (or $(\rho_L, 0)$). Therefore since ξ is surrounded by vacuum, a change its slope does not lead to a change in the total variation of the solution until the turning curve interacts with an incoming shock or a rarefaction wave. At $t = \tau^*$, a new Riemann problem needs solved. See the next section. We next discuss two cases studies in which $\mathrm{TV}\rho(t,\cdot)$ increases as a result of changes in the slope of the turning curve.

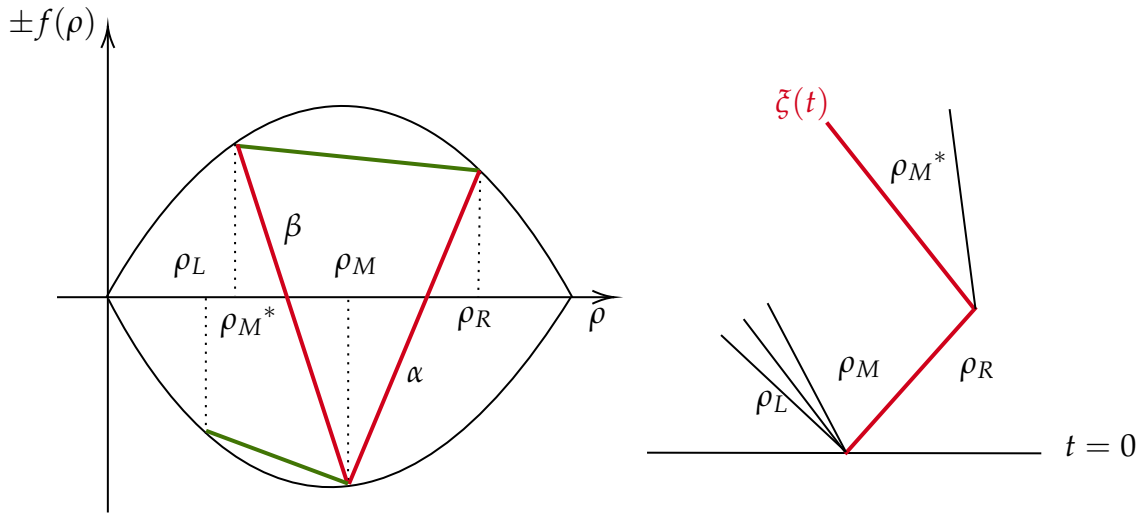

FIGURE 3.2: Left: Geometric representation of the how to Riemann solver after the change of $\xi'(t)$ corresponding to ***Case:*** $\alpha > v(\rho_R)$ *and* $\beta < -v(\rho_L)$. Right: characteristic solution in the $x - t$ plane for ***Case:*** $\alpha > v(\rho_R)$ *and* $\beta < -v(\rho_L)$.

Case: $\alpha > v(\rho_R)$ *and* $\beta < -v(\rho_L)$. Using points 2 and 3 of Definition 3.2, there exist a unique $\rho_M \in (0, \rho_R)$ and $\rho_M^* \in (0, \rho_M)$ respectively such that

$$\alpha = \frac{f(\rho_R) + f(\rho_M)}{\rho_R - \rho_M} \text{ and } \beta = \frac{f(\rho_M^*) + f(\rho_M)}{\rho_M^* - \rho_M}.$$

Note that the wave (ρ_L, ρ_M) is a rarefaction wave if $\rho_L < \rho_M$ but a shock wave otherwise and the wave (ρ_M^*, ρ_R) is a shock wave since $\rho_M^* < \rho_R$ and $-f$ is convex. See the Figure 3.2. Denoting by $\Delta \mathrm{TV}\rho(\tau, \cdot)$ the change in total variation at $t = \tau$, we have

$$\begin{aligned}
\Delta \mathrm{TV}\rho(\tau, \cdot) &= \mathrm{TV}\rho(\tau+, \cdot) - \mathrm{TV}\rho(\tau-, \cdot), \\
&= |\rho_L - \rho_M| + |\rho_M - \rho_M^*| + |\rho_R - \rho_M^*| - |\rho_L - \rho_M| - |\rho_R - \rho_M|, \\
&= 2\,(\rho_M - \rho_M^*)\,.
\end{aligned}$$

Clearly, there is an increase in total variation in the solution as a consequence of the change in the slope of the turning curve.

3.2.2 Analysis of interactions

In this section, we consider selected case studies of interactions between waves (shock or rarefaction wave) and the turning curve that also results in a change in $\mathrm{TV}\rho(t,\cdot)$. Without loss of generality, we assume that any incoming wave approach the turning curve from the right if $\xi'(t) > 0$. On the other hand, if $\xi'(t) < 0$, then any incoming wave approaches ξ from the left. Since the solution structure is symmetric, we simplify the presentation by considering only interaction cases with $\xi' \geq 0$.

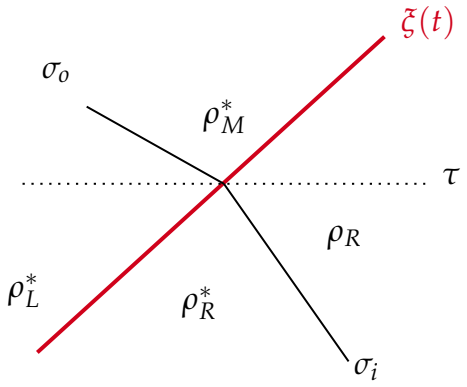

FIGURE 3.3: Illustrating a generic interaction (or collision) of incoming wave $\sigma_i^{\pm}(\rho_R^*, \rho_R)$ with the turning curve $\xi(t)$ at time $t = \tau$ in the $x - t$ plane.

For notation convenience, we let $\sigma_i^{\pm}(\rho_R^*, \rho_R)$ represent an incoming wave connecting ρ_R^* to ρ_R with a speed, $\dot{\sigma}_i^{\pm}$, and $\sigma_o^{\pm}(\rho_R^*, \rho_R)$, the outgoing wave after the interaction connecting ρ_R^* to ρ_R with a speed of $\dot{\sigma}_o^{\pm}$. The superscripts $\pm$ allows for easy identification of the flux function $\pm f$. See Figure 3.3. Clearly, an interaction between the turning curve and a wave $\sigma_i^{\pm}(\rho_R^*, \rho_R)$ occurs only if $\xi'(t) > \dot{\sigma}_o^{\pm}$. By the geometry of the flux function, the Lax admissibility condition requires that if an incoming wave is a shock wave, then the corresponding outgoing wave will be a rarefaction and vice versa after the interaction.

We assume further that the slope of ξ remains constant before and after an interaction. The following are the main types of interactions between the turning curve and waves. The first set of cases concerns incoming shock, thus $\rho_R^* < \rho_R$.

(I1) Case $\rho_L^* = 0$. The incoming shock wave $\sigma_i^+(\rho_R^*, \rho_R)$ has a Rankine-Hugoniot speed $\dot{\sigma}_i^+ = \left(f(\rho_R) - f(\rho_R^*)\right) / (\rho_R - \rho_R^*)$. Moreover, $\rho_L^* = 0$ implies that $\xi'(t) = v(\rho_R^*)$ for $t < \tau$. After the interaction, a new Riemann problem needs to be resolved at $(\tau, \xi(\tau))$. Since $v(\rho_R^*) > v(\rho_R)$, the Riemann problem is

resolved by introducing a unique intermediate state $\rho_M \in [0, \rho_R]$ such that the slope of the turning curve is kept constant and satisfies

$$\xi'(t) = \left(f(\rho_R) + f(\rho_M)\right) / (\rho_R - \rho_M) \tag{3.14}$$

for $t \geq \tau$. See the Figure 3.4. The outgoing wave $\sigma_o^-(0, \rho_M)$ is a rarefaction.

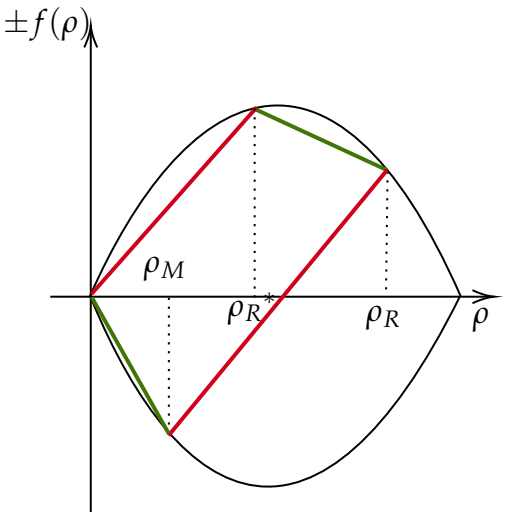

FIGURE 3.4: Geometric interpretation of resolving the new Riemann problem in Case **I1**.

The change in the total variation is

$$\begin{aligned} \Delta \mathrm{TV}\rho(\tau, \cdot) &= \mathrm{TV}\rho(\tau+, \cdot) - \mathrm{TV}\rho(\tau-, \cdot) \\ &= |\rho_R - \rho_R^*| - |\rho_R - \rho_M| \\ &= \rho_M - \rho_R^*. \end{aligned}$$

Therefore the total variation decreases after the interaction $t = \tau$ since $\rho_M < \rho_R^*$.

(I2) Case $\rho_L^* \in (0, \rho_R)$. This case implies that $\xi'(t) > v(\rho_R^*)$ for $t < \tau$. Note also that $v(\rho_R*) > v(\rho_R)$. The new Riemann solver at $t = \tau$ requires a unique intermediate state $\rho_M^* \in [\rho_L^*, \rho_R)$ such that $\xi'(t)$ remains constant for $t \geq \tau$ and satisfies the same condition as in (3.14). In this case there is no net change

in the total variation after the interaction as

$$\begin{aligned}\Delta \mathrm{TV}\rho(\tau,\cdot) &= \mathrm{TV}\rho(\tau+,\cdot) - \mathrm{TV}\rho(\tau-,\cdot)\\ &= |\rho_M - \rho_L^*| + |\rho_R - \rho_M| - (|\rho_R^* - \rho_L^*| + |\rho_R - \rho_R^*|)\\ &= 0.\end{aligned}$$

We now consider the cases $\rho_R < \rho_R^*$ which is equivalent to an incoming rarefaction wave. Here, we reckon that the interaction of the rarefaction wave $\sigma_o^+(\rho_R, \rho_R^*)$ with the turning curve not instantaneous. As such, let $t = \tau_1$ and $t = \tau_N$, be the initial and final times at which the first and last characteristics in the rarefaction wave collide with the turning curve where N is a positive integer. The total variation for $t < \tau_1$ is given by

$$\begin{aligned}\mathrm{TV}\rho(\tau-,\cdot) &= |\rho_R^* - \rho_L^*| + |\rho_R - \rho_R^*|\\ &= 2\rho_R^* - (\rho_L + \rho_R).\end{aligned}$$

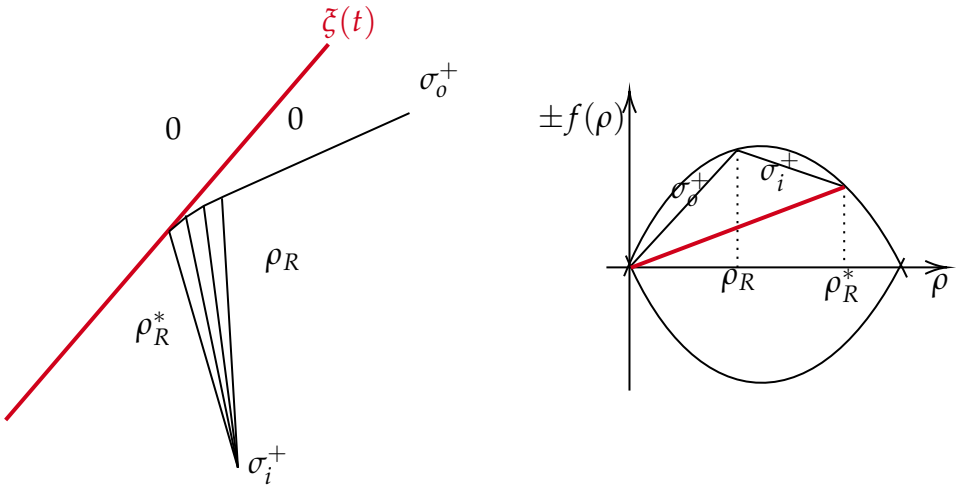

FIGURE 3.5: Interaction between ξ and incoming rarefaction waves (ρ_R^*, ρ_R) from the right corresponding to case **(I3)**.

(I3) Case $\rho_L^* = 0$. Here $\rho_L^* = 0$ implies $\xi'(t) = v(\rho_R^*)$ for $t < \tau_1$. Since $v(\rho_R) > v(\rho_R^*)$, the new Riemann problem at $t = \tau_1$ can only be solved with $\rho_M = 0$ and an outgoing shock wave $\sigma_o^+(0, \rho_R)$ that travels with a speed of $v(\rho_R)$. See Figure 3.5. The change in the total variation in the solution after the

interaction at $t = \tau_N$ is given by

$$\begin{aligned}\Delta \mathrm{TV}\rho(\tau, \cdot) &= \rho_R - [\rho_R^* + (\rho_R^* - \rho_R)] \\ &= 2(\rho_R - \rho_R^*),\end{aligned}$$

which is clearly negative indicating that the total variation after the interaction decreases after the interaction.

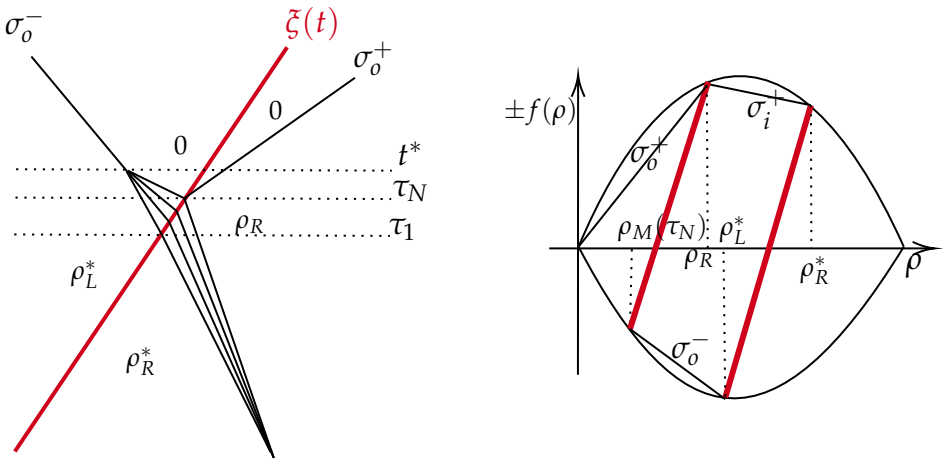

FIGURE 3.6: Interaction between ξ and incoming rarefaction waves (ρ_R^*, ρ_R) from the right corresponding to case **(I4)**.

(I4) Case $\rho_L^* \neq 0$. Here the new Riemann problem for $\tau_1 \leq t < \tau_N$ is resolved by a set of unique time-dependent intermediate densities $\{\rho_M(\tau_1), \rho_M(\tau_2), \ldots, \rho_M(\tau_N)\}$ where $\rho_M(\tau_1) < \rho_M(\tau_2) < \ldots < \rho_M(\tau_N)$, such that each small wave $\sigma_o^*(\rho_M(\tau_{i-1}), \rho_M(\tau_i))$ for $2 \leq i \leq N$ is a shock wave having a Rankine-Hugoniot speed

$$\dot{\sigma}_o^* = \frac{f(\rho_M(\tau_i)) - f(\rho_M(\tau_{i-1}))}{\rho_M(\tau_i) - \rho_M(\tau_{i-1})}.$$

As illustrated in Figure 3.6 (left), these small shocks focus at time $t = t^* > \tau_N$ to form a large shock σ_o^- that travels with a speed of $\dot{\sigma}_o^- = v(\rho_L^*)$. Then at $t = \tau_N$, an outgoing shock wave $\sigma_o^+(0, \rho_R)$ detaches from the turning curve and moves with a speed of $\dot{\sigma}_o^+ = v(\rho_R)$.

In this case the total variation in the solution for $\tau_1 \leq t < \tau_N$ becomes:

$$\begin{aligned}\mathrm{TV}\rho(t,\cdot) &= |\rho_L^* - \rho_M(\tau_1)| + \sum_{i=2}^{N} |\rho_M(\tau_{i-1}) - \rho_M(\tau_i)| + |\rho_R^* - \rho_R| \\ &= \rho_L^* - \rho_M(\tau_1) + \rho_M(\tau_1) - \rho_M(\tau_N) + \rho_R^* - \rho_R \\ &= \rho_L^* - \rho_M(\tau_N) + \rho_R^* - \rho_R,\end{aligned}$$

and if $t \geq \tau_N$, the total variation becomes

$$\mathrm{TV}\rho(t,\cdot) = \rho_L^* + \rho_R.$$

Therefore the change in total variation after the interaction is

$$\begin{aligned}\Delta\mathrm{TV}(\tau,\cdot) &= [\rho_L^* + \rho_R] - [(\rho_R^* - \rho_L^*) + (\rho_R^* - \rho_R)] \\ &= 2(\rho_R^* - \rho_R^*) + 2\rho_R.\end{aligned}$$

Granted that the above presentation demonstrates the increase in the total variation both on the changes in the slope of the flux interface and on interactions with classical waves it would be desirable to estimate this increment with the aim of controlling it. In [32, 68] and other works, the authors defined for BV solutions, a type of Glimm functional and show that it is non-increasing in time. This gives an estimate on the bound of the total variation as expected. Other authors achieve the same goal by the singular mapping approach for spatial discontinuous problems. Compare [86, 87]. We know of no result where compactness was established with a bound on the TV for the space-time discontinuous problems and at the moment have not obtained a BV bound on the solution for (3.1). For this reason, we yet consider an alternate approach to prove a well-posedness result.

3.3 Stability and uniqueness of entropy solution

In this section, we study the uniqueness and derive some stability properties of the solution to the Cauchy (3.1). We begin with the next theorem which estimates the $\mathbf{L^1}$ distance of two solutions to the Riemann problems

$$\begin{cases} \partial_t\rho + \partial_x\left(\mathrm{sign}(x-\xi_1(t))f(\rho)\right) = 0 \\ \rho(0,x) = \begin{cases} \rho_L & \text{for } x<0, \\ \rho_R & \text{for } x>0, \end{cases} \end{cases} \qquad \begin{cases} \partial_t\rho + \partial_x\left(\mathrm{sign}(x-\xi_2(t))f(\rho)\right) = 0, \\ \rho(0,x) = \begin{cases} \rho_L & \text{for } x<0, \\ \rho_R & \text{for } x>0, \end{cases} \end{cases} \tag{3.15}$$

where $\rho_1(t,x)$ and $\rho_2(t,x)$ are solutions to the appropriate Riemann's problem (3.15) when ξ_1 and ξ_2 are given respectively. We consider two constants α and β in the interval $(-f'(0), f'(0))$. To fix our notations we assume $\alpha < \beta$ and we call $\xi_1(t) = \alpha t$ and $\xi_2(t) = \beta t$ the corresponding turning point curves. We recall that $f(\rho) = \rho v(\rho)$, for some smooth function v representing the velocity of the density ρ.

Theorem 3.1. *Let $\rho_1(t,x)$ and $\rho_2(t,x)$ be the two solutions to Riemann problems respectively in (3.15) when $\xi_1(t) = \alpha t$ and $\xi_2(t) = \beta t$ are given, with $\alpha < \beta$ and $\rho_L, \rho_R \in [0,1]^2$ then we have that*

$$\int_{-\infty}^{+\infty} |\rho_1(t,x) - \rho_2(t,x)|\, dx \leq 2t \cdot \max\{\rho_L, \rho_R\} \cdot \big([\beta - v(\rho_R)]_+ + [-\alpha - v(\rho_L)]_+\big), \tag{3.16}$$

where $[x]_\pm$ stands for the positive/negative part of the real number x.

Proof. First, we observe that $-v(\rho_L) < v(\rho_R)$ if $\rho_L \neq \rho_R$. In this case, α and β are chosen in one of the following ways:

1. $-v(\rho_L) \leq \alpha \leq \beta < v(\rho_R)$;
2. $-v(\rho_L) \leq \alpha < v(\rho_R) \leq \beta$;
3. $-v(\rho_L) < v(\rho_R) \leq \alpha < \beta$;
4. $\alpha \leq -v(\rho_L) < v(\rho_R) \leq \beta$;
5. $\alpha \leq -v(\rho_L) < \beta \leq v(\rho_R)$;
6. $\alpha < \beta \leq -v(\rho_L) < v(\rho_R)$.

Case (1) is trivial. Cases (2) and (5) are analogous in the same way as cases (3) and (6). Therefore to avoid duplication of results, we only provide detailed computations for cases (2), (3) and (4) to prove the theorem.

Case (2): With $-v(\rho_L) \leq \alpha < v(\rho_R) \leq \beta$, the solutions to (3.15) are constructed using the Riemann's solver introduced in Section 3.1.3 and applying lemma 3.2,

$\rho_1(t,x)$ is given as in (3.9) and ρ_2 given by (3.10). Then for every $t > 0$

$$\begin{aligned}
&\int_{-\infty}^{+\infty} |\rho_1(t,x) - \rho_2(t,x)|dx \\
&= \int_{-\infty}^{st} |\rho_L - \rho_L|dx + \int_{-v(\rho_L)t}^{st} |0 - \rho_L|dx + \int_{st}^{\xi_1} |0 - \rho_M|dx \\
&\qquad + \int_{\xi_1}^{v(\rho_R)t} |0 - \rho_M|dx + \int_{v(\rho_R)t}^{\xi_2} |\rho_R - \rho_M|dx + \int_{v(\rho_R)t}^{+\infty} |\rho_R - \rho_R|dx \\
&= t\left\{\rho_L(s + v(\rho_L)) + \rho_M(v(\rho_R) - s) + (\beta - v(\rho_R)(\rho_R - \rho_M))\right\},
\end{aligned}$$

where $s = -\left(f(\rho_L) - f(\rho_M)\right)/(\rho_L - \rho_M)$ is the speed of the shock in $\mathcal{R}^-(\rho_L, \rho_M)$ of ρ_2. If we expand and re-arrange the first two terms in the previous line to obtain: $s(\rho_L - \rho_M) + \rho_L v(\rho_L) + \rho_M v(\rho_R)$, and then apply lemma 3.2 again, we have

$$\int_{-\infty}^{+\infty} |\rho_1(t,x) - \rho_2(t,x)|\, dx = t\left\{f(\rho_M) + \rho_M v(\rho_R) + (\beta - v(\rho_R))(\rho_R - \rho_M)\right\}.$$

Now add and subtract $f(\rho_R)$, and using the fact that the condition (3.11) is satisfied across ξ_2 leads to

$$\begin{aligned}
\int_{-\infty}^{+\infty} |\rho_1(t,x) - \rho_2(t,x)|\, dx &= 2t\left\{(\beta - v(\rho_R))(\rho_R - \rho_M)\right\} \\
&\leq 2t \cdot \max\{\rho_R\}[\beta - v(\rho_R)]_+.
\end{aligned}$$

Analogously, by similar argument the following result can be obtained for case (5): $\alpha \leq -v(\rho_L) < \beta \leq v(\rho_R)$, leading to

$$\int_{-\infty}^{+\infty} |\rho_1(t,x) - \rho_2(t,x)|\, dx \leq 2t \cdot \max\{0, \rho_L\}[v(\rho_R) + \alpha]_-.$$

Next consider the case (3). For every $t > 0$, we have

$$\begin{aligned}
\int_{-\infty}^{+\infty} |\rho_1(t,x) - \rho_2(t,x)|\, dx =& t\big\{(s_2 - s_1)(\rho'_M - \rho_L) + (\alpha - s_2)(\rho'_M - \rho''_M) \\
&+ (\beta - \alpha)(\rho_R - \rho''_M)\big\},
\end{aligned}$$

where s_1 and s_2 are the speed of the shocks due to ρ_1 and ρ_2 respectively, and $\rho'_M \in (0, \rho_L)$ and $\rho''_M \in (0, \rho_L)$ are the corresponding intermediate states formed

according to lemma 3.2 with $\rho''_M - \rho'_M > 0$. Then the above equation can be simplified as

$$\begin{aligned}\int_{-\infty}^{+\infty} |\rho_1(t,x) - \rho_2(t,x)|\, dx &= (\beta-\alpha)(\rho_R - \rho''_M) + (\beta-\alpha)(\rho_R - \rho'_M) \\ &\leq 2t \cdot \max\{0, \rho_R\}[\beta-\alpha]_+.\end{aligned}$$

Finally, case (4). It can be observed that this case is equivalent to $\alpha < -v(\rho_L) < v(\rho_R) < \beta$. By setting $\tilde{\rho}(t,x)$ as solution to the trivial case (1), we have for every $t > 0$

$$\begin{aligned}&\int_{-\infty}^{+\infty} |\rho_1(t,x) - \rho_2(t,x)|\, dx \\ &\quad\leq \int_{-\infty}^{+\infty} |\rho_1(t,x) - \tilde{\rho}(t,x)|\, dx + \int_{-\infty}^{+\infty} |\tilde{\rho}(t,x) - \rho_2(t,x)|\, dx\end{aligned} \tag{3.17}$$

Again observe that the first term of the right hand side of (3.17) coincides with case (5) whereas the second term corresponds to case (2). Hence

$$\int_{-\infty}^{+\infty} |\rho_1(t,x) - \rho_2(t,x)|\, dx \leq 2t \cdot \max\{\rho_L, \rho_R\} \cdot \left([\beta - v(\rho_R)]_+ + [-\alpha - v(\rho_L)]_+\right), \tag{3.18}$$

completing the proof. □

In the Lemma below, we derive an entropy jump condition at the interface.

Lemma 3.3. *Let ρ be a weak solution of the Cauchy problem (3.1), then the following entropy jump condition in the flux $\pm f$ at $x = \xi(t)$ is satisfied*

$$f(\gamma^r\rho) + \xi'(c - \gamma^r\rho) \leq f(c), \text{ if } \gamma^l\rho \leq c \leq \gamma^r\rho, \tag{3.19}$$

$$-f(\gamma^l\rho) + \xi'(c - \gamma^l\rho) \geq -f(c), \text{ if } \gamma^r\rho \leq c \leq \gamma^l\rho, \tag{3.20}$$

and

$$\Phi(\gamma^r\rho(t), c) + \Phi(\gamma^l\rho(t), c) \leq \xi'(t)\left[|\gamma^r\rho(t) - c| - |\gamma^l\rho(t) - c|\right] + 2f(c), \tag{3.21}$$

holds for $t \in \mathbb{R}^+$, where $\Phi(\rho, c) = \operatorname{sign}(\rho - c)(f(\rho) - f(c))$.

Proof. The proof follows the one of [59, Lemma 6.3]. If ρ is weak solution then the integral identity (1.32) is satisfied for every $\psi \in \mathcal{D}([0, +\infty[\times\mathbb{R})$. Choose a test function

$$\psi(t,x) = \theta_\varepsilon(x - \xi(t))\varphi(t), \tag{3.22}$$

such that for $\varepsilon > 0$, θ_ε is a Lipschitz compact function defined as

$$\theta_\varepsilon(x) = \begin{cases} \frac{1}{\varepsilon}(\varepsilon + x), & x \in [-\varepsilon, 0] \\ \frac{1}{\varepsilon}(\varepsilon - x), & x \in [0, \varepsilon] \\ 0, & |x| \geq \varepsilon, \end{cases}$$

and $\varphi(t) \in \mathcal{D}([0,T])$, $T > 0$ is an arbitrary test function. Noting that $\psi_x = \theta'_\varepsilon(x - \xi(t))\varphi(t)$ and $\psi_t = \theta_\varepsilon(x - \xi(t))\varphi'(t) - \xi'(t)\theta'_\varepsilon(x - \xi(t))\varphi(t)$, we see from (1.32) that

$$\int_{-\infty}^{\infty}\int_0^{\infty} \big[\rho\big(\theta_\varepsilon(x - \xi(t))\varphi'(t) - \theta_\varepsilon(x - \xi(t))\xi'(t)\big) + F(t,x,\rho)\theta'_\varepsilon(x - \xi(t))\varphi(t)\big]\, dtdx = 0\,. \tag{3.23}$$

The first term in the integrand is

$$\begin{aligned} &\int_0^{\infty}\int_{-\infty}^{\infty} \rho\big[\theta_\varepsilon(x - \xi(t))\varphi'(t) - \theta_\varepsilon(x - \xi(t))\xi'(t)\big]dxdt \\ &\quad = \int_0^{\infty}\int_{-\infty}^{\infty} \rho\varphi'(t)\theta_\varepsilon(x - \xi(t))dxdt \\ &\qquad - \frac{1}{\varepsilon}\int_0^{\infty}\int_{\xi(t)-\varepsilon}^{\xi(t)} \xi'(t)\varphi(t)\rho(t,x)dxdt + \frac{1}{\varepsilon}\int_0^{\infty}\int_{\xi(t)}^{\xi(t)+\varepsilon} \xi'(t)\varphi(t)\rho(t,x)dxdt, \end{aligned}$$

where $\int_0^{\infty}\int_{-\infty}^{\infty} \rho\varphi'(t)\theta_\varepsilon(x - \xi(t)) \to 0$ as $\varepsilon \to 0$ in $\mathbf{L^1}(\mathbb{R})$ and the sum of other integral terms becomes

$$\int_0^{+\infty} (-\gamma^l\rho(t) + \gamma^r\rho(t))\xi'(t)\varphi(t)dt \tag{3.24}$$

as $\varepsilon \to 0$. Similarly, the next term in (3.23) gives

$$\begin{aligned} \int_0^{+\infty}\int_{-\infty}^{+\infty} F(t,x,\rho)\theta'_\varepsilon(x - \xi(t))\varphi(t)dtdx &= -\frac{1}{\varepsilon}\int_0^{+\infty}\int_{\xi(t)-\varepsilon}^{\xi(t)} f(\rho)\varphi(t)dxdt \\ &\quad - \frac{1}{\varepsilon}\int_0^{+\infty}\int_{\xi(t)}^{\xi(t)+\varepsilon} f(\rho)\varphi(t)dxdt \end{aligned}$$

Again letting $\varepsilon \to 0$, we have for a.e $t \in \mathbb{R}^+$

$$\frac{1}{\varepsilon}\int_0^{+\infty}\int_{\xi(t)-\varepsilon}^{\xi(t)} f(\rho)\varphi(t)dxdt \to \int_0^{+\infty} f(\gamma^l\rho(t))\varphi(t)dt$$
$$\frac{1}{\varepsilon}\int_0^{+\infty}\int_{\xi(t)}^{\xi(t)+\varepsilon} f(\rho)\varphi(t)dxdt \to \int_0^{+\infty} f(\gamma^r\rho(t))\varphi(t)dt$$

and so summation gives

$$-\int_0^{+\infty}\left[f(\gamma^r\rho(t)) + f(\gamma^r\rho(t))\right]\varphi(t)dt.$$

Combining this with (3.24) leads to

$$\int_0^{+\infty}\left[-f(\gamma^r\rho(t)) - f(\gamma^r\rho(t)) + \xi'(t)(\gamma^r\rho(t) - \gamma^l\rho(t))\right]\varphi(t)dt = 0 \tag{3.25}$$

Since φ is not zero, then

$$-f(\gamma^r\rho(t)) - f(\gamma^r\rho(t)) + \xi'(t)(\gamma^r\rho(t) - \gamma^l\rho(t)) = 0$$

which is (3.6).
In a similar way, if ρ is entropy solution then the Kruzkhov-type entropy solution (1.8) is satisfied for test function in (3.22) as earlier. With ψ_t and ψ_x given above, the integral becomes

$$\int_0^{\infty}\int_{-\infty}^{\infty}\underbrace{|\rho - c|\left(\varphi'(t)\theta_\varepsilon(x-\xi(t)) - \xi'(t)\theta_\varepsilon(x-\xi(t))\varphi(t)\right)}_{A_1(t,x)}dxdt$$
$$+\int_0^{\infty}\int_{-\infty}^{\infty}\underbrace{\mathcal{F}(t,x,\rho,c)\theta'_\varepsilon(x-\xi(t))\varphi(t)}_{A_2(t,x)}dxdt \tag{3.26}$$
$$-\int_0^{\infty}\int_{-\infty}^{\infty}\operatorname{sign}(\rho-c)F(t,x,c)_x\theta_\varepsilon(x-\xi(t))\varphi(t)dxdt + 2\int_0^{\infty} f(c)\psi(t,\xi(t))dt \geq 0.$$

By the definition of the test function, the first term in the second line goes to zero as $\varepsilon \to 0$ in $\mathbf{L^1}(\mathbb{R})$. Checking the other terms

$$\begin{aligned}
&\int_0^\infty \int_{-\infty}^\infty A_1(t,x)dxdt \\
&\quad = \int_0^\infty \int_{-\infty}^\infty |\rho - c|\theta_\varepsilon(x - \xi(t))\varphi'(t) - \frac{1}{\varepsilon}\int_0^\infty \int_{\xi(t)-\varepsilon}^{\xi(t)} |\rho - c|\xi'(t)\varphi(t)dxdt \\
&\qquad + \frac{1}{\varepsilon}\int_0^\infty \int_{\xi(t)}^{\xi(t)+\varepsilon} |\rho - c|\xi'(t)\varphi(t)dxdt
\end{aligned}$$

As done earlier, it can be observed that as $\varepsilon \to 0$, the first term goes to 0 and so

$$\int_0^\infty \int_{-\infty}^\infty A_1(t,x)dxdt \to \int_0^{+\infty} \xi'(t)\left(-|\gamma^l\rho(t) - c| + |\gamma^r\rho(t) - c|\right)\varphi(t)dt \quad (3.27)$$

as $\varepsilon \to 0$. Furthermore

$$\begin{aligned}
&\int_0^\infty \int_{-\infty}^\infty A_2(t,x)dxdt \\
&\quad = \frac{1}{\varepsilon}\int_0^\infty \int_{\xi(t)}^{\xi(t)+\varepsilon} \mathcal{F}(t,x,\rho,c)\varphi(t)dxdt - \frac{1}{\varepsilon}\int_0^\infty \int_{\xi(t)-\varepsilon}^{\xi(t)} \mathcal{F}(t,x,\rho,c)\varphi(t)dxdt
\end{aligned}$$

which, as $\varepsilon \to 0$, converges to

$$\begin{aligned}
-\int_0^{+\infty} \Big[&\operatorname{sign}(\gamma^l\rho(t) - c)(f(\gamma^l\rho(t)) - f(c)) \\
&+ \operatorname{sign}(\gamma^l\rho(t) - c)(f(\gamma^l\rho(t)) - f(c))\Big]\varphi(t)dt\,.
\end{aligned} \quad (3.28)$$

Combining (3.27), (3.28) and the last term of (3.26) leads to

$$\begin{aligned}
\int_0^{+\infty} \Big[&\xi'(t)(-|\gamma^l\rho(t) - c| + |\gamma^r\rho(t) - c|) - \operatorname{sign}(\gamma^l\rho(t) - c)(f(\gamma^l\rho(t)) - f(c)) \\
&- \operatorname{sign}(\gamma^r\rho(t) - c)(f(\gamma^r\rho(t)) - f(c)) + 2f(c)\Big]\varphi(t)dt \geq 0.
\end{aligned}$$

Since $\varphi(t)$ is arbitrary, then

$$\begin{aligned}
&\operatorname{sign}(\gamma^r\rho(t) - c)(f(\gamma^r\rho(t)) - f(c)) + \operatorname{sign}(\gamma^l\rho(t) - c)(f(\gamma^l\rho(t)) - f(c)) \\
&\qquad - \xi'(t)(|\gamma^r\rho(t) - c| - |\gamma^l\rho(t) - c|) \leq 2f(c)
\end{aligned}$$

which is (3.21). □

In passing, the uniqueness result shall depend on the so-called *flux crossing condition*.

Assumption 3.1. Given the discontinuous coefficient, $k(t,x) = \text{sign}(x - \xi(t))$, with jump at $\xi(t)$ and (ρ_L, ρ_R) be states in solution left and right of $\xi(t)$ for every $t > 0$, then the crossing condition must hold:

$$f(\rho_L) < 0 < f(\rho_R) \implies \rho_L < \rho_R. \tag{3.29}$$

As mentioned in [59], the geometric interpretation of the crossing condition given therein implies that the graphs of $-f$ and f do not cross except if graph of $-f$ lies above f to the left of any crossing point. The geometry of our flux function implies that it there is no point in $\rho \in [0, R]$ that violates assumption 3.1 and therefore we can conclude that the flux crossing condition holds for our flux function. With this in mind, we state and prove the stability and uniqueness result for our problem.

Theorem 3.2. *Let ρ and $\tilde{\rho}$ be two entropy solutions of the Cauchy problem associated with (3.1) with the same turning curve $\xi(t)$ such that $k(t,x)$ is defined and initial conditions $\rho_0, \tilde{\rho}_0 \in \mathbf{L}^\infty(\mathbb{R})$ respectively. Assuming that the crossing condition of assumption 3.1, and existence of traces then for* a. e. *$t > 0$, we have for $r > 1$ that*

$$\int_{-r}^{r} |\rho(t,x) - \tilde{\rho}(t,x)| dx \leq \int_{-r-\|\partial_\rho F\| t}^{r+\|\partial_\rho F\| t} |\rho_0(x) - \tilde{\rho}_0(x)| dx, \forall x \in \mathbb{R}. \tag{3.30}$$

Proof. Let $\rho(t,x)$ and $\tilde{\rho}(t,x)$ be two entropy solutions according to the definition 3.1, the following contraction holds for a non-negative test function $\psi \in \mathcal{D}(\Omega \setminus \xi)$ and a constant C:

$$-\int_0^{+\infty} \int_{-\infty}^{+\infty} \left[|\rho - \tilde{\rho}| \psi_t + \mathcal{F}(t,x,\rho,\tilde{\rho}) \psi_x \right] dxdt \leq C \int_0^{+\infty} \int_{-\infty}^{+\infty} |\rho - \tilde{\rho}| \psi dxdt. \tag{3.31}$$

The above integral is derived from [58] for scalar conservation laws with space flux discontinuity by using the Kruzkhov's doubling of variable technique with a test function that vanishes on the discontinuity and has been extended to the case of time dependent flux discontinuity in [59]. Following the proof of [58, Theorem A.1], we observe that the inequality (3.31) leads to

$$-\int_0^{+\infty} \int_{-\infty}^{+\infty} \left[|\rho - \tilde{\rho}| \psi_t + \mathcal{F}(t,x,\rho,\tilde{\rho}) \psi_x \right] dxdt \leq 0, \tag{3.32}$$

since the time dependent coefficients, $k(t,x)$ are constants and bounded away from ξ without the diffusion term. To account for the flux discontinuity, let $\varphi \in \mathcal{D}(\Omega)$

be an arbitrary test function that doesn't vanish near ξ for all $t > 0$ and introduce

$$\theta_h(x) := \begin{cases} \frac{1}{h}(2h + x) & \text{if } x \in [-2h, -h], \\ 1 & \text{if } x \in [-h, h] \\ \frac{1}{h}(2h - x) & \text{if } x \in [h, 2h] \\ 0, & \text{if } |x| \geq 2h \end{cases}$$

a Lipschitz function for a real number $h > 0$ such that $\theta_h(x) \to 1$ as $h \to 0$. Set $\Psi_h(x - \xi(t)) = 1 - \theta_h(x - \xi(t))$ so that $\Psi_h \to 1$ in L^1 but vanishes near $\xi(t)$. Then for any test function φ, we have $\psi = \varphi\Psi_h$ is an admissible test function. This is implied by the fact that sending $h \to 0$, we have $\varphi - \varphi\theta_h \to \varphi$, in the neighbourhood of $\xi(t)$ and $\psi \to \varphi$ away from $\xi(t)$. Inserting this into (3.32) with the following derivatives

$$\begin{aligned} \partial_t \Psi_h(x - \xi(t)) &= \theta_h'(x - \xi(t))\xi'(t), \\ \partial_t \psi(t, x) &= \varphi_t \Psi_h(x - \xi(t)) + \varphi\theta_h'(x - \xi(t))\xi'(t), \\ \partial_x \psi(t, x) &= \varphi_x \Psi_h(x - \xi(t)) - \varphi\theta_h'(x - \xi(t)), \end{aligned}$$

leads to

$$\begin{aligned} &- \int_0^{+\infty} \int_{-\infty}^{+\infty} \left(|\rho - \tilde{\rho}|\varphi_t + \mathcal{F}(t, x, \rho, \tilde{\rho})\varphi_x\right) \Psi_h dx dt \\ &\quad \underbrace{- \int_0^{+\infty} \int_{-\infty}^{+\infty} \left(|\rho - \tilde{\rho}|\xi'(t)\theta_h'(x - \xi(t)) - \mathcal{F}(t, x, \rho, \tilde{\rho})\theta_h'\right) \varphi dx dt}_{I_h(t,x)} \\ &\qquad \leq 0. \end{aligned}$$

Expanding $I_h(t, x)$ and performing a change of variables in the neigbhourhood of ξ for $h > 0$ gives

$$\begin{aligned} I_h(t, x) &= - \int_0^{+\infty} \int_{-2h}^{2h} \left(|\rho - \tilde{\rho}|\xi'(t) - \mathcal{F}(t, x, \rho, \tilde{\rho})\right) \varphi\theta_h'(x - \xi(t)) dx dt \\ &= -\frac{1}{h} \int_0^{+\infty} \int_{\xi(t)+h}^{\xi(t)+2h} \left(|\rho - \tilde{\rho}|\xi'(t) - \mathcal{F}(t, x, \rho, \tilde{\rho})\right) \varphi dx dt \\ &\quad + \frac{1}{h} \int_0^{+\infty} \int_{\xi(t)-2h}^{\xi(t)-h} \left(|\rho - \tilde{\rho}|\xi'(t) - \mathcal{F}(t, x, \rho, \tilde{\rho})\right) \varphi dx dt. \end{aligned}$$

Sending $h \to 0$ leads to

$$\lim_{h\downarrow 0} I_h(t,x) = \int_0^{+\infty} \left[|\rho-\tilde{\rho}|\xi'(t) - \mathcal{F}(t,x,\rho,\tilde{\rho})\right]_{x=\xi^+}^{x=\xi^-} \varphi(t,\xi)dt$$

and so (3.32) becomes

$$\begin{aligned} -\int\int \left[|\rho-\tilde{\rho}|\varphi_t + \mathcal{F}(t,x,\rho,\tilde{\rho})\varphi_x\right] dxdt \\ \leq \int_0^{+\infty} \left[\mathcal{F}(t,x,\rho,\tilde{\rho}) - \xi'(t)|\rho-\tilde{\rho}|\right]_{x=\xi^-}^{x=\xi^+} \varphi(t,\xi)dt, \end{aligned} \tag{3.33}$$

where the signs are used to indicate the left and right limits of $x = \xi$. The next thing to do is to show that $\lim_{h\downarrow 0} I_h(t,x) \leq 0$ by using the entropy conditions in lemma 3.3 and the crossing condition of Assumption 3.1. From the contribution at $\xi(t)$ this is equivalent to showing that

$$\Gamma_\xi(t) = \mathcal{F}(t,x,\gamma^r\rho,\gamma^r\tilde{\rho}) - \mathcal{F}(t,x,\gamma^l\rho,\gamma^l\tilde{\rho}) - \xi'(t)|\gamma^r\rho-\gamma^r\tilde{\rho}| - \xi'(t)|\gamma^l\rho-\gamma^l\tilde{\rho}| \leq 0.$$

Proceeding as in the proof of theorem 6.5 of [59], we choose the modified flux

$$\pm\hat{f}(\rho) := \pm f(\rho) - \xi'\rho$$

so that the associated entropy flux

$$\hat{\mathcal{F}}(t,x,\rho,c) := \mathcal{F}(t,x,\rho,c) - \xi'|\rho-c|.$$

Here the $\hat{f}$ and f admits the same crossing condition, in that there's $\rho \in [0,R]$ such that the crossing condition is satisfied. In this way, we can write from the $\Gamma_\xi(t)$

$$\hat{\Gamma}_{\xi(t)} = \hat{\mathcal{F}}(t,x,\gamma^r\rho,\gamma^r\tilde{\rho}) - \hat{\mathcal{F}}(t,x,\gamma^l\rho,\gamma^l\tilde{\rho}). \tag{3.34}$$

Now we check on case by case basis that $\hat{\Gamma}_{\xi(t)}$ with the aid of the following entropy jump condition in the flux $\pm f$

$$f(\gamma^r\rho) + \xi'(c-\gamma^r\rho) \leq f(c), \text{ if } \gamma^l\rho \leq c \leq \gamma^r\rho, \tag{3.35}$$

$$-f(\gamma^l\rho) + \xi'(c-\gamma^l\rho) \geq -f(c), \text{ if } \gamma^r\rho \leq c \leq \gamma^l\rho, \tag{3.36}$$

which is obtained by using the fact that $-f(c) \leq f(c)$ for any constant c. We check the following cases for (3.34) for a fixed ξ'

Case 1:($\gamma^l\rho = \gamma^l\tilde{\rho}, \gamma^r\rho = \gamma^r\tilde{\rho}$). This case is trivial in that $\hat{\Gamma}_{\xi(t)} = 0$.

Case 2:$(\gamma^l\rho = \gamma^l\tilde{\rho}, \gamma^r\rho \neq \gamma^r\tilde{\rho})$. Assume $\gamma^r\rho > \gamma^r\tilde{\rho}$, then (3.34) becomes

$$\hat{\Gamma}_{\xi(t)} = f(\gamma^r\tilde{\rho}) - f(\gamma^r\rho) - \xi'(\gamma^r\tilde{\rho} - \gamma^r\rho) \leq 0,$$

and the inequality is due to (3.35) with $c = \gamma^r\tilde{\rho}$. On the other hand if we assume $\gamma^r\rho < \gamma^r\tilde{\rho}$ the same computation is made and so omitted.
Case 3: $(\gamma^r\rho = \gamma^r\tilde{\rho}, \gamma^l\rho \neq \gamma^l\tilde{\rho})$. Assume $\gamma^l\rho < \gamma^l\tilde{\rho}$, then

$$\begin{aligned}\hat{\Gamma}_{\xi(t)} &= -f(\gamma^l\rho) + f(\gamma^l\tilde{\rho}) + \xi'(\gamma^l\tilde{\rho} - \gamma^l\rho) \\ &= -\left[f(\gamma^l\rho + \xi'(\gamma^l\rho - \gamma^l\tilde{\rho})\right] + f(\gamma^l\tilde{\rho}).\end{aligned}$$

The jump condition of (3.36) allows the conclusion that

$$\hat{\Gamma}_{\xi(t)} \leq -f(\gamma^l\tilde{\rho}) + f(\gamma^l\tilde{\rho}) = 0.$$

If $\gamma^l\rho > \gamma^l\tilde{\rho}$, we proceed with same computation and apply (3.36) with $c = \gamma^l\tilde{\rho}$.
Case 4: $(\gamma^r\rho < \gamma^r\tilde{\rho}$ and $\gamma^l\rho < \gamma^l\tilde{\rho})$. Here (3.34) becomes

$$\begin{aligned}\hat{\Gamma}_{\xi(t)} &= -\big(f(\gamma^r\rho) - f(\gamma^r\tilde{\rho})\big) - \xi'(\gamma^r\tilde{\rho} - \gamma^r\rho) - f(\gamma^l\rho) + f(\gamma^l\tilde{\rho}) + \xi'(\gamma^l\tilde{\rho} - \gamma^l\rho) \\ &= \xi'(\gamma^r\rho - \gamma^l\rho) + \xi'(\gamma^r\tilde{\rho} - \gamma^l\tilde{\rho}) - \xi'(\gamma^r\tilde{\rho} - \gamma^r\rho) + \xi'(\gamma^l\tilde{\rho} - \gamma^l\rho)\end{aligned}$$

by the Rankine-Hugoniot jump condition and leads to 0 by cancellation.
Case 5: $(\gamma^r\rho > \gamma^r\tilde{\rho}$ and $\gamma^l\rho > \gamma^l\tilde{\rho})$. Same as the preceding case.
Case 6: $(\gamma^r\rho < \gamma^r\tilde{\rho}$ and $\gamma^l\rho > \gamma^l\tilde{\rho})$. Again (3.34) becomes

$$\begin{aligned}\hat{\Gamma}_{\xi(t)} &= -f(\gamma^r\rho) + f(\gamma^r\tilde{\rho}) - \xi'(\gamma^r\tilde{\rho} - \gamma^r\rho) + f(\gamma^l\rho) - f(\gamma^l\tilde{\rho}) + \xi'(\gamma^l\rho - \gamma^l\tilde{\rho}) \\ &= -\big(f(\gamma^r\rho) + f(\gamma^r\tilde{\rho})\big) + \big(f(\gamma^l\rho) + f(\gamma^l\tilde{\rho})\big) - \xi'(\gamma^r\tilde{\rho} - \gamma^r\rho) + \xi'(\gamma^l\rho - \gamma^l\tilde{\rho})\end{aligned}$$

which again leads to zero by applying the Rankine Hugoniot condition and cancellation of terms.
Case 7: $(\gamma^r\rho > \gamma^r\tilde{\rho}$ and $\gamma^l\rho < \gamma^l\tilde{\rho})$. This case can also be concluded as the previous case.
The above computations implies that (3.33) holds for any non-negative test function, φ and becomes

$$-\int_0^\infty \int_{-\infty}^\infty \left[|\rho - \tilde{\rho}|\varphi_t + \mathcal{F}(t, x, \rho, \tilde{\rho})\varphi_x\right] dxdt \leq 0. \tag{3.37}$$

With this inequality, we now choose for any fixed positive real s_0, s such that $0 < s_0 < s < T$ a piecewise linear function:

$$\beta_{\tau,\kappa}(t) = \begin{cases} 0, & \text{if } t \in [0, s_0] \cup [s+\kappa, T], \\ \frac{1}{\tau}(t-\tau), & \text{if } t \in [s_0, s_0+\tau], \\ 1, & \text{if } t \in [s_0+\tau, s], \\ \frac{1}{\kappa}(\kappa - t), & \text{if } t \in [s, s+\kappa], \end{cases} \tag{3.38}$$

where τ, κ are chosen to satisfy $0 < s_0 < s_0 + \tau < s < s + \kappa < T$ for any fixed $T > 0$. Furthermore, consider the trapezoid Ω_T given by:

$$\Omega_T := \left\{(t,x) : \ |x| \leq r + \left\|F_\rho\right\|(T-t), \ s_0 \leq t \leq T\right\}$$

and define $A_r : \mathbb{R} \mapsto [0,1]$, a characteristic function by

$$A_r(x) = \begin{cases} 1, & \text{if } x \in \Omega_T, \\ 0, & \text{otherwise,} \end{cases}$$

then set test function to be $\varphi(t,x) = A_r(x - \xi(t))\beta_{\tau,\kappa}(t)$. If we compute the derivatives

$$\begin{aligned} \varphi_t &= -\xi'(t)A_r'(x-\xi(t))\beta_{\tau,\kappa}(t) + \beta_{\tau,\kappa}'(t)A_r(x-\xi(t)) \\ \varphi_x &= A_r'(x-\xi(t))\beta_{\tau,\kappa}(t) \end{aligned}$$

and insert them into (3.37), we have

$$\begin{aligned} -\frac{1}{\tau}\int_{s_0}^{s_0+\tau}\int_{-r}^{r} |\rho(t,x) - \tilde{\rho}(t,x)| A_r(x-\xi(t))dxdt \\ + \frac{1}{\kappa}\int_{s}^{s+\kappa}\int_{-r}^{r} |\rho(t,x) - \tilde{\rho}(t,x)| A_r(x-\xi(t))dxdt \leq 0. \end{aligned}$$

Sending $s_0 \to 0$, leads to

$$\frac{1}{\kappa}\int_{s}^{s+\kappa}\int_{-r}^{r} |\rho(t,x) - \tilde{\rho}(t,x)|dxdt \leq \frac{1}{\tau}\int_{0}^{\tau}\int_{-r}^{r} |\rho(t,x) - \tilde{\rho}(t,x)|dxdt. \tag{3.39}$$

Insert $\pm\rho_0(t,x)$ and $\pm\tilde{\rho}_0(t,x)$ into the r.h.s of (3.39) and apply the triangle inequality, it becomes

$$\frac{1}{\tau}\int_0^\tau\int_{-r}^{r}|\rho(t,x)-\tilde{\rho}(t,x)|dxdt \leq \int_{-r-\|\partial_\rho F\|t}^{r+\|\partial_\rho F\|t}|\rho_0(x)-\tilde{\rho}_0(x)|dx + \frac{1}{\tau}\int_0^\tau\int_{-r}^{r}|\rho(t,x)-\rho_0(x)|dxdt + \frac{1}{\tau}\int_0^\tau\int_{-r}^{r}|\tilde{\rho}(t,x)-\tilde{\rho}_0(x)|dxdt.$$

Letting $\tau \to 0$, the last two terms of the above integral tends to 0 (uniformly in r) and so (3.39) becomes

$$\frac{1}{\kappa}\int_s^{s+\kappa}\int_{-r}^{r}|\rho(t,x)-\tilde{\rho}(t,x)|dxdt \leq \int_{-r-\|\partial_\rho F\|t}^{r+\|\partial_\rho F\|t}|\rho_0(x)-\tilde{\rho}_0(x)|dx \tag{3.40}$$

□

Considering the observation that $\rho \in \mathbf{L}^\infty$ of (3.1) admits one-sided strong traces at the interface, we consider the possibility of reducing the problem to finding an appropriate flux connection across the interface [8], so-called dissipative coupling or *dissipative germs*. Introduced in [14] with a spatial flux discontinuous example, this interface coupling conditions is referred to as (A,B)-connection in [3], employ the principal tools of satisfying the Kato inequalities away from the interface and near the interface, strong traces theory [76], adapted entropies [16] and monotone finite volume schemes with the Godunov solver at the interface [11], entropy process solutions and weak BV estimates arguments [13, 15]. Here in this work, we extend the notion of admissible germs to (3.1).

The presentation of section 3.1.3 demonstrates how this connection are derived for the present problem. This allows one to study the problem well-posedness of solution to the problem with $\mathbf{L}^\infty$ data within the framework of entropy process solutions as was done in [13, 38, 11] and other papers. Later in Chapter 4 of this thesis, the finite volume method with adapted moving near ξ generates the $\mathbf{L}^\infty$ representation of the solution to equation (3.1). In the next section however, we re-formulate the problem following the theory of admissibility germs formally for our problem, establish the equivalence of adapted entropy and entropy process solutions. These two sections would allow the treatment of convergence of approximate solutions to the entropy solutions already introduced.

3.4 Admissibility germs and entropy solutions

In this section, we formulate the weak entropy solutions of (3.1) in the framework of $\mathcal{G}$-entropy solutions via the admissible germs theory, $\mathcal{G}$ introduced in [14] with $\mathbf{L}^\infty$ data. In doing so, we reckon that since $\xi'(t) \in \mathbb{R}$ is given *a priori*, and that there exist strong trace at ξ (see remark 3.3, we expect that ρ equivalently satisfies the following Cauchy-Dirichlet problems in the sense of distributions

$$\partial_t \rho - \partial_x f(\rho) = 0, \text{ in } \mathcal{D}(\Omega_l),\ t > 0 \tag{3.41}$$

$$\partial_t \rho + \partial_x f(\rho) = 0, \text{ in } \mathcal{D}(\Omega_r),\ t > 0 \tag{3.42}$$

$$f(\gamma^r \rho(t)) + f(\gamma^l \rho(t)) = \xi'(\gamma^r \rho(t) - \gamma^l \rho(t)), \text{ on } x = \xi(t),\ t > 0, \tag{3.43}$$

and

$$\rho(0,x) = \begin{cases} \rho_L & \text{if } x < 0 \\ \rho_R, & \text{if } x > 0. \end{cases} \tag{3.44}$$

The discontinuous flux function can equivalently be set to

$$F(t,x,\cdot) := -f(\cdot)\mathbf{1}_{x<\xi(t)} + f(\cdot)\mathbf{1}_{x>\xi(t)}, \tag{3.45}$$

where for every $t \geq 0$, $\pm f(\cdot)$ are non-linear functions in ρ satisfying the conditions **(F)**, implying that $(t,x) \mapsto F(t,x,\cdot)$ has a jump across the interface discontinuity. Throughout this section we shall consider $\xi(t) = \alpha t$, to simplify the analysis even though the result can be extended in general to Lipschitz continuous functions of ξ.

3.4.1 Flux connections and the dissipative germ

We hereby define the admissible germ for the equation (3.1) in this section. This is a family of piecewise constant weak solutions of the form $p_l \mathbb{1}_{x<\xi(t)} + p_r \mathbb{1}_{x>\xi(t)}$, with p_l and p_r in $[0,R]$. Of course, each of these solutions is completely characterized by the values of p_l and p_r, so that we describe the germ as a set of ordered couples. This tool will be used later to prove the convergence of approximate solutions to a weak entropy solution.

Equivalently, the germ can be defined as a set of possible couples of traces $\gamma^{l,r}\rho(t)$ at the sides of the interface ξ. We stress that since by assumption $\pm f$ are continuous over $[0,R]^2$ and the measure of set $\{s \in [0,1] \text{s.t.} f'(s) = 0\}$ is zero, we conclude that $\gamma^{l,r}\rho(t)$ are in fact one-sided strong traces based on the [14, Theorem 2.1].

Definition 3.3. Let $\xi(t) = \alpha t$, with $\alpha \in \mathbb{R}$ fixed. The germ of admissible solutions $\mathcal{G}_\alpha$ for the conservation law (3.1) is

$$\mathcal{G}_\alpha := \left\{ (0, \rho_\alpha) \in [0, R]^2 : f(\rho_\alpha) = \alpha \rho_\alpha \right\}. \tag{3.46}$$

Definition 3.4. A germ $\mathcal{G}$ is L^1-dissipative (L^1D for short), if for any two pairs (p_l, p_r), $(q_l, q_r) \in \mathcal{G}$ the following dissipative property holds

$$\mathcal{F}(t, x, p_l, q_l) - \mathcal{F}(t, x, p_r, q_r) \geq \alpha(\eta(p_l, q_l) - \eta(p_r, q_r)), \tag{3.47}$$

where $\mathcal{F}(t, x, \rho, c)$ is defined in Definition (3.1) and $\eta(\rho, c) := |\rho - c|$.

Proposition 3.1. *The unique maximal L^1D extension of $\mathcal{G}_\alpha$ is the subset of $[0, R]^2$ defined by*

$$\widetilde{\mathcal{G}}_\alpha := \left\{ (p_l, p_r) \in [0, R]^2 : f(p_r) + f(p_l) = \alpha(p_r - p_l) \right\}. \tag{3.48}$$

Proof. The fact that $\widetilde{\mathcal{G}}_\alpha$ contains $\mathcal{G}_\alpha$ is obvious as

$$f(\rho_\alpha) + f(0) = \alpha \rho_\alpha - 0.$$

To show that $\widetilde{\mathcal{G}}_\alpha$ is L^1D we distinguish three cases : $\alpha = 0$, $\alpha > 0$, and $\alpha < 0$.

If $\alpha = 0$ the germ only contains four elements $(0, 0)$, $(0, R)$, $(R, 0)$, (R, R) and we can check that (3.47) holds as an equality by direct computations.

If $\alpha > 0$ we consider two sub-cases

I. If $q_l = q_r = 0$ we have

$$\begin{aligned} \mathcal{F}(t, x, p_l, 0) - \mathcal{F}(t, x, p_r, 0) &= (-f(p_l) + f(0)) - (f(p_r) - f(0)) \\ &= -(f(p_r) + f(p_l)) = \alpha(p_l - q_r) \\ &= \alpha(\eta(p_l, 0) - \eta(p_r, 0)), \end{aligned}$$

for all $p_l, p_r \in [0, R]^2$. The case in which $q_l = q_r = R$ is similar.

II. If $q_l < q_r$ (the reverse inequality being impossible due to the sign of α and the geometry of the problem) we can observe that

$$\operatorname{sign}(p_l - q_l) = \operatorname{sign}(p_r - q_r).$$

Therefore

$$\begin{aligned}\mathcal{F}(t,x,p_l,q_l)-\mathcal{F}(t,x,p_r,q_r) &= \operatorname{sign}(p_l-q_l)\big[-f(p_l)+f(q_l)\\ &\quad -f(p_r)+f(q_r)\big]\\ &= \operatorname{sign}(p_l-q_l)\alpha\left(q_r-q_l-p_r+p_l\right)\\ &= \alpha(\eta(p_l,q_l)-\eta(p_r,q_r))\,.\end{aligned}$$

If $\alpha<0$ the analysis is exactly the same as in the previous case.

It is also clear that $\widetilde{\mathcal{G}}_\alpha$ is maximal : given any L^1D germ $\mathcal{G}$ one can look for its possible L^1D extensions, the largest of which is its dual $\mathcal{G}^*$, i.e. the set containing all couples $(q_l,q_r)\in[0,R]^2$ which satisfy the Rankine-Hugoniot conditions and (3.47) for any $(p_l,p_r)\in\mathcal{G}$. Of course $\widetilde{\mathcal{G}}_\alpha$ and $\widetilde{\mathcal{G}}_\alpha^*$ coincide.

□

Additionally, given any piecewise constant initial condition $\rho_l\mathbb{1}_{x<\xi(t)}+\rho_r\mathbb{1}_{x>\xi(t)}$, for, $(\rho_l,\rho_r)\in[0,R]^2$, the left and right side traces of the solution of the associate Riemann problem correspond to an element of $\widetilde{\mathcal{G}}_\alpha$.

Lemma 3.4. *For any $\xi=\alpha t$, the L^1D germ $\widetilde{\mathcal{G}}_\alpha$ is complete.*

Proof. This lemma immediately follows from the study of the Riemann problem at the interface in Section 3.1.3. □

Definition 3.5. Assume that f, ξ satisfy, (3.2) and (3.3) respectively. We say that map $(t,x)\mapsto\rho(t,x)$ is a $\mathcal{G}$-entropy solution to the initial-boundary value problem (3.1), if ρ is in $\mathbf{L}^\infty\big(\Pi;\,[0,R]\big)$, is a weak solution of this problem and for any $(p_l,p_r)\in\mathcal{G}$, and any test function $\varphi\in\mathbf{C}_\mathbf{c}^\infty\left(\Omega;\,[0,+\infty[\right)$ we have

$$\begin{aligned}&\int_0^{+\infty}\!\!\int_{-1}^{1}\left[|\rho-c(t,x)|\partial_t\varphi+\mathcal{F}(t,x,\rho,c(t,x))\partial_x\varphi\right]\mathrm{d}x\mathrm{d}t\\ &+\int_{-1}^{1}|\rho_0(x)-c(t,x)|\varphi(0,x)\mathrm{d}x\\ &+\int_0^{+\infty}\left[f(\rho(t,1-))-f(c_r)\right]\varphi(t,1)\mathrm{d}t+\\ &+\int_0^{+\infty}\left[f(\rho(t,-1+))-f(c_l)\right]\varphi(t,-1)\mathrm{d}t\geq 0,\end{aligned}\tag{3.49}$$

where $c(t,x)=c_l\mathbb{1}_{x<\xi(t)}(x)+c_r\mathbb{1}_{x>\xi(t)}(x)$ and $\mathcal{F}(t,x,\rho,c)$ the same as in Definition 3.1.

Remark 3.4. Following [14, Remark 3.12 and Th. 3.18] we recall that

- $\rho \in \mathbf{L}^\infty(\Pi;\,[0,R])$ is a $\mathcal{G}_\alpha$-entropy solution if and only if it is a weak solution and for almost every $t > 0$ the couple given by its traces at $x = \xi(t)$, $(\gamma^l\rho(t), \gamma^r\rho(t))$, is in $\widetilde{\mathcal{G}}_\alpha = \mathcal{G}_\alpha^*$.
- In our setting $\mathcal{G}_\alpha$- and $\widetilde{\mathcal{G}}_\alpha$-entropy solutions coincide.

The consequence of Remark 3.4 is that one can consider the existence of a measure-valued solution, herein referred to as $\mathcal{G}$-entropy process solution, to which approximate solutions of (3.1) obtained by a finite volume scheme converges. The definition of entropy solution with global adapted entropy inequality is given next.

Definition 3.6. Assume that f, ξ satisfy (3.2), (3.3) respectively. We say that a function $\mu \in \mathbf{L}^\infty(\Pi;\,[0,R])$ is a $\widetilde{\mathcal{G}}_\alpha$-entropy process solution to the initial-boundary value problem (3.1), if the following conditions hold :

1. For any test function $\varphi \in \mathbf{C}_\mathbf{c}^\infty(\Pi;\,[0,+\infty[)$ we have

$$\int_0^1\int_0^{+\infty}\int_{-1}^1 \left[\mu(t,x,a)\partial_t\varphi + F(t,x,\mu(t,x,a))\partial_x\varphi\right]\mathrm{d}x\mathrm{d}t\mathrm{d}a + \int_{-1}^1 \rho_0(x)\varphi(0,x)\mathrm{d}x = 0. \tag{3.50}$$

2. The inequality

$$\int_0^1\int_0^{+\infty}\int_{-1}^1 \left[|\mu(t,x,a)-c(t,x)|\partial_t\varphi + \mathcal{F}(t,x,\mu(t,x,a),c(t,x))\partial_x\varphi\right]\mathrm{d}x\mathrm{d}t\mathrm{d}a + \int_{-1}^1 |\rho_0(x)-c(0,x)|\varphi(0,x)\mathrm{d}x \geq 0, \tag{3.51}$$

where $\mathcal{F}(t,x,\rho,c) = \mathrm{sign}(\rho-c)\,[F(t,x,\rho)-F(t,x,c)]$, is satisfied

- for any test function $\varphi \in \mathbf{C}_\mathbf{c}^\infty(\Pi;\,[0,+\infty[)$ and for any
$$c(t,x) = p_l\mathbb{1}_{x<\xi(t)}(x) + p_r\mathbb{1}_{x>\xi(t)}(x)$$
such that $(p_l,p_r) \in \widetilde{\mathcal{G}}_\alpha$;
- for any test function $\varphi \in \mathbf{C}_\mathbf{c}^\infty(\Pi;\,[0,+\infty[)$ such that $\varphi = 0$ on $x = \xi(t)$ and any constant $c(x) = c \in \mathbb{R}$.

Remark 3.5. We could define $\mathcal{G}_\alpha$-entropy process solutions, but since they do not coincide in general with $\widetilde{\mathcal{G}}_\alpha$-entropy process solutions, we do not use them here.

The fact that $\widetilde{\mathcal{G}}_\alpha$ is maximal L^1D is a necessary hypothesis in the following theorem, see [14, Th: 3.28].

Theorem 3.3. *Let $\mathcal{G}$ be a maximal L^1D germ and let ρ_0 be an initial condition for which the Cauchy problem (3.1) admits a $\mathcal{G}$-entropy solution, ρ. Then there exists a unique $\mathcal{G}$-entropy process solution μ associated to the initial condition ρ_0 and $\mu(a) = \rho$ for almost every $a \in (0,1)$.*

Thanks to the existence result proved in [58] we are then sure that our problem admits a unique solution.

In Chapter 4 of this thesis, we shall prove the convergence of the scheme relying on the $\mathbf{L}^\infty$ estimate and on the discrete solution.

3.5 A note on boundary conditions

The main equation considered in this work posed as a Cauchy problem in $\mathbb{R}$ needs to be supplemented with boundary conditions if considered in a boundary domain. Indeed implementing a finite volume scheme for (3.1) also requires a restriction of $\mathbb{R}$ to a bounded domain accompanied by appropriate set of boundary conditions that must also satisfy the weak formulations previously defined. By approximate set of boundary conditions, we mean conditions that are physically meaningful to the problem at hand and the same time fulfills the corresponding PDE. We hereby state the initial-boundary value problem for the equation studied in this work by setting $\Pi := [0,+\infty)\times]-1,1[$ and $\Pi_x =]-1,1[$.

$$\begin{cases} \partial_t \rho + \partial_x F(t,x,\rho) = 0, \ (t,x) \in \Pi, \\ \rho(0,x) = \rho_0(x), \ \text{ for } x \in \Pi_x, \\ \rho(t,\pm 1) = 0, \ \text{for } \ t > 0, \end{cases} \tag{3.52}$$

where $\rho \in [0,R]$, $F(t,x,\rho) := \operatorname{sign}(x-\xi) f(\rho)$ have the same meaning as introduced for the Cauchy problem (3.1). Following [7], we look for weak solutions in the following sense:

Definition 3.7. Assume that F, ξ satisfy the same hypothesis as in (3.1), we say that the map $(t,x) \mapsto \rho(t,x)$ is a weak entropy solution to the initial-boundary value problem (3.52), if ρ is in $\mathbf{C^0}\left([0,+\infty[;\ \mathbf{L^1}(\Omega;\ [0,R])\right)$ and for any $c \in [0,R]$, and any test function $\varphi \in \mathbf{C_c^\infty}\left(\mathbb{R}^2;\ [0,+\infty[\right)$, the following Kružkov-type entropy

inequality holds:

$$\begin{aligned}&\int_0^{+\infty}\int_{-1}^{1}\left[|\rho-c|\partial_t\varphi+\mathcal{F}(t,x,\rho,c)\partial_x\varphi\right]\mathrm{d}x\mathrm{d}t\int_{-1}^{1}|\rho_0(x)-c|\varphi(0,x)\mathrm{d}x+\\&+\int_0^{+\infty}\left[f(\rho(t,1-))-f(c)\right]\varphi(t,1)\mathrm{d}t+2\int_0^{+\infty}f(c)\varphi(t,\xi(t))\mathrm{d}t+\\&+\int_0^{+\infty}\left[f(\rho(t,-1+))-f(c)\right]\varphi(t,-1)\mathrm{d}t\geq 0,\end{aligned}\tag{3.53}$$

where $\mathcal{F}(t,x,\rho,c)=\operatorname{sign}(\rho-c)\left[F(t,x,\rho)-F(t,x,c)\right]$.

The first line in (3.53) originates from the Kružkov definition of entropy weak solution as would be in the case of a Cauchy problem, [63]. The first term in the second line and the last line comes from the boundary condition introduced by Bardos *et al* [18] where as the last term of the second line accounts for the discontinuity in the flux along the turning curve. These boundary conditions are intended in the weak form meaning that the following inequalities

$$\begin{aligned}-f(\rho(t,-1+))\geq -f(k),\text{ for all } k\in[0,\rho(t,-1+)],\\ f(\rho(t,1-))\geq f(k),\text{ for all } k\in[0,\rho(t,1-)],\end{aligned}$$

are satisfied. Compare [7] and [40] where these conditions are verified for the boundary conditions in the Hughes' model.

Chapter 4

Approximate solution and Convergence to the entropy weak solution

4.1 Introduction

In this chapter, we derive a numerical scheme that converges to the weak solution of the problem studied in this thesis. For clarity, we re-state the problem introduced in Chapter 3 below

$$\begin{cases} \partial_t \rho + \partial_x F(t,x,\rho) = 0, \ (t,x) \in \Pi, \\ \rho(0,x) = \rho_0(x), \ \text{ for } x \in \Pi_x, \\ \rho(t,\pm 1) = 0, \ \text{for } \ t > 0. \end{cases} \tag{4.1}$$

In equation (4.1), there is the existence of a function $t \mapsto \xi(t)$, here referred to as the *turning curve* or the flux interface function. Taking ξ to be piecewise linear in time, we seek to approximate weak entropy solutions to (4.1) in $\mathbf{L}^\infty$-setting using a mixture of standard and non-standard finite volume method with a moving mesh strategy near the turning curve, ξ.

There are multiple approaches that could be applied to solve equations of type (4.1) for given initial data, such as the vanishing viscosity limit [21, 75], numerical schemes such as the wave front tracking method [48, 46, 27, 23], and finite difference/volume method [24, 11, 2, 59, 60] or by solving the corresponding Hamilton-Jacobi equation of the problem, [1, 21, 4]. In this work, we use the Godunov-type scheme [50] which is an example of of finite volume methods and has been extensively used to approximate entropy weak solutions of scalar conservation laws with discontinuous flux functions. See for instance [2, 60, 10]. It is based on a numerical flux function whose input argument is the exact solution of a local Riemann problem at each vertical interface (discrete) with data from adjacent cells

ensuring that there is less numerical diffusion, the numerical flux is conservative and consistent with the flux function of the problem at hand [67]. This makes the Godunov scheme a natural choice for us. For a detailed discussion, see Chapter 2 of this thesis.

A straightforward application of the Godunov scheme in its standard form to problem (4.1) could lead to numerical inaccuracies in the solution at the turning curve. There are two main issues here that need to be addressed, namely the undercompressive (non-classical) wave at the turning curve and the space-time discretization near the turning curve. We already know from chapter 3 that the Riemann problem at the interface admits non-classical solutions, i.e. non compressive waves, and hence a non-classical Riemann solver was devised to in order to have an 'entropy' flux connection between the left and right state value of the solution at the flux interface. Furthermore, unique intermediate states appears in the evolution of the solution so as to satisfy the Rankine-Hugoniot jump condition at the interface whenever the slope of the turning curve changes in time. This leads to a non-classical Riemann solver, $\mathcal{R}^{\alpha}$ at $\xi(t)$ in which the intermediate states are captured. Therefore, the Godunov-type scheme we propose in this work uses a standard Godunov flux away from $x = \xi(t)$ and a modified numerical flux that is consistent with $\mathcal{R}^{\alpha}$ 'near' $x = \xi(t)$ for a.e $t > 0$.

On the second issue, we note that since the turning curve is time-dependent, one should expect that it may not coincide with at most one cell interface point as the solution evolves. This shall lead to severe numerical instabilities in the solution as the turning curve may interact with the self-similar solution of the local Riemann problem. Even if the turning curve does not coincide with a cell interface point but is very close to it, the 'wave' emanating from the local Riemann solver at that interface point may interact with the turning curve before the next time level. The occurrence of these scenarios shall lead to a breakdown of the straightforward application of the standard Godunov scheme to (4.1). We deal with this issue by introducing a moving mesh strategy into the scheme where the turning curve replaces any nearby interface point (i.e within $1/2\Delta x$), recomputes the density averages in adjacent cells affected by this replacement before applying the modified flux function mentioned earlier.

Finite volume schemes with moving mesh were originally developed to approximate solutions to hyperbolic problems with propagating phase boundaries, [93], and have been successfully applied to solve several problems. For instance, see [31], for an application to the study of traffic dynamics in the presence of a slow moving vehicle like a bus, which acts as a moving bottleneck. In order to satisfy the flux constraint and deal with interactions with incoming waves, a non-classical Riemann's solver at the bottleneck was enforced by locally shifting the closest cell

interfaces. The scheme used a locally nonuniform mesh at the bus trajectories and a tracking algorithm which reconstructs the bus position through its interaction with the density waves. Other applications in [26] can be found for traffic flow models with different flow regimes and in [39] for phase transition model of liquid-vapour fluids.

The chapter is organized as follows: we begin with Section 4.2 where we show that a straightforward application of the standard Godunov scheme to problem (4.1) fails. The motivates the presentation of our proposed scheme with the moving mesh near ξ in the Section 4.3. We then deduce some key properties of the scheme in Section 4.4 which would enable us to prove the convergence of the scheme in Section 4.5. Finally in Section 4.6, we validate the scheme with several examples including application to the Hughes' model of pedestrian flow. We demonstrate a numerical convergence of the scheme to the weak entropy solution in this final section.

4.2 The Godunov Scheme

In this section, we demonstrate the failure of the standard Godunov scheme when applied to (4.1). To introduce the notations, let the spatial and temporal discretization parameters $\Delta x > 0$ and $\Delta t > 0$ respectively be given such that the ratio $\frac{\Delta t}{\Delta x}$ is kept constant. Then the space domain is discretized into cells $\left[x_{j-1/2}, x_{j+1/2}\right)$, $j \in \mathbb{Z}$, where $x_{j\pm1/2} = (j \pm 1/2)\Delta x$ and the centers of each of these cells are located at $x_j = j\Delta x$. Similarly, the time interval $[0, T]$ is discretized via $t^n = n\Delta t$, for $n = 0, 1, 2, \ldots, N$, where $N := \left\lfloor T/\Delta t \right\rfloor + 1$. We denote by ρ_j^n, the piecewise constant approximate solution $x \mapsto \rho(t^n, x)$ of (4.1).

Given $\rho_0(x) \in \mathbf{L}^\infty$, discretize the initial data in each cell by

$$\rho_j^0 = \frac{1}{\Delta x} \int_{x_{j-1/2}}^{x_{j+1/2}} \rho_0(x)dx, \quad \text{for all } j \in \mathbb{Z}. \tag{4.2}$$

With the slope of the turning curve given *a priori*, we assign $\xi^0 = \xi(0)$ as the initial position of ξ and discretize $k(t, x)$, the flux coefficient at $t = 0$ as $k_{j+1/2}^0 = \text{sign}(x_{j+1/2} - \xi^0)$. The standard Godunov scheme consists in two main steps:

Step 1:
Solve the following Riemann problem of our PDE model at each interface $x_{j+1/2}$:

$$\begin{cases} \partial_t \hat{\rho} + \partial_x \left(\text{sign}(x_{j+1/2} - \xi^n) f(\hat{\rho}) \right) = 0, \\ \hat{\rho}_0(x) = \begin{cases} \rho_j^n & x < x_{j+1/2} \\ \rho_{j+1}^n & x \geq x_{j+1/2}, \end{cases} \end{cases} \tag{4.3}$$

for $t \in [0, \Delta t]$ to obtain

$$\hat{\rho}(t,x) = \hat{\rho}\left(\frac{x - x_{j+1/2}}{t - t^n}; \rho_j^n, \rho_{j+1}^n \right) \text{ for all } (t,x) \in [0, \Delta t] \times C_j,$$

a self-similar solution of (4.3). Note that here the data at $t = 0$ is obtained from (4.2) above and the temporal parameter Δt, is chosen according to the CFL condition

$$\Delta t \leq \frac{\Delta x}{2 \cdot \max \left\| f_{\hat{\rho}} \right\|}. \tag{4.4}$$

The solution to (4.3) over the entire space domain is given by "gluing together" all the self-similar solutions at each interface so that $\hat{\rho}(t,x)$ is piecewise constant at each time.

Step 2:
In the next step, we project the piecewise constant solution obtained in step **1** over each cell C_j at time t^{n+1}, via the update formula:

$$\rho_j^{n+1} = \frac{1}{\Delta x} \int_{x_{j-1/2}}^{x_{j+1/2}} \hat{\rho}(\Delta t, x) dx, \quad \text{for all } j \in \mathbb{Z}. \tag{4.5}$$

The following simplifications can be made from (4.5). In the figure 4.1, we integrate the PDE in (4.3) over the element $E = (pqrs)$ and apply the Green's theorem to get

$$\begin{aligned} 0 &= \int \int_E \partial_t \hat{\rho} + \partial_x \left(\text{sign}(x_{j+1/2} - \xi^n) f(\hat{\rho}) \right) dx dt \\ 0 &= \Delta x \rho_j^{n+1} - \Delta x \rho_j^n + \int_0^{\Delta t} k_{j+1/2}^n f(\hat{\rho}(\mathbf{0}^-; \rho_j^n, \rho_{j+1}^n)) dt \\ &\quad - \int_0^{\Delta t} k_{j-1/2}^n f(\hat{\rho}(\mathbf{0}^+; \rho_{j-1}^n, \rho_j^n)) dt, \end{aligned} \tag{4.6}$$

where $\mathbf{0}^{\pm}$ represents the traces in the Riemann solution at the interfaces $x_{j \pm 1/2}$. We

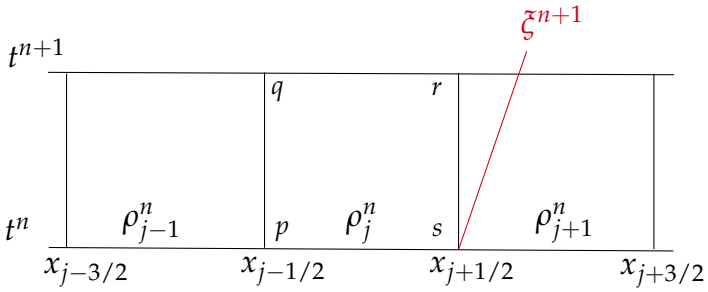

FIGURE 4.1: Cell averages with the Riemann problems at each interface.

use $\mathbf{0}$ with the inspiration that the cell interface is vertical w.r.t. time and hence the quantity $(x - x_{j+1/2})/(t - t^n)$ is zero at each interface. If the flux across the interface is defined by

$$F\left(k^n_{j\pm1/2}; \rho^n_j, \rho^n_{j+1}\right) := k^n_{j\pm1/2} f(\hat{\rho}(\mathbf{0}^{\pm}; \rho^n_j, \rho^n_{j+1})),$$

the the time marching formula can be obtained from (4.6) as

$$\rho^{n+1}_j = \rho^n_j - \frac{\Delta t}{\Delta x}\left[F\left(k^n_{j+1/2}; \rho^n_j, \rho^n_{j+1}\right) - F\left(k^n_{j-1/2}; \rho^n_{j-1}, \rho^n_j\right)\right]. \tag{4.7}$$

For any given $k^n_{j+1/2} < 0$(or $k^n_{j+1/2} > 0$), the numerical flux function satisfies the Rankine-Hugoniot condition at $x_{j+1/2}$

$$k^n_{j+1/2} f(\hat{\rho}(\mathbf{0}^+; \rho^n_j, \rho^n_{j+1})) = k^n_{j+1/2} f(\hat{\rho}(\mathbf{0}^-; \rho^n_j, \rho^n_{j+1})) \tag{4.8}$$

if $\hat{\rho}(\mathbf{0}^-; \rho^n_j, \rho^n_{j+1})$ is continuous or discontinuous along the line $x_{j+1/2}$. In the latter case, a stationary shock located at the interface leads to the condition (4.8). Let's introduce the standard Godunov flux

$$\bar{h}(p, q) = \begin{cases} \min\limits_{\rho\in[p,q]} f(\rho), & \text{if} \quad p < q, \\ \max\limits_{\rho\in[q,p]} f(\rho), & \text{if} \quad p \geq q, \end{cases} \tag{4.9}$$

which can be deduced on case by case basis from the solution of the Riemann problem at the cell interface from which the numerical flux in (4.7), can be written

as

$$F\left(k^n_{j+1/2};\rho^n_j,\rho^n_{j+1}\right) = \begin{cases} \bar{h}(\rho_j,\rho_{j+1}), & \text{if } k^n_{j+1/2} < 0, \\ h^\alpha(\rho_j,\rho_{j+1}), & \text{if } k^n_{j+1/2} = 0, \\ \bar{h}(\rho_{j+1},\rho_j), & \text{if } k^n_{j+1/2} > 0, \end{cases} \tag{4.10}$$

where h^α is defined by

$$h^\alpha(\rho^n_j,\rho^n_{j+1}) = \begin{cases} \bar{h}(\rho_j,\rho_{j+1}), & \text{if } \alpha > v(\rho^n_{j+1}), \\ \bar{h}(\rho_{j+1},\rho_j), & \text{if } \alpha < -v(\rho^n_j), \\ 0, & \text{otherwise}, \end{cases} \tag{4.11}$$

is the modified flux at the turning curve. At the next time step, the turning curve is

$$\xi^{n+1} = \xi^n + \alpha_n \Delta t, \quad \forall n \in \mathbb{N}. \tag{4.12}$$

It must be noted that the Godunov's flux $\bar{h}(q,p)$ is Lipschitz continuous with respect to both arguments and consistent with f, meaning that $\bar{h}(p,p) = f(p)$. This also implies that the flux function (4.10) is consistent with the flux function of the problem (4.3) and hence holds also for (4.1).

4.2.1 The failure of the standard scheme

Since the solution to the Riemann problem is explicitly known from section 3.1.3, computing the traces at $\mathbf{0}^+$ and $\mathbf{0}^-$ away from the turning curve is does not present a problem in the scheme presented above. Indeed the Rankine-Hugoniot condition (4.8) is trivially satisfied at the turning curve (which also correspond to $x_{j+1/2} = \xi^n$ for any fixed $n \in \mathbb{N}$). However, observe that the Riemann solver at the turning curve is not classical and so, where the turning curve coincides with the interface, the line $x_{j+1/2}$ is no longer a straight vertical line. Without a proper treatment of the turning curve and the closest cell interface from the previous time step, the state value ρ^{n+1}_j resulting from the update formula can be over- or underestimated since the averaging procedure at the next time step shall not consider the varying size of the adjacent. This leads to the following two implications: (1) the input of the numerical flux may not result from the non-classical Riemann solver at ξ as presented in section 3.1.3. This shall occur at the next time step where after applying (4.12), the turning curve coincides with no cell interface. (2) If the scheme is designed to ensure that the turning curve coincides with at most one interface, then the cells adjacent to the turning curve have non-uniform sizes. The standard scheme fails to accommodate the non-uniform sizes of these cells. As a consequence of point (1), we yet modify the numerical flux at the turning curve where

we introduce a moving mesh strategy in the scheme to resolve the problem posed by (2).

4.3 A finite volume scheme with moving mesh

In this section, we present the numerical scheme that deals with the numerical instabilities observed at the turning curve in the straightforward application of the standard Godunov scheme to (4.1). Our strategy consists in adapting the finite volume mesh near to ξ such that ξ is actually a cell interface point at which the solution of the non classical Riemann solver $(\mathcal{R}^\alpha)$ will have to be computed and a modified numerical flux defined accordingly. This is a slight departure from the mesh adaptation strategy introduced in [93] and applied in [31], where one replaces the cell interface nearest to ξ and shifts an adjacent interface point after which new temporal density averages are computed in the two adjacent cells by a Lagrange interpolation formula. Even though this scheme is conservative, the re-computation of the new averages makes it impossible to proof the well-balanced property of such scheme.

As the scheme introduced here does not use a re-computation formula, the well-balanced property is straightforward. This would allow one to prove the convergence of the scheme to the weak entropy solution.

We use the following notations, let

- $\Delta t > 0$ be the time step,
- $x^n_{j+1/2}$ be the set of grid points for $j \in \mathbb{Z}$, at time t^n,
- C_j, be a computational cell, and C^n_j the computational cells at t^n,
- Δx be the length of the cell C_j and Δx^n_j, the length of each cell at time t^n.

4.3.1 Discretization

Let $\Delta x > 0$ fixed, and $x_{j+1/2} := (j + 1/2)\Delta x$ be the set of cell interface points with centers $x_j = j\Delta x$, for $J_0 < j < J_1$, where

$$J_0 = \left[-\frac{1}{\Delta x} + \frac{1}{2}\right], \qquad J_1 = \left[\frac{1}{\Delta x} - \frac{1}{2}\right].$$

Here above, $[x]$ denotes the integer part of the real number x, that is, the only integer that satisfies $[x] \leq x < [x] + 1$. Then, let set $\mathbb{Z}^* := \{j \in \mathbb{Z} : J_0 \leq j \leq J_1\}$. That is J_0, J_1 are indices of the computational cells (to be properly defined later) satisfying $-1 \in \overline{C}_{J_0}$ and $1 \in \overline{C}_{J_1}$ respectively.

For a fixed $T > 0$, choose $\Delta t > 0$, and discretize the time interval $[0, T]$ by $t^n = n\Delta t$, for all $n \in \mathbb{N}$. Suppose that the turning point curve is given by $t \mapsto \xi(t) \in \mathbf{Lip}\big([0,T],(-1,1)\big)$, and denote by $\alpha \in \mathbb{R}$ its slope discretized by

$$\alpha^n = \frac{1}{\Delta t}\int_{t^n}^{t^{n+1}} \xi'(t)dt, \qquad n \in \mathbb{N},$$

then trajectories of the turning curve is discretized by (4.12) which we repeat as $\xi^{n+1} = \xi^n + \alpha^n \Delta t$.

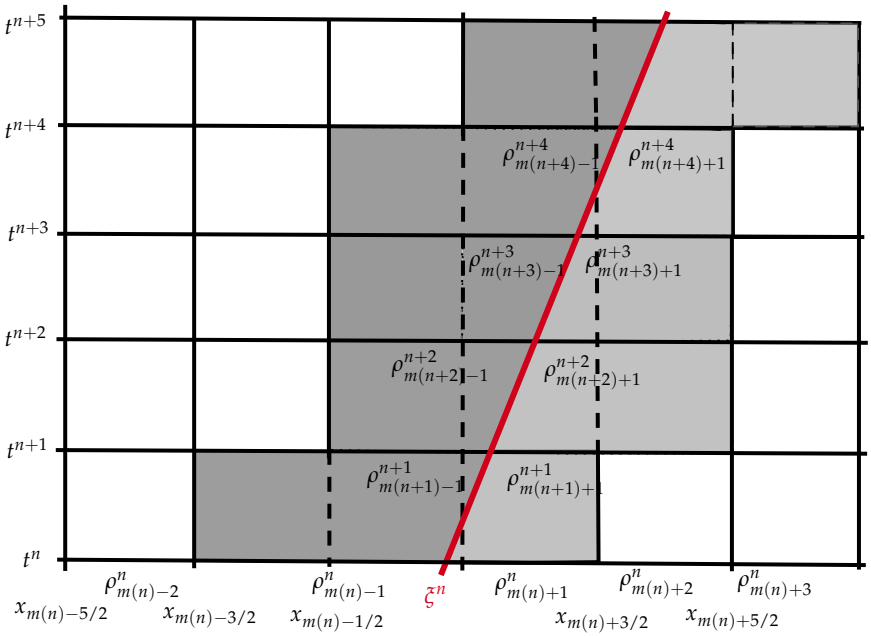

FIGURE 4.2: Illustration of cases A and B. Dashed lines is used to imply that the corresponding cell boundary is cancelled.

Starting from $x_{j+1/2}$, the *moving mesh* at each time t^n, denote $\mathcal{T}^n_{j+1/2}$ is given as

$$\mathcal{T}^n_{j+1/2} := \begin{cases} x_{j-1/2}, & \text{if } j \le m(n)-1, \\ \xi^n, & \text{if } j = m(n), \\ x_{j+1/2}, & \text{if } j \ge m(n)+1, \end{cases} \tag{4.13}$$

where $m(n) \in \mathbb{Z}^*$ is unique such that $\xi^n \in \Big[x_{m(n)-1/2},\ x_{m(n)+1/2}\Big)$ for every n.

This implies that the set of intervals $C_j := \big[x_{j-1/2}, x_{j+1/2}\big)$ for each $j \le m(n)-2$ and $C_{j+1} := \big[x_{j-1/2}, x_{j+1/2}\big)$ for each $j \ge m(n)+2$ have fixed length of Δx, and are

parts of the computational cell. The remaining parts are for $j = m(n) \pm 1$ defined by $C_{m(n)-1} := \left[x_{m(n)-3/2},\, \xi^n\right)$ and $C_{m(n)+1} := \left[\xi^n,\, x_{m(n)+3/2}\right)$ with variable sizes $\Delta x_{m(n)-1} := \xi^n - x_{m(n)-3/2}$ and $\Delta x_{m(n)+1} := x_{m(n)+3/2} - \xi^n$ respectively. Then

$$C_j^n := C_j \times \left[t^n, t^{n+1}\right), \quad \forall j \in \mathbb{Z}^* \setminus m(n), \ \ \forall n \in \mathbb{N},$$

represents the computational cells and

$$\widetilde{\Pi} := \bigcup_{n\in\mathbb{N}} \bigcup_{j\neq m(n)} C_j^n.$$

as the cell grid discretization of Π. Assume the following CFL condition

$$\Delta t \max\left\{\left\|f'\right\|_\infty, \left\|\xi'\right\|_\infty\right\} \leq \frac{1}{2}\Delta x, \tag{4.14}$$

then in projecting the grid at time t^{n+1}, three cases arises for the definition of the moving mesh $\mathcal{T}_{j+1/2}^{n+1}$ namely, Case **A**: $m(n+1) = m(n)$, Case **B**: $m(n+1) = m(n)+1$ and Case **C**: $m(n+1) = m(n)-1$.

Indeed, if the CFL condition (4.14), holds then $\left|\xi^{n+1} - \xi^n\right| \leq 1/2\Delta x$ and that the turning curve $\xi(t)$ crosses at most one boundary cell in the time strip $\left[t^n, t^{n+1}\right)$. The third case is possible only if $\alpha_n < 0$ and since the solution to (4.1) is symmetric, we conclude that this case is very similar to that of cases **A** with **B**. For this reason, we shall present the scheme in the light of only cases **A** and **B**.

Case A: $m(n+1) = m(n)$. This case leads to the same definition of the mesh as in (4.13). Then $\mathcal{T}_{j+1/2}^{n+1} = \mathcal{T}_{j+1/2}^{n}$, $\forall j \in \mathbb{Z}^*$ and $\forall n \in \mathbb{N}$. See Figure 4.3.

Case B: $m(n+1) = m(n)+1$. Here it can be noticed that the line joining (ξ^n, t^n) and (ξ^{n+1}, t^{n+1}) crosses the vertical line $x = x_{m(n)+1/2}$. See Figure 4.4. The moving mesh at t^{n+1}, is similarly updated as

$$\mathcal{T}_{j+1/2}^{n+1} := \begin{cases} x_{j-1/2}, & \text{if } j \leq m(n+1)-1, \\ \xi^{n+1}, & \text{if } j = m(n+1), \\ x_{j+1/2}, & \text{if } j \geq m(n+1)+1. \end{cases} \tag{4.15}$$

The intervals $\left[x_{m(n)-1/2},\, \xi^{n+1}\right)$ and $\left[\xi^{n+1},\, x_{m(n)+5/2}\right)$ are the cells adjacent to ξ^{n+1} respectively from the left and right. With the exception of these two intervals, all other intervals at t^{n+1} have the fixed size of Δx. The computational cells are then updated accordingly.

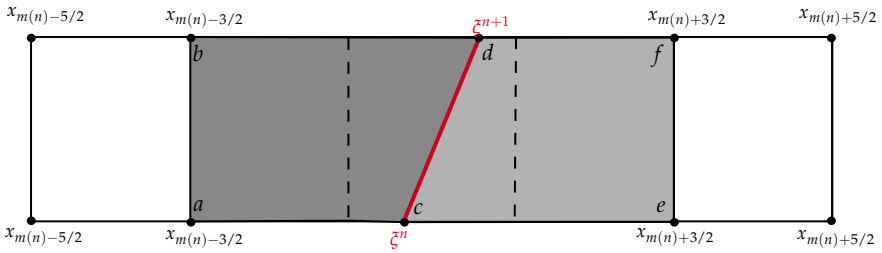

FIGURE 4.3: Illustration of mesh adaptation for Case **A**.

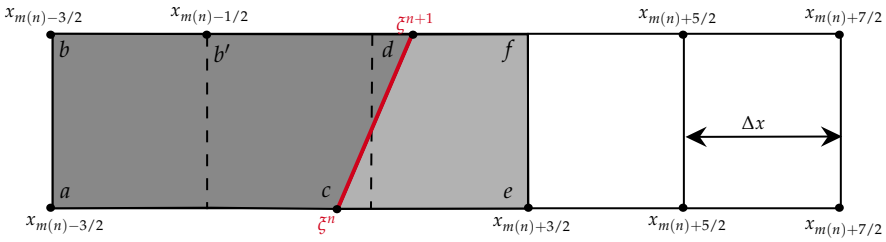

FIGURE 4.4: Illustration of mesh adaptation for Case **B**. In this case, the indices of the mesh is shifted forward by one after projecting the mesh at t^{n+1}.

Remark 4.1. In Case **B**, note that while the grid point $x_{m(n)-1/2}$ is now included in the mesh, the grid point $x_{m(n)+3/2}$ is excluded at t^{n+1}.

Remark 4.2. This discretization procedure ensures that at each time, t^n the total length of the two cells adjacent to ξ^n, from the left and right is $3\Delta x$. Furthermore, the total number of computational cells at each time is kept constant. See Figure 4.2.

4.3.2 The Numerical scheme

We now proceed to derive the numerical scheme. Recall that ρ_j^n, is the piecewise constant approximate solution $x \mapsto \rho(t^n, x)$ of (4.1). At t^n, the approximate solution is

$$\rho(t^n,x) = \sum_{j=J_0}^{m(n)-2} \rho_j^n \mathbb{1}_{C_j}(x) + \rho_{m(n)-1}^n \mathbb{1}_{[x_{m(n)-3/2},\xi^n)}(x) + \rho_{m(n)+1}^n \mathbb{1}_{[\xi^n, x_{m(n)-3/2})}(x) + \sum_{j=m(n)+2}^{J_1} \rho_j^n \mathbb{1}_{C_{j+1}}(x). \tag{4.16}$$

We start by discretizing the initial data $\rho_0(x) \in \mathbf{L}^\infty(\mathbb{R})$ with discretized by:

$$\rho_j^0 = \begin{cases} \frac{1}{\Delta x}\int_{x_{j-1/2}}^{x_{j+1/2}} \rho_0(x)dx, & j \neq m(0) \pm 1, \\ \frac{1}{\xi^0 - x_{m(0)-3/2}}\int_{x_{m(0)-3/2}}^{\xi^0} \rho_0(x)dx, & j = m(0)-1, \\ \frac{1}{x_{m(0)+3/2}-\xi^0}\int_{\xi^0}^{x_{m(0)+3/2}} \rho_0(x)dx, & j = m(0)+1. \end{cases} \tag{4.17}$$

This choice implies that $\left(\rho_j^0\right)_{j\in\mathbb{Z}^*\setminus m(0)}$ is its mean value on the computational cells. To simplify the notations, lets denote the following functions

$$h^{n-}_{j+1/2}(a,b) = \bar{h}(b,a) \qquad h^{n+}_{j+1/2}(a,b) = \bar{h}(a,b) \tag{4.18}$$

as the numerical flux if $x < \xi(t)$, and $x > \xi(t)$ respectively, where $\bar{h}$ represents the Godunov flux function already given in (4.9). At $x = \xi(t)$, we use the modified flux h^α,

$$h^\alpha(a,b) = \begin{cases} f(b) - \alpha b, & \text{if } \alpha > v(b), \\ -f(a) - \alpha a, & \text{if } \alpha < -v(a), \\ 0, & \text{otherwise}, \end{cases} \tag{4.19}$$

coming from the non-classical Riemann solver $\mathcal{R}^\alpha$ introduced in section 3.1.3.

If $j \leq m(n) - 2$ and $j \geq m(n) + 2$, the standard time marching formulas with the standard Godunov flux from (4.9) (here denoted as $h^{n-}_{j+1/2}(\rho_j^n, \rho_{j+1}^n)$ if $j \leq m(n) - 2$ and $h^{n+}_{j+1/2}(\rho_j^n, \rho_{j+1}^n)$ if $j \geq m(n) + 2$) becomes respectively as

$$\rho_j^{n+1} = \rho_j^n - \frac{\Delta t}{\Delta x}\left[h^{n-}_{j+1/2}(\rho_j^n, \rho_{j+1}^n) - h^{n-}_{j-1/2}(\rho_{j-1}^n, \rho_j^n)\right]. \tag{4.20a}$$

and

$$\rho_j^{n+1} = \rho_j^n - \frac{\Delta t}{\Delta x}\left[h^{n+}_{j+1/2}(\rho_j^n, \rho_{j+1}^n) - h^{n+}_{j-1/2}(\rho_{j-1}^n, \rho_j^n)\right]. \tag{4.20b}$$

If $j = m(n) \pm 1$, we derive first the formulae of the Riemann solver at ξ^n for case **B** and infer for the other cases. Consider the elements $E_1 = (acdb)$ and $E_2 = (cefd)$ to be computational cells of interest. See Figure 4.4. Then by conservation, the following integral over $E = E_1 \cup E_2$ should satisfy:

$$\iint_E \left(\partial_t \rho + \partial_x F(t,x,\rho)\right) dxdt = 0.$$

We detail the derivation over E_1. By applying the Green's theorem and integrating along the interface in E_1 give:

$$\int_{x_{m(n+1)-3/2}}^{\xi^{n+1}} \rho(t^{n+1},x)dx = \int_{x^n_{m(n)-3/2}}^{\xi^n} \rho(t^n,x)dx$$
$$- \int_{t^n}^{t^{n+1}} \left[F\left(t,\xi(t),\mathcal{R}^{\alpha^n}(\rho^n_{m(n)-1},\rho^n_{m(n)+1})\right) - F\left(t,x_{m(n)-3/2},\mathcal{R}^-(\rho^n_{m-2},\rho^n_{m(n)-1})\right)\right] dt.$$

Set $\rho^{n+1}_{m(n+1)-1}$ the average of ρ on $\left[x^{n+1}_{m(n+1)-3/2},\xi^{n+1}\right)$ defined by

$$\rho^{n+1}_{m(n+1)-1} := \frac{1}{\xi^{n+1}-x_{m(n+1)-3/2}} \int_{x_{m(n+1)-3/2}}^{\xi^{n+1}} \rho(t^{n+1},x)dx.$$

This leads to the marching formula

$$\left(\xi^{n+1}-x_{m(n+1)-3/2}\right)\rho^{n+1}_{m(n+1)-1} = \left(\xi^n - x_{m(n)-3/2}\right)\rho^n_{m(n)-1}$$
$$- \Delta t\left[h^{\alpha^n}\left(\rho^n_{m(n)-1},\rho^n_{m(n)+1}\right) - h^{n-}\left(\rho^n_{m(n)-2},\rho^n_{m(n)-1}\right)\right] \tag{4.21}$$

Similarly the update formula in $C_{m(n)+1}$ writes

$$\left(x_{m(n+1)+3/2}-\xi^{n+1}\right)\rho^{n+1}_{m(n+1)+1} = \left(x_{m(n)+3/2}-\xi^n\right)\rho^n_{m(n)+1} + \Delta x\rho^n_{m(n)+2}$$
$$- \Delta t\left[h^{n+}(\rho^n_{m(n)+1},\rho^n_{m(n)+2}) - h^{\alpha^n}\left(\rho^n_{m(n)-1},\rho^n_{m(n)+1}\right)\right] \tag{4.22}$$

For case **A**, the same procedure yields the time marching formula if $j = m(n)-1$

$$\left(\xi^{n+1}-x_{m(n+1)-3/2}\right)\rho^{n+1}_{m(n+1)-1} = \left(\xi^n - x_{m(n)-3/2}\right)\rho^n_{m(n)-1}$$
$$- \Delta t\left[h^{\alpha^n}\left(\rho^n_{m(n)-1},\rho^n_{m(n)+1}\right) - h^{n-}\left(\rho^n_{m(n)-2},\rho^n_{m(n)-1}\right)\right], \tag{4.23}$$

whereas if $j = m(n)+1$, it writes

$$\left(x_{m(n+1)+3/2} - \xi^{n+1}\right)\rho^{n+1}_{m(n+1)+1} = \left(x_{m(n)+3/2} - \xi^{n}\right)\rho^{n}_{m(n)+1} - \Delta t\left[h^{n+}\left(\rho^{n}_{m(n)+1}, \rho^{n}_{m(n)+2}\right) - h^{\alpha^n}\left(\rho^{n}_{m(n)-1}, \rho^{n}_{m(n)+1}\right)\right]. \tag{4.24}$$

Compared with the scheme presented of the section 4.2, this modified scheme has a moving grid at $x = \xi(t)$ where a non-classical Godunov-type flux is also applied. Obviously, the interface line corresponding to the turning curve is non-vertical. Therefore the discretization ensures that $\xi(t)$ is also a numerical cell interface point. A key advantage of the scheme is that it accounts for the non-uniform sizes of the two cells adjacent to the turning curve at each time. Using the equations (4.20 - 4.24), the approximate solution over the entire domain a.e. is obtained by patching together the piecewise constant values

$$\rho^{\Delta}(t,x) := \sum_{n\in\mathbb{N}}\sum_{j=J_0}^{m(n)-1}\rho^{n}_{j}\mathbb{1}_{[n\Delta t,(n+1)\Delta t)}(t)\mathbb{1}_{[x_{j-1/2},x_{j+1/2})} + \sum_{n\in\mathbb{N}}\sum_{j=m(n)+1}^{J_1}\rho^{n}_{j}\mathbb{1}_{[n\Delta t,(n+1)\Delta t)}(t)\mathbb{1}_{[x_{j-1/2},x_{j+1/2})}. \tag{4.25}$$

We make the following remarks:

Remark 4.3. Following Remark 4.1, numerical conservation in (4.20a), implies putting the same density value over the sub-intervals $\left[x_{m(n)-3/2},\ x_{m(n)-1/2}\right)$, and $\left[x_{m(n)-1/2},\ \xi^{n+1}\right)$ at time t^{n+1}.

4.4 Analysis of the scheme

It would be interesting to analyse the mathematical properties of the above scheme so that questions regarding consistency, stability, entropy conditions and convergence to entropy solutions can be addressed. The non-uniform meshes near the turning curve which also leads to the moving mesh complicates the rigorous analysis of the convergence of the scheme. In this section, we deduce some preliminary properties that could pave way to further prove the of the numerical scheme presented above.

4.4.1 Conservation and well-balanced

It is well-known that in general non conservative schemes converges to wrong solutions [55]. Indeed our choice of flux function in the above scheme as well as the mesh adaptation near the flux interface obscures the obviousness of the conservative property of the scheme. In the next proposition, we show that the scheme is conservative and so by the Lax-Wendroff Theorem [64] gives hope that it converges to a weak solution of (4.1).

Proposition 4.1. *The numerical scheme proposed is conservative and thus satisfies*

$$\sum_{\substack{j=J_0,\\ j\neq m(n+1)}}^{J_1} \rho_j^{n+1}\Delta x_j^{n+1} = \sum_{\substack{j=J_0,\\ j\neq m(n)}}^{J_1} \rho_j^{n}\Delta x_j^{n} - \Delta t\left(h^{n+}_{J_1+1/2} - h^{n-}_{J_0-1/2}\right) \tag{4.26}$$

Proof. To show that the scheme is conservative, we start by observing that the approximate solution satisfies the following integral

$$\int_{-1}^{1}\rho(t^{n+1},x)dx = \int_{-1}^{\xi^{n+1}}\rho(t^{n+1},x)dx + \int_{\xi^{n+1}}^{1}\rho(t^{n+1},x)dx. \tag{4.27}$$

Equivalently, this can be written for Case **B** as

$$\begin{aligned}\sum_{\substack{j=J_0,\\ j\neq m(n)+2}}^{J_1} \rho_j^{n+1}\Delta x_j^{n+1} = \sum_{j=J_0}^{m(n)-2} \rho_j^{n+1}\Delta x_j^{n+1} + \left(\xi^{n+1} - x_{m(n+1)-3/2}\right)\rho^{n+1}_{m(n+1)-1}\\ + \left(x_{m(n+1)+3/2} - \xi^{n+1}\right)\rho^{n+1}_{m(n+1)+1} + \sum_{j=m(n)+3}^{J_1}\rho_j^{n+1}\Delta x_j^{n+1}.\end{aligned} \tag{4.28}$$

Substituting (4.20), (4.21) and (4.22) for ρ_j^{n+1}, performing telescoping summation, collecting and cancelling the flux terms leads to

$$\begin{aligned}\sum_{\substack{j=J_0,\\ j\neq m(n)+2}}^{J_1} \rho_j^{n+1}\Delta x_j^{n+1} = \sum_{j=J_0}^{m(n)-2} \rho_j^{n}\Delta x + \left(\xi^{n} - x_{m(n)-3/2}\right)\rho^{n}_{m(n)-1}\\ + \left(x_{m(n)+3/2} - \xi^{n}\right)\rho^{n}_{m(n)+1} + \Delta x\rho^{n}_{m(n)+2} + \sum_{j=m(n)+3}^{J_1}\rho_j^{n}\Delta x\\ -\Delta t\left(h^{n+}_{J_1+1/2} - h^{n+}_{J_0-1/2}\right).\end{aligned}$$

The r.h.s of the above equation is clearly equivalent to that of (4.26). A similar consideration if case **A** leads to the same conclusion concluding the proof. □

We now turn our attention to the 'well-balanced' property of the scheme. The basic idea of well-balanced schemes the approximate solution exactly preserves the steady states solution of the problem. According to the analysis of Chapter 3 of this thesis, we shall be interested in stationary solutions that the form $\rho(t,x) = \rho_L \mathbb{1}_{x<\xi(t)} + \rho_R \mathbb{1}_{x>\xi(t)}$ with ρ_L, ρ_R belonging $\mathcal{G}_\alpha$ [15]. Indeed, the definition of the numerical flux functions and the consistency, this scheme verifies the *well-balance property* of the solutions of (4.1). We prove this property in the next lemma.

Lemma 4.1. *Let $t \mapsto \xi(t) = \alpha t$ for $\alpha \in \mathbb{R}$ and choose $(\rho_L, \rho_R) \in [0,R]^2$ such that*

$$f(\rho_R) - \alpha\rho_R = -f(\rho_L) - \alpha\rho_R, \tag{4.29}$$

holds and consider the initial condition

$$\rho_0(x) = \begin{cases} \rho_L, & \text{if } x < \xi(0), \\ \rho_R, & \text{if } x > \xi(0). \end{cases} \tag{4.30}$$

Then numerical scheme (4.20 - 4.24) preserves the exact states from (4.30), $\rho(t,x) = \rho_L \mathbb{1}_{\{x<\xi(t)\}} + \rho_R \mathbb{1}_{\{x>\xi(t)\}}$. Thus

$$\rho_j^n = \rho_L \mathbb{1}_{\{j\le m(n)-1\}} + \rho_R \mathbb{1}_{\{j\ge m(n)+1\}}, \qquad \forall n \ge 0. \tag{4.31}$$

Proof. We prove by induction. We make the prove for case B, case A is analogous. Suppose we are given the initial mesh, $\mathcal{T}^0_{j+1/2}$, then clearly $\rho_j^0 = \rho_L$, if $j \le m(0) - 1$, and $\rho^0_{m(0)+1} = \rho_R$ if $j \ge m(0) + 1$ thanks to the discretized $\rho_0(x)$ in (4.17).
This implies that If $j \le m(1) - 2 = m(0) - 1$, then

$$\rho_j^1 = \rho_j^0 - \frac{\Delta t}{\Delta x}\left[h^{0-}(\rho_j^0, \rho_{j+1}^0) - h^{0-}(\rho_{j-1}^0, \rho_j^0)\right] = \rho_L,$$

and if $j \ge m(1) + 2$

$$\rho_j^1 = \rho_j^0 - \frac{\Delta t}{\Delta x}\left[h^{0+}(\rho_j^0, \rho_{j+1}^0) - h^{0+}(\rho_{j-1}^0, \rho_j^0)\right] = \rho_R,$$

Indeed if $j = m(1) - 1$, then (4.21) writes

$$\begin{aligned}\rho^1_{m(1)-1} &= \frac{\rho^0_{m(0)-1}\left(\xi^0 - x_{m(0)-3/2}\right) - \Delta t\left[h^\alpha - h^{0-}_{m(0)-3/2}\right]}{\xi^1 - x_{m(1)-3/2}} \\ &= \frac{\rho_L(\xi^0 - x_{m(0)-3/2}) + \alpha^0\rho_L\Delta t}{\xi^1 - x_{m(1)-3/2}} = \rho_L,\end{aligned}$$

using $h^\alpha\left(\rho^0_{m(0)-1}, \rho^0_{m(0)+1}\right) = -f(\rho_L) - \alpha\rho_L$ by (4.29) and $\xi^1 = \xi^0 + \alpha^0\Delta t$, and that $x_{m(1)-3/2} = x_{m(0)-1/2}$ for the Case **B**.

Similarly if $j = m(1) + 1$, then the right density average (4.22) leads to

$$\begin{aligned}\rho^1_{m(1)+1} &= \frac{(x_{m(0)+3/2} - \xi^0)\rho^0_{m(0)+1} + \Delta x\rho^0_{m(0)+2} - \Delta t\left[h^{0+}_{m(0)+3/2} - h^\alpha\right]}{x_{m(1)+3/2} - \xi^1} \\ &= \frac{(x_{m(0)+3/2} - \xi^0)\rho_R + \Delta x\rho_R - \Delta t\left[h^{0+}_{m(0)+3/2} - h^\alpha\right]}{x_{m(0)+5/2} - \xi^1} = \rho_R,\end{aligned}$$

since $h^{0+}_{m(0)+3/2} - h^\alpha = \alpha\rho_R$ and $\rho^0_j = \rho_R, j \geq m(0) + 1$. A similar computation for the Case **A** yields the same result and hence omitted to avoid repetition. This implies that for $n \geq 1$, we can iterate this to have

$$\rho^n_j = \frac{1}{|C^n_j|}\int_{x^n_{j-1/2}}^{x^n_{j+1/2}} \rho(t^n, x)dx, \qquad \forall j \in \mathbb{Z}^* \setminus \{m(n)\},$$

given in (4.31), completing the proof. □

Recall the complete admissibility germ, $\mathcal{G}_\alpha$ defined in Chapter 3 of this thesis. A useful interpretation of this lemma is that if $\rho_0 \in \mathcal{G}_\alpha$, then the approximate solution with the adapted mesh scheme also belongs to the germ. This will come in handy when one needs to prove convergence of the scheme to $\mathcal{G}$ entropy process solutions using the $\mathbf{L}^\infty$ stability estimate and the discrete entropy inequality.

For the remaining sections, we introduce the following functions in order to keep the presentation of the scheme simple

$$\mathcal{H}_{m(n)-1}(a, b, c) = \frac{\left(\xi^n - x_{m(n)-3/2}\right)b - \Delta t\left[h^\alpha(b, c) - h^{n-}(a, b)\right]}{\xi^{n+1} - x_{m(n+1)-3/2}}, \tag{4.32a}$$

$$\mathcal{H}_{m(n)}(a,b,c) = \frac{\left(x_{m(n)+3/2} - \xi^n\right) b - \Delta t \left[h^{n+}(b,c) - h^{\alpha}(a,b)\right]}{x_{m(n+1)+3/2} - \xi^{n+1}}, \tag{4.32b}$$

$$\mathcal{H}_{m(n)+1}(a,b,c) = \frac{\left(x_{m(n)+3/2} - \xi^n\right) b + \Delta x c - \Delta t \left[h^{n+}(b,c) - h^{\alpha}(a,b)\right]}{x_{m(n+1)+3/2} - \xi^{n+1}}. \tag{4.32c}$$

These functions are the distinct marching formulae based on the equations (4.21), (4.22) and (4.24).
The resulting finite volume scheme comes down to the following set of equations:

for $j \leq m(n+1) - 2$,

$$\rho_j^{n+1} = \rho_j^n - \frac{\Delta t}{\Delta x}\left[h^{n-}_{j+1/2}(\rho_j^n, \rho_{j+1}^n) - h^{n-}_{j-1/2}(\rho_{j-1}^n, \rho_j^n)\right], \quad \forall n \in \mathbb{N}, \tag{4.33}$$

$$\rho^{n+1}_{m(n+1)-1} = \mathcal{H}_{m(n)-1}\left(\rho^n_{m(n)-2}, \rho^n_{m(n)-1}, \rho^n_{m(n)+1}\right), \quad \text{either } \mathbf{A} \text{ or } \mathbf{B}\ , \forall n \in \mathbb{N}, \tag{4.34}$$

$$\rho^{n+1}_{m(n+1)+1} = \begin{cases} \mathcal{H}_{m(n)}(\rho^n_{m(n)-1}, \rho^n_{m(n)+1}, \rho^n_{m(n)+2}), & \text{if Case } \mathbf{A}, \\ \mathcal{H}_{m(n)+1}(\rho^n_{m(n)-1}, \rho^n_{m(n)+1}, \rho^n_{m(n)+2}), & \text{If Case } \mathbf{B}, \end{cases} \quad \forall n \in \mathbb{N}, \tag{4.35}$$

for $j \geq m(n+1) + 2$,

$$\rho_j^{n+1} = \rho_j^n - \frac{\Delta t}{\Delta x}\left[h^{n+}_{j+1/2}(\rho_j^n, \rho_{j+1}^n) - h^{n+}_{j-1/2}(\rho_{j-1}^n, \rho_j^n)\right], \quad \forall n \in \mathbb{N}, \tag{4.36}$$

with ρ_j^0 given by (4.17), $\forall j \in \mathbb{Z}^*$.

4.4.2 Stability of the scheme

In the next lemma, we prove an $\mathbf{L}^\infty-$estimate on the approximate solution of (4.1). For the following sections, let's introduce the notation $\partial_i\mathcal{H} : [0,R]^3 \mapsto \mathbb{R}$ be the partial derivative w.r.t. the $i-$th dependent argument of the function $\mathcal{H}$. The function in (4.32a - 4.32c) allows the scheme to be written as a function of up to four arguments and from this function, one can prove the stability and monotonicity of the scheme. See [41].

Lemma 4.2. *Assume that $\rho_0 \in \mathbf{L}^\infty(\Omega; [0,R])$, $R > 0$ and τ_ξ be the mesh by the discretization scheme, then under the CFL condition (4.14), the numerical scheme is monotone and the finite volume approximate solution $\rho^\Delta(t,x)$ given by the scheme satisfies*

$$0 \leq \rho_j^n \leq R, \quad \forall\ J_0 \leq j \leq J_1,\ \forall n \in \mathbb{N}.$$

Proof. In what follows, we drop the superscript n on ρ and α for notation convenience. We first verify that the scheme is monotone *i.e.* $h^{n\pm}$ and h^{α}, defined at (4.18) and (4.19) respectively, are non-decreasing in their first argument and non-increasing in their second argument.

Observe immediately that $h^{\alpha}(\rho_{m(n)-1}, \rho_{m(n)+1})$ and $h^{n\pm}_{j\pm 1/2}$ Lipschitz continuous in both arguments with Lipschitz constant $\|f'\|_{\infty}$ and $\max\{\|f'\|_{\infty}, |\alpha|\}$. Therefore the montonicity of the scheme can be studied using their derivatives. Since the flux is classical for $j \notin \{m(n)-1, m(n)+1\}$, it is easy to infer monotonicity of the scheme from the classical properties of the standard Godunov fluxes $h^{n\pm}$. See also [87, Proposition 2.1]. We then focus on h^{α}.

Recall from Lemma 3.2 of Chapter 3 of this thesis that if $\alpha > v(\rho_{m(n)+1})$, there exist a unique ρ^* such that interface numerical flux writes, $h^{\alpha} = h^{\alpha}(\rho_{m(n)-1}, \rho_{m(n)+1}) = -f(\rho^*) - \alpha\rho^* = f(\rho_{m(n)+1}) - \alpha\rho_{m(n)+1}$.
This implies that, $\partial_1 h^{\alpha} = 0$ and

$$\partial_2 h^{\alpha} = f'(\rho_{m(n)+1})) - \alpha = \rho_{m(n)+1} v'(\rho_{m(n)+1}) + v(\rho_{m(n)+1}) - \alpha < 0,$$

since v is a decreasing function. Similarly, if $\alpha < -v(\rho_{m(n)-1})$ then $h^{\alpha} = f(\rho^*) - \alpha\rho^* = -f(\rho_{m(n)-1}) - \alpha\rho_{m(n)-1}$ and the partial derivative w.r.t. first argument is given by

$$\partial_1 h^{\alpha} = -f'(\rho_{m(n)-1}) - \alpha = -\rho_{m(n)-1} v'(\rho_{m(n)-1}) - v(\rho_{m(n)-1}) - \alpha > 0,$$

and $\partial_2 h^{\alpha} = 0$. Next, we show that the functions $\mathcal{H}_{m(n)-1}$ and $\mathcal{H}_{m(n)+1}$ defined in (4.32a) and (4.32c) respectively are non-decreasing functions in all their arguments.

Lets start with $\mathcal{H}_{m(n)+1}$ and differentiate w.r.t. the first argument

$$\partial_1 \mathcal{H}_{m(n)+1}(a, b, c) = \frac{\Delta t \partial_1 h^{\alpha}(a, b)}{x_{m(n+1)+3/2} - \xi^{n+1}} \geq 0$$

by the monotone arguments of h^α presented above and

$$\begin{aligned}\partial_3\mathcal{H}_{m(n)+1}(a,b,c) &= \frac{\Delta x}{x_{m(n+1)+3/2}-\xi^{n+1}} - \frac{\Delta t\partial_2 h^{n+}_{m(n)+3/2}(b,c)}{x_{m(n+1)+3/2}-\xi^{n+1}}\\ &\geq \frac{\Delta x-\Delta t\max\{\|f'\|_\infty,\|\xi'\|_\infty\}}{x_{m(n+1)+3/2}-\xi^{n+1}}\\ &\geq \frac{\Delta x-1/2\Delta x}{x_{m(n+1)+3/2}-\xi^{n+1}}\geq 0.\end{aligned}$$

The partial derivative w.r.t. the second argument also gives

$$\partial_2\mathcal{H}_{m(n)+1}(a,b,c) = \frac{(x_{m(n)+3/2}-\xi^n)-\Delta t\left[\partial_1 h^{n+}_{m(n)+3/2}(b,c)-\partial_2 h^\alpha(a,b)\right]}{x_{m(n+1)+3/2}-\xi^{n+1}}. \tag{4.37}$$

We now verify that (4.37) is non-negative for all α.

1) If $\alpha\in[-v(\rho_{m(n)-1}),v(\rho_{m(n)+1})]$ or $\alpha<-v(\rho^n_{m(n)-1})$, then (4.37) is

$$\begin{aligned}\partial_2\mathcal{H}_{m(n)+1}(a,b,c) &= \frac{x_{m(n)+3/2}-\xi^n-\Delta t\partial_1 h^{n+}_{m(n)+3/2}(b,c)}{x_{m(n+1)+3/2}-\xi^{n+1}}\\ &\geq \frac{\Delta x-\Delta t\partial_1 h^{n+}_{m(n)+3/2}(b,c)}{x_{m(n+1)+3/2}-\xi^{n+1}},\end{aligned}$$

which is non-negative by the same deduction as in $\partial_3\mathcal{H}_{m(n)+1}$ above.

2) If $\alpha > v(\rho_{m(n)+1})$, then (4.37) becomes

$$\begin{aligned}
\partial_2 \mathcal{H}_{m(n)+1}(a,b,c) &\geq \frac{\Delta x - \Delta t \left[\partial_1 h^{n+}_{m(n)+3/2}(b,c) - \partial_2 h^{\alpha}(a,b)\right]}{x_{m(n+1)+3/2} - \xi^{n+1}} \\
&= \frac{\Delta x - \Delta t \left[\partial_1 h^{n+}_{m(n)+3/2}(b,c) - f'(b) + \alpha\right]}{x_{m(n+1)+3/2} - \xi^{n+1}} \\
&\geq \frac{\Delta x - \Delta t \left(2\|f'\|_\infty + |\xi'\|_\infty\right)}{x_{m(n+1)+3/2} - \xi^{n+1}} \\
&\geq \frac{\Delta x - 3\Delta t \max\{\|f'\|_\infty, |\xi'\|_\infty\}}{x_{m(n+1)+3/2} - \xi^{n+1}} \\
&\geq \frac{2/3\Delta x}{x_{m(n+1)+3/2} - \xi^{n+1}} \geq 0,
\end{aligned}$$

provided that a stricter version of the CFL condition (4.14) holds:

$$\Delta t \max\{\|f'\|_\infty, \|\xi'\|_\infty\} \leq \frac{1}{3}\Delta x.$$

Next, we proof the stability of the scheme. That is to verify that $\left(\rho_j^n\right)_{j=J_0}^{J_1}$ lies in $[0,R]$, then $\left(\rho_j^{n+1}\right)_{j=J_0}^{J_1}$ also belongs to $[0,R]$. It is easy to verify that

$$\mathcal{H}_{m(n)-1}(0,0,0) = 0$$

and

$$\mathcal{H}_{m(n)}(0,0,0) = \mathcal{H}_{m(n)+1}(0,0,0) = 0,$$

because of the consistency of $h^{n\pm}$ and h^{α}. Similarly

$$\begin{aligned}
\mathcal{H}_{m(n)+1}(R,R,R) &= \frac{(x_{m(n)+3/2} - \xi^n)R + \Delta x R - \Delta t \left[h^{n+}_{m(n)+3/2}(R,R) - h^{\alpha^n}(R,R)\right]}{x_{m(n+1)+3/2} - \xi^{n+1}}, \\
&= \frac{(x_{m(n)+3/2} - \xi^n)R + \alpha \Delta t R}{x_{m(n+1)+3/2} - \xi^{n+1}} = R,
\end{aligned}$$

for all $\alpha \in \mathbb{R}$. The same calculations for $\mathcal{H}_{m(n)-1}(R,R,R)$ and $\mathcal{H}_{m(n)}(R,R,R)$ yields

the same results and hence is omitted to avoid repetition. Therefore we can conclude that

$$0 \leq \rho_j^n \leq R \quad \forall \ J_0 \leq j \leq J_1, \ \forall n \in \mathbb{N},$$

to complete the proof. □

Another important property of a scheme that justifies the convergence of scheme to entropy weak solutions, is to show that it possesses a discrete per cell entropy inequality. Using this inequality allows one to pass to the continuous entropy inequality as $\Delta x \to 0$. See [41]. We shall adapt the following notations,

$$a \perp b = \min(a, b) \quad \text{and} \quad a \top b = \max(a, b).$$

Proposition 4.2. *Let ρ_j^n, $\forall n, j$ be the finite volume approximate solution obtained by the monotone scheme (4.20 - 4.24). Suppose the pair of constants $(\kappa^-, \kappa^+) \in [0, R]^2$ satisfying (4.29) defines the peicewise constant function*

$$\kappa_j^n = \begin{cases} \kappa^- & \text{if } j < m(n) - 1, \\ \kappa^+ & \text{if } j \geq m(n) + 1. \end{cases} \tag{4.38}$$

Then under the CFL *condition (4.14), the following discrete 'per cell' entropy inequality holds:*

$$|\rho_j^{n+1} - \kappa_j^{n+1}|\Delta x \leq \begin{cases} |\rho_j^n - \kappa^-|\Delta x - \Delta t \left(H_{j+1/2}^{n-} - H_{j-1/2}^{n-} \right) & \text{if } j \leq m(n+1) - 2, \\ |\rho_j^n - \kappa^+|\Delta x - \Delta t \left(H_{j+1/2}^{n+} - H_{j-1/2}^{n+} \right), & \text{if } j \geq m(n+1) + 2. \end{cases} \tag{4.39}$$

Furthermore, if $j = m(n+1) - 1$

$$\left| \rho_j^{n+1} - \kappa^- \right| \leq \frac{\xi^n - x_{m(n)-3/2}}{\xi^{n+1} - x_{m(n+1)-3/2}} \left| \rho_{m(n)-2}^n - \kappa^- \right| - \frac{\Delta t}{\xi^{n+1} - x_{m(n+1)-3/2}} \left(H^\alpha - H_{m(n)-3/2}^{n-} \right) \tag{4.40}$$

and if $j = m(n+1)+1$,

$$\left|\rho_j^{n+1} - \kappa^+\right| \leq \frac{x_{m(n)+3/2} - \xi^n}{x_{m(n+1)+3/2} - \xi^{n+1}} \left|\rho_{m(n)+1}^n - k^+\right| + \frac{\Delta x}{x_{m(n+1)+3/2} - \xi^{n+1}} \left|\rho_{m(n)+2}^n - k^+\right| - \frac{\Delta t}{x_{m(n+1)+3/2} - \xi^{n+1}} \left(H_{m(n)+3/2}^{n+} - H^\alpha\right), \tag{4.41}$$

where,

$$H_{j+1/2}^{n+} = h_{j+1/2}^{n-}(\rho_j^n \top \kappa^+, \rho_{j+1}^n \top \kappa^+) - h_{j+1/2}^{n+}(\rho_j^n \perp \kappa^+, \rho_{j+1}^n \perp \kappa^+),$$

$$H_{j+1/2}^{n-} = h_{j+1/2}^{n-}(\rho_j^n \top \kappa^-, \rho_{j+1}^n \top \kappa^-) - h_{j+1/2}^{n-}(\rho_j^n \perp \kappa^-, \rho_{j+1}^n \perp \kappa^-),$$

$$H^\alpha = h^\alpha(\rho_{m(n)-1}^n \top \kappa^-, \rho_{m(n)+1}^n \top \kappa^+) - h^\alpha(\rho_{m(n)-1}^n \perp \kappa^-, \rho_{m(n)+1}^n \perp \kappa^+).$$

Proof. First, let's observe that the constants, κ^- and κ^+ are 'steady state solutions' of (4.1) thanks to the well-balanced property given in Lemma 4.1.
Since we use the classical Godunov flux and marching formulas for $j \neq m(n)$, $m(n)+2$ then the discrete entropy inequality is simply

$$\frac{|\rho_j^{n+1} - \kappa_j^n| - |\rho_j^n - \kappa_j^n|}{\Delta t} - \frac{H_{j+1/2}^{n\pm} - H_{j-1/2}^{n\pm}}{\Delta x} \leq 0, \tag{4.42}$$

using case **B**. This can be verified using the same approach in [41]. However, for $j = m(n+1)-1$ and $m(n+1)$, we deduce the following using Case **B**. If $j = m(n+1)-1$, then

$$\begin{aligned}\mathcal{H}_{m(n)-1}(\kappa_j^n, \kappa_j^n, \kappa_j^n) &= \frac{\kappa^-(\xi^n - x_{m(n)-3/2}) - \Delta t\left[h^\alpha(\kappa^-, \kappa^+) - h^{n-}(\kappa^-, \kappa^-)\right]}{\xi^{n+1} - x_{m(n+1)-5/2}} \\ &= \kappa^-.\end{aligned}$$

The monotonicity of $\mathcal{H}_{m(n)-1}$ implies,

$$\begin{aligned}\rho^{n+1}_{m(n+1)-1} \perp \kappa^- \geq & \frac{(\xi^n - x_{m(n)-3/2})\rho^n_{m(n)-2} \perp \kappa^-}{\xi^{n+1} - x_{m(n+1)-3/2}} \\ & - \frac{\Delta t}{\xi^{n+1} - x_{m(n+1)-3/2}} \Big[h^\alpha(\rho^n_{m(n)-1} \perp \kappa^-, \rho^n_{m(n)+1} \perp \kappa^-) \\ & - h^{n-}(\rho^n_{m(n)-2} \perp \kappa^-, \rho^n_{m(n)-1} \perp \kappa^-)\Big], \\ & = \mathcal{H}_{m(n)-1}(\rho^n_{m(n)-2} \perp \kappa^-, \rho^n_{m(n)-1} \perp \kappa^- \rho^n_{m(n)+1} \perp \kappa^-).\end{aligned}$$

Similarly

$$\rho^{n+1}_{m(n+1)-1} \top \kappa^- \leq \mathcal{H}_{m(n)-1}(\rho^n_{m(n)-2} \top \kappa^-, \rho^n_{m(n)-1} \top \kappa^-, \rho^n_{m(n)+1} \top \kappa^-).$$

Therefore

$$\begin{aligned}\left|\rho^{n+1}_{m(n)-1} - \kappa^-\right| &= \rho^{n+1}_{m(n)-1} \top \kappa^- - \rho^{n+1}_{m(n)-1} \perp \kappa^-, \\ &\leq \frac{\xi^n - x_{m(n)-3/2}}{\xi^{n+1} - x_{m(n+1)-3/2}} \left(\rho^n_{m(n)-2} \perp \kappa^- - \rho^n_{m(n)-2} \perp \kappa^-\right) \\ &- \frac{\Delta t}{\xi^{n+1} - x_{m(n+1)-5/2}} \left(H^\alpha - H^{n-}_{m(n)-3/2}\right), \\ &= \frac{\xi^n - x_{m(n)-3/2}}{\xi^{n+1} - x_{m(n)-3/2}} \left|\rho^n_{m(n)-2} - \kappa^-\right| - \frac{\Delta t}{\xi^{n+1} - x_{m(n)-3/2}} \left(H^\alpha - H^{n-}_{m(n)-3/2}\right),\end{aligned}$$

which is exactly (4.40).

In a similar way, if $j = m(n+1)$, we know that the function $\mathcal{H}_{m(n)+1}$ is also non-decreasing in all its argument. We deduce that

$$\begin{aligned}\left|\rho^{n+1}_{m(n+1)} - \kappa^+\right| &\leq \mathcal{H}_{m(n)+1}(\rho^n_{m(n)-1} \top \kappa^+, \rho^n_{m(n)+1} \top \kappa^+, \rho^n_{m(n)+2} \top \kappa^+) \\ &- \mathcal{H}_{m(n)+1}(\rho^n_{m(n)-1} \perp \kappa^+, \rho^n_{m(n)+1} \perp \kappa^+, \rho^n_{m(n)+2} \perp \kappa^+) \\ &= \frac{x_{m(n)+3/2} - \xi^n}{x_{m(n+1)+3/2} - \xi^{n+1}} \left|\rho^n_{m(n)+1} - k^+\right| + \frac{\Delta x}{x_{m(n+1)+3/2} - \xi^{n+1}} \left|\rho^n_{m(n)+2} - k^+\right| \\ &- \frac{\Delta t}{x_{m(n+1)+3/2} - \xi^{n+1}} \left(H^{n+}_{m(n)+3/2} - H^\alpha\right),\end{aligned}$$

which is the inequality (4.41). The same deductions can be done for case **A**. □

4.5 On the convergence of scheme

In this section, we study the convergence of the scheme defined by (4.20) - (4.24). The first step to prove convergence of a numerical scheme is to establish the compactness of the approximate solution. It consists in obtaining a spatial bound on the total variation, and then pass to the limit of the solution along a converging subsequence. As scalar conservation laws with discontinuous flux are known to be resonant systems, thus a system with no spatial total variation bound for the conserved variable ρ, it is almost impossible to establish convergence using this standard approach [3, 4]. Nevertheless, this difficulty has been overcome by several authors who have studied conservation laws with space discontinuous flux function via the so-called *Temple functionals*. The functional is named after Temple [85], who was the first to propose the singular differentiable transformation denoted $\Phi : (\rho, k) \mapsto (z, k)$ such that the variation of the approximate solutions remains uniformly bounded in the $zc-$plane and therefore the Helly's theorem, when applied on this functional, gives convergence (along a subsequence) of the approximate solutions. As mentioned in the previous chapter of this thesis, the problem considered in this work has no bound on the total variation to the best of our knowledge. For this reason, we look for an alternative approach to prove the convergence of the scheme.

An alternative analytical tools utilized to prove convergence for discontinuous flux problems are the compensated compactness approach originally introduced in [84] and first applied in [59] to prove convergence of approximate solutions by the Lax-Friedrichs scheme to the weak entropy solution. It was shown that compensated compactness method handles sign changes in the discontinuous coefficient very well and does not required any convex/concave assumptions on the flux function as well. However, it must be noted that the Lax-Friedrichs scheme has a numerical viscosity, an approximating term in the r.h.s of (1.13), with which $W^{-1,2}_{\text{loc}}$ compactness was established and relied upon to prove convergence. Given that the Godunov's scheme has no viscosity, we cannot use compensated compactness to the present problem.

4.6 Numerical examples and validation

In this final section, we apply the numerical scheme proposed in this work to approximate solution to selected Riemann problem, investigate the performance and accuracy of the proposed scheme and finally study the order of convergence of the method through the $\mathbf{L^1}$-norm.

Algorithm 1: Algorithm for the Finite volume method with the local mesh adaptation

Input: Initial and boundary data for (4.1) and ξ
Output: Computes the densities at t^{n+1} from the densities at t^n.
Data: I space domain is discretized into $N_x + 1$ grid points.
$m_1 = m(n), m_2 = m(n+1) \in \mathbb{Z}$, the numerical indices to track the position of the turning curve at t^n, t^{n+1} respectively.
X is an $N_t \times (N_x + 1)$ matrix of interface points.
Find m_1,
$X[1][1 : m_1 - 1] = I[1 : m_1 - 1]$
$X[1][m_1] = \xi^1$
$X[1][m_1 + 1 : N_x + 1] = I[m_1 + 1 : N_x + 1]$
while $n < N_t$ *OR* $|\xi^n| < 1$ **do**
  Compute ξ^{n+1} and m_2,
  if $m_2 = m_1 + 1$ **then**
    $X[n+1][1 : m_2 - 1] = I[1 : m_2 - 1]$
    $X[n+1][m_2] = \xi^{n+1}$
    $X[n+1][m_2 + 1 : N_x + 1] = I[m_2 + 1 : N_x + 1]$
    Compute ρ^{n+1} using formula (4.20), (4.21) and (4.22).
  else if $m_2 = m_1$ **then**
    $X[n+1][1 : m_2 - 1] = I[1 : m_2 - 1]$
    $X[n+1][m_2] = \xi^{n+1}$
    $X[n+1][m_2 + 1 : N_x + 1] = I[m_2 + 1 : N_x + 1]$
    Compute ρ^{n+1} using formula (4.20), (4.23) and (4.24).
  Update $\xi^{n+1} = \xi^n + \alpha^n \Delta t$, m_2

We also compare our results with other classical finite volume methods and show that our scheme captures non-classical shocks without oscillations. Furthermore, we apply our scheme to solve the 1D Hughes' model [57] of pedestrian flow model and compare the order of convergence to similar results obtained in the literature. In the following examples, we use the turning curve given as a piecewise linear function of the form:

$$\xi(t) = \xi_0 + \int_0^t \xi'(s)ds, \tag{4.43}$$

and the following sets of initial data and slopes for ξ :

	Initial data	$\dot{\xi}(s)$
Ex. 4.1:	$\rho_0(x) = \begin{cases} 0.6, & \text{if } -1 < x < 0.3 \\ 0.9, & \text{if } 0.3 \leq x < 1\,. \end{cases}$	$\xi' = \begin{cases} 4/10, & \text{if } 0 < s < 0.6 \\ 0, & \text{if } s \geq 0.6 \end{cases}$
Ex. 4.2:	$\rho_0(x) = \begin{cases} 0.9, & \text{if } -0.1 \leq x \leq 0.5 \\ 0.6, & \text{if otherwise.} \end{cases}$	$\xi' = \begin{cases} 1/10, & \text{if } 0 < s \leq 0.3, \\ 1/4, & \text{if } 0.3 < s \leq 0.6, \\ 0, & \text{if } s > 0.6. \end{cases}$

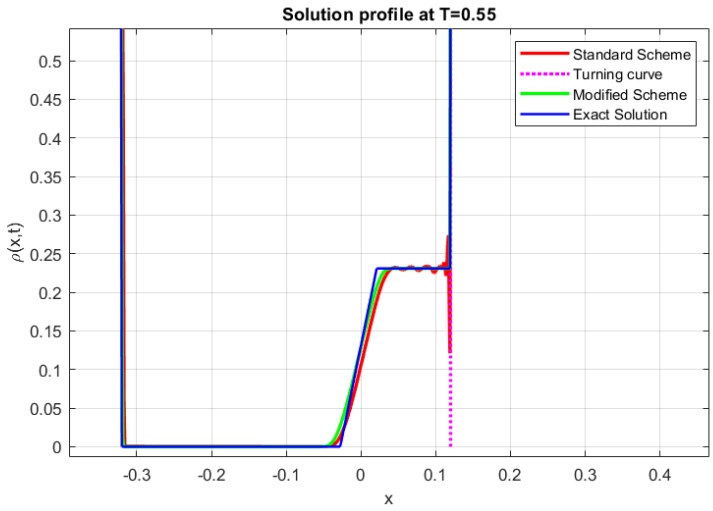

FIGURE 4.5: A zoomed view of exact solution and the numerical solutions with the standard Godunov's flux and the modified flux at $T = 0.55$ with $\Delta x = 1/1000$.

These examples are chosen in order to observe changes in slope of the turning curve discontinuity as well as its interactions with the classical waves out of which non-classical waves are formed. The exact weak solutions are constructed by the

method of characteristics. For both examples, since $\rho(0,x) > 1/2$, the boundary conditions dictates that rarefaction waves enters the boundary points $\{(t,-1^+)\}$ and $\{(t,1^-)\}$ such that $\rho(t,\pm 1) \geq 1/2$ for every $t > 0$.

Example 4.1. At $x = 0.3$, a shock defined by $\sigma_1(t) = 0.3 - 0.5t$ is created and at $x = -0.1$ two undercompressive shocks separated with vacuum and defined $\sigma_L(t) = -1/10(1+4t)$ and $\sigma_R(t) = -1/10(1-4t)$ are created. Observing that $\xi(t) = \sigma_R(t)$ and since $\dot{\sigma}_L > \dot{\sigma}_1$, the turning curve discontinuity shall collide with the classical shock σ_1 at $t = 4/9$. The weak solution for $t \in [0, 4/9)$ writes

$$\rho(t,x) = \begin{cases} 0.6 & \text{if } -1 < x < \sigma_L(t) \\ 0 & \text{if } -\sigma_L(t) \leq x < \xi(t) \\ 0.6 & \text{if } \xi(t) \leq x < \sigma_R(t) \\ 0.9 & \text{if } \sigma_R(t) \leq x < 1. \end{cases}$$

At $t = 4/9$, a small rarefaction is formed and a solution of a new Riemann problem at ξ is solved with an intermediate state $\rho_M = 1/10\left(7 - 1/2\sqrt{\frac{88}{10}}\right)$ for $4/9 \leq t < 6/10$. The solution in this time interval writes

$$\rho(t,x) = \begin{cases} 0.6 & \text{if } -1 < x < \sigma_L(t), \\ 0 & \text{if } -\sigma_L(t) \leq x < 7/90 - (t-4/9), \\ \frac{x-7/90}{2(t-4/9)} + \frac{1}{2} & \text{if } 7/90 - (t-4/9) \leq x < 7/90 - \dot{R}_{\max}(t-4/9), \\ \rho_M & \text{if } 7/90 - \dot{R}_{\max}(t-4/9) \leq x < \xi(t), \\ 0.9 & \text{if } \xi(t) \leq x < 1. \end{cases}$$

Here $\dot{R}_{\max} = 1/5\left(2 - 1/2\sqrt{\frac{88}{10}}\right)$, denotes the maximum slope of the rarefaction fan.

Example 4.2. In this example, at $x = 0.5$ a rarefaction given by $R^0(t) := 1/2 + f'(\rho)t$, where $\rho \in [0.6, 0.9]$ is formed and two shocks defined by $\sigma_L(t) = -0.1 + 0.4t$ and $\sigma_R = -0.1 + 0.1t$ emanates from $\xi(0) = -0.1$ for $0 < t \leq 3/10$. The

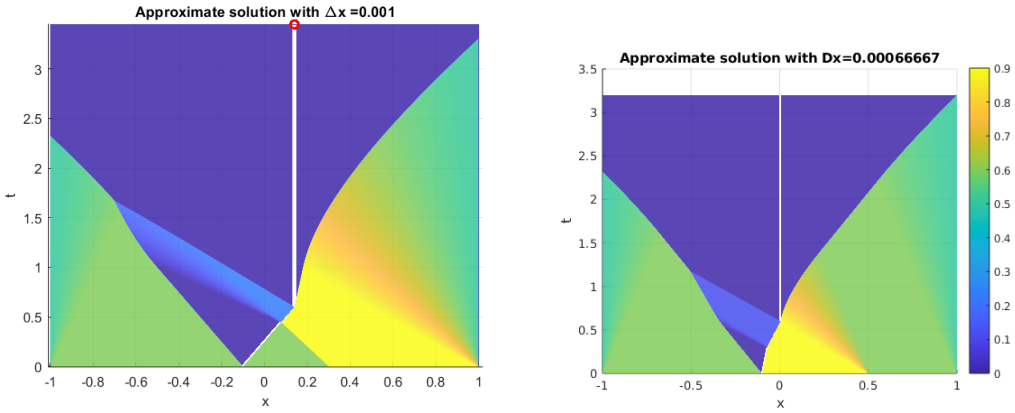

FIGURE 4.6: Approximate solution of examples 4.1 (left) and 4.2 (right) with $\Delta x = 1000$ and CFL = 0.45 in each case.

solution writes

$$\rho(t,x) = \begin{cases} 6/10 & \text{if } -1+8t/10 \le x \le \sigma_L(t), \\ 0 & \text{if } \sigma_L(t) < x < \xi(t), \\ 0.9 & \text{if } \xi(t) < x \le R^0_{\min}(t), \\ (t-x)/2t & \text{if } \dot{R}^0_{\min}(t) < (x-1/2)/t \le \dot{R}^0_{\max}(t), \\ 6/10, & \text{if } 1/2(1-t/5) < x < 1-8t/10, \end{cases}$$

where $\dot{R}^0_{\min}$ and $\dot{R}^0_{\max}$ represents the minimum and maximum speeds of the R^0. At $t = 3/10$, turning curve increases velocity with $\xi' > \dot{\sigma}_r$ and so a new Riemann problem at ξ is solved with an intermediate state of $\rho_M := \frac{1}{80}(50 - \sqrt{1636})$ and a small rarefaction denoted $R^1(t) := -\frac{1}{40} - f'(\rho)\left(t - \frac{3}{10}\right)$, where $\rho \in [0, \rho_M]$, after ξ interacts with σ_R. For $3/10 \le t < 6/10$

$$\rho(t,x) = \begin{cases} 6/10 & \text{if } -1+8t/10 \le x \le \sigma_L(t), \\ 0 & \text{if } \sigma_L(t) < x < R^1_{\min}(t), \\ \frac{1}{2} + \frac{x+1/40}{2(t-3/10)}, & \text{if } \dot{R}^1_{\min}(t) \le x \le \dot{R}^1(t) \\ \frac{1}{80}(50 - \sqrt{1636}), & \text{if } R^1_{\max}(t) \le x < \xi(t) \\ 9/10, & \text{if } \xi(t) \le x < R^0_{\min}(t) \\ (t-x)/2t & \text{if } \dot{R}^0_{\min}(t) < (x-1/2)/t \le \dot{R}^0_{\max}(t), \\ 6/10 & R^0_{\max}(t) \le x < 1-8t/10, \end{cases}$$

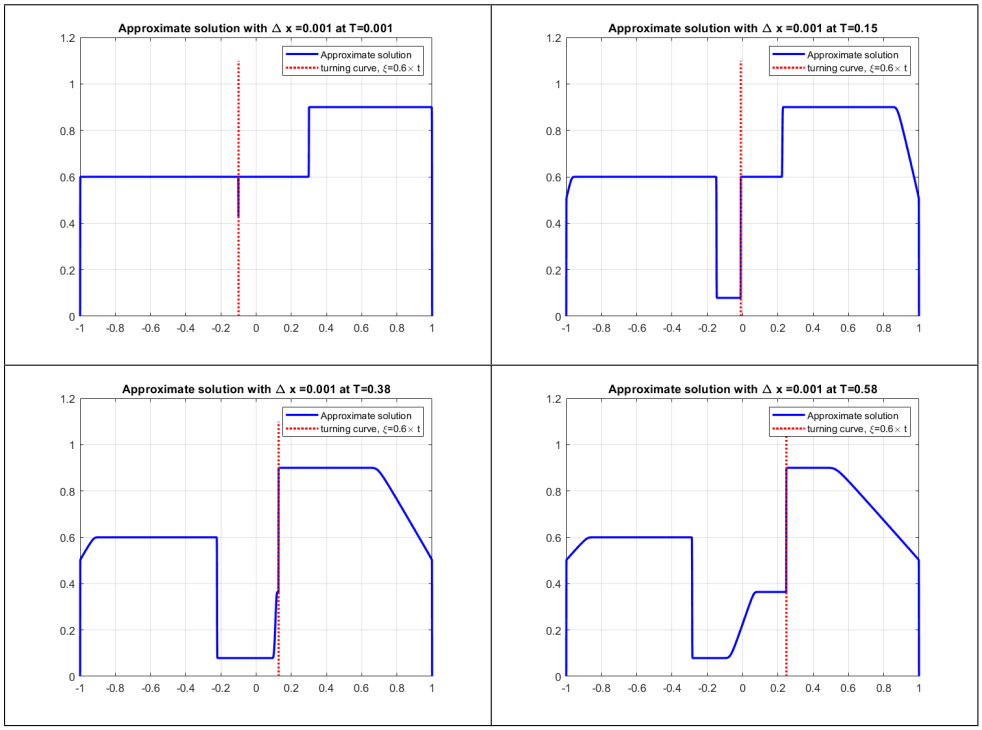

FIGURE 4.7: Evolution of example 4.1.

	Example 4.1		Example 4.2	
Δx	$Err(\Delta x)$	$\frac{\ln(Err(\Delta x))}{\ln(\Delta x)}$	$Err(\Delta x)$	$\frac{\ln(Err(\Delta x))}{\ln(\Delta x)}$
$1/50$	$4.3335e-2$	0.802	$4.8727e-2$	0.66
$1/100$	$2.3590e-2$	0.814	$2.3218e-3$	0.71
$1/250$	$1.0639e-2$	0.823	$1.1388e-2$	0.73
$1/500$	$5.8867e-3$	0.826	$6.5496e-3$	0.73
$1/1000$	$3.2550e-3$	0.829	$3.7091-3$	0.74
$1/1500$	$2.3086e-3$	0.830	$2.7588e-3$	0.74

TABLE 4.1: $\mathbf{L^1}$*−errors at* $T = 0.55$*, for Example 4.1 and at* $T = 0.58$ *for Example 4.2 with mesh size from* $\Delta x = 1/50, \ldots, 1/1500$.

4.6.1 Order of convergence

In this section, we analyse the accuracy of the proposed numerical scheme with the above examples. To do this, we estimate the $\mathbf{L^1}$ errors of the scheme and use it to deduce the order of convergence on examples 4.1 and 4.2. These examples are carefully chosen to enable us observe the performance of our scheme during collisions between the turning curve discontinuity and incoming waves.
We define the $\mathbf{L^1}$-norm at $k = T/\Delta t$ as:

$$Err(k, \Delta x) = \sum_{j=J_0}^{J_1} \left| \rho(T, x_j^k) - \rho_j^k \right| \Delta x_j^k, \tag{4.44}$$

where $\rho(T, x)$ is the exact solution which we use as the reference solution and ρ_j^k is the approximate solution obtained with our scheme. Though the two cells adjacent to the turning curve from the left and right have variable sizes, the total number of cells at each time is constant. In the following simulations, we use a CFL number of 0.45, choose Δx that ranges from $1/50$ to $1/1500$, and plot the log-log graph of the errors against Δx values at the time levels where the turning curve discontinuity collide with the classical incoming waves. Table 4.1 contains the numerical values representing the order of convergence for Examples 4.1 and 4.2.

We now show the graph of the approximate solution in the $x - t$ plane for examples 4.1 and 4.2. It can be observed from Figure 4.6 (left) that the approximate solution of Example 4.1 contains a shock wave that starts from $x = 0.3$ at $t = 0$ and travels left with a speed less than ξ' and then collides with the turning curve discontinuity at approximately $t = 0.444$. In Example 4.2, we could observe an interaction between the turning curve and a rarefaction. These are also confirmed by the presentations of the exact solution given above.

To observe the performance and accuracy of the scheme against the standard Godunov's flux, we compare in Example 4.1 at $T = 0.55$, where the interaction between classical shock wave and the turning curve occurs in figure 4.5. From the figure, the approximate solution by the standard Godunov's flux exhibits spurious oscillations at $x = \xi(t)$ during interactions between ξ and an incoming shock wave from the right. On the other hand, the modified scheme do not only eliminate these oscillation but also effectively captures the non-zero intermediate state created after the interaction.

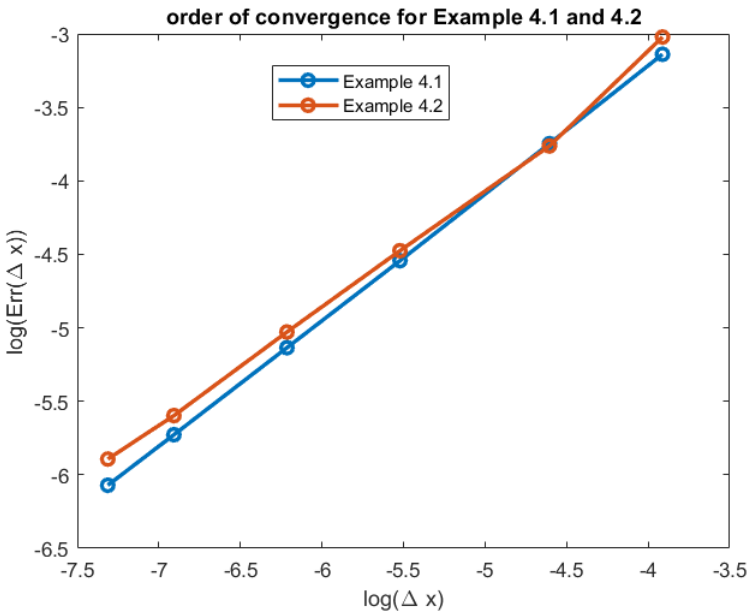

FIGURE 4.8: log-log graph of example 4.1 and 4.2 at $T = 0.55$ and $T = 0.58$ respectively against the log of Δx.

4.6.2 An application to the Hughes' model

Finally, we attempt to apply the modified scheme (4.20 - 4.24), to generate a simulation of the one dimensional Hughes' model for pedestrian flow where the position of the turning curve, $\xi(t)$ is not known *a priori* but satisfies a non-local condition (5). To specify the model (4), we re-write the equation as a scalar conservation law with space-time discontinuous flux:

$$\partial_t \rho + \partial_x \big(\text{sign}(x - \xi(t)) f(\rho)\big) = 0, \tag{4.45}$$

where, $\rho \mapsto f(\rho)$ is defined by $f(\rho) := \rho v(\rho)$ and $t \mapsto \xi(t)$ satisfies the implicit relation (5) for each $(t, x) \in \Pi$. In order to check the accuracy of our approximation, we use the same initial as used in [48]:

$$\rho_0(x) = \begin{cases} 0, & \text{if } -1 < x < 0, \\ 0.9, & \text{if } 0 < x < 1. \end{cases} \tag{4.46}$$

and a cost function $c(\rho) = 1/v(\rho)$. Actually in [48], the model was solved with the wave front tracking (WFT) and referenced as the exact solution to which the approximate solution by the Godunov scheme was compared. Also, in [40], the authors studied the associated Riemann-type problems by constructing explicit solutions for small times, after which the Godunov and Rusanov schemes were applied. Except for the wave front tracking algorithm where the Riemann solver at the turning curve was explicitly calculated for the approximation, the Godunov and Rusanov schemes in these works were applied in standard ways. Compare [87, 48, 40].

The main difficulty here concerns the determination of ξ at each time. Given a Riemann data, the initial position of the turning curve is determined by

$$\xi(0) = \begin{cases} \frac{1}{2}\left(1 - \frac{c(\rho_L)}{c(\rho_R)}\right) & \text{if } \rho_L \leq \rho_R, \\ \frac{1}{2}\left(\frac{c(\rho_R)}{c(\rho_L)} - 1\right) & \text{if } \rho_L \geq \rho_R. \end{cases} \tag{4.47}$$

With a general initial datum $\rho(0, x) = \rho_0(x)$ and the boundary conditions (4d), (4c), the simplest way to apply our scheme, is to solve once the Eikonal equation (4b) with the fast sweeping method [92] at $t = 0$ to determine the starting point of the turning curve and then approximate by a linear function the turning point curve such it has a 'local' slope determined by

$$\xi'(t)\left[c(\rho^+) + c(\rho^-)\right] = -\int_{-1}^{\xi(t)} c(\rho(t,y))_t dy + \int_{\xi(t)}^{1} c(\rho(t,y))_t dy \tag{4.48}$$

for small time $t > 0$, where $\rho^{\pm}(t) = \rho(t, \xi(t)\pm)$ are the traces at ξ. By discretization, (4.48) with $\xi^n = \xi(t^n)$ can be re-written for every m,

$$\alpha_n\left[c(\rho^n_{m+1}) + c(\rho^n_m)\right] \approxeq \\ -\sum_{j=1}^{m} c(\rho^n_j)(x^n_{j+1/2} - x^n_{j-1/2}) + \sum_{j=m+1}^{N} c(\rho^n_j)(x^n_{j+1/2} - x^n_{j-1/2}),$$

where $m = m(n)$ is such that $x_{m-1/2} < \xi^n \leq x_{m+1/2}$. The turning curve position

	With mesh adaptation		Without mesh adaptation		
Δx	$Err(\Delta x)$	$\frac{\ln(Err(\Delta x))}{\ln(\Delta x)}$	Δx	$Err(\Delta x)$	$\frac{\ln(Err(\Delta x))}{\ln(\Delta x)}$
$1/250$	$2.09e-2$	-0.62	$1/250$	$2.49e-2$	-0.66
$1/500$	$6.20e-3$	-0.74	$1/500$	$1.52e-2$	-0.67
$1/1000$	$2.30e-3$	-0.80	$1/1000$	$9.03e-3$	-0.68
$1/1500$	$1.60e-3$	-0.80	$1/1500$	$6.66e-3$	-0.69
$1/2000$	$1.10e-3$	-0.82	-	-	-
$1/4000$	$6.41e-4$	-0.82	-	-	-

TABLE 4.2: Comparison of the $\mathbf{L}^1$-norm error between the Godunov's scheme by [48] and our scheme using the approximate solution by WFT method as the reference solution at $T = 1.2$.

is then updated with $\xi^{n+1} = \xi^n + \alpha_n \Delta t$ and ρ is approximated by (4.20 - 4.24) using the modified flux at the ξ for all $n \in \mathbb{N}$. Recall that the implicit relations (5) and (4.48) are non local and at each time require information on the 'global' distribution of ρ. Therefore a straightforward updating the position of ξ by the proposed scheme of this work may lead to inaccuracies in comparison with the values by [48]. One way to overcome this problem is to apply the fast sweeping method at each time to generate $\{\xi^n\}$ and then use a linear interpolation formula on the generated values, ξ^n so that at each time step we can determine the slope and next position of ξ. More precisely, let $\varphi_j^n := \varphi(t^n, x_j)$ for simplicity,

- Given ρ_j^n, solve the eikonal equation (4b) by the fast sweeping method to obtain $\varphi = (\varphi_1^n, \ldots, \varphi_N^n)$. For each $n > 1$, there exist $m \in \mathbb{Z}$ such that $\varphi_{\max}(t^n, x_m) = \max_j \varphi_j^n$ and $\xi^n := x_m$.

- We then update ξ

$$\xi(t) = \frac{t^n - t}{t^n - t^{n-1}} \xi^{n-1} + \frac{t - t^{n-1}}{t^n - t^{n-1}} \xi^n$$

  and $\alpha_n = (\xi^n - \xi^{n-1})/\Delta t$ for $n \geq 1$.

It should be noticed that the WFT solution is not associated to an uniform grid as it is the case for the approximate solution computed by our scheme. As such, a data processing step is needed in order to compare the two approximations with the WFT method and the finite volume method. To do this comparison, one needs to define a reference grid on $x \in [-1, 1]$ with a fixed size, Δx, compare them to the position of the finite volume flux interface and select the corresponding solution at that point. The finite volume solution at this point is then compared to the

reference 'exact' solution obtained by the WFT method. Once this is done, we use the formula (4.44).

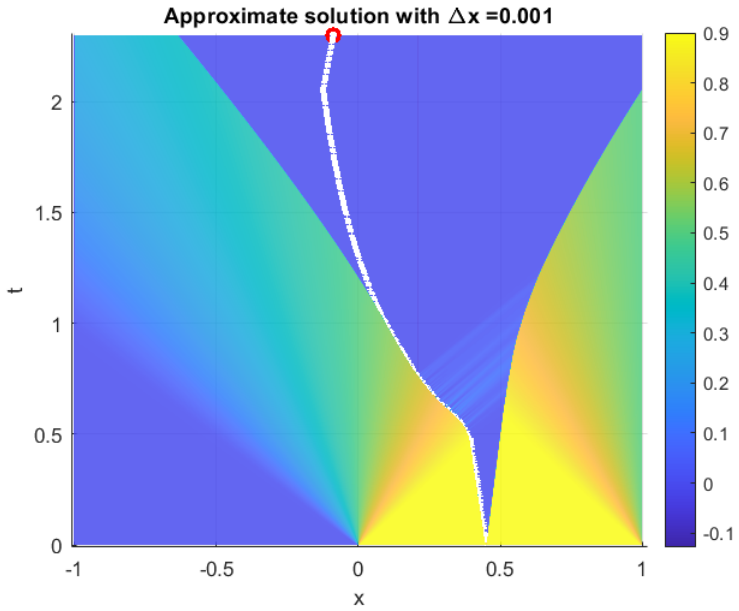

FIGURE 4.9: application of the scheme to the Hughes' model with $\Delta x = 1000$, CFL = 0.45 and up to time $T = 2.3$.

Chapter 5

Conclusions and Discussion

In this thesis, we considered a first order PDE with discontinuous space-time flux coefficients. In general, the time dependent jump discontinuity is given *a priori* as a Lipschitz continuous function. However, we use a piecewise linear function in order to simplify the analysis. The flux function is genuinely non-linear and satisfies the same assumption as the commonly used flux functions for traffic flow models. With the appropriate modification and assumption the equation could serve as starting equation for pedestrian and traffic flow models. For this reason we briefly recalled examples of models by hyperbolic conservation law with variable coefficients such as the traffic flow models with variable speed ramp and road conditions, the Hughes' model of pedestrian flow and the ion etching model in the introduction section.

The equation featured new theoretical aspects of wave interactions and entropy admissible weak solution. Toward this goal, the theory of entropy solutions for the general scalar conservation law was revisited and reviewed with examples. A definition of entropy solutions with Kruzkhov admissible flux away from the interface was derived. This framework of solution was taken in the same sense of that developed by Karlsen, Risebro and Towers [58]. This enabled us to further derive some stability properties of the solution, including L^1 distance and L^1-contraction principle. The former was based on the construction of exact solutions of the Riemann problem at the interface. This led to the well-posedness of the Riemann problem. Furthermore, analysis of the total variation in the solution reveals that it is higher than the total variation in the solution. A literature search further revealed that this phenomena is common for problems of the nature considered in this work. In such cases, a singular mapping approach are used to overcome this difficulty. However, for our problem it is not clear if it is even possible to obtain a global bound on the total variation. In the absence of this estimate, we extended to the notion of admissible germs, which elucidate a dissipative behavior across the flux interface.

Finally in Chapter 4, we proposed a finite volume scheme with local mesh adaptation near the flux interface that results in a moving mesh. The mesh adaptation was done to accommodate for the local non-uniform mesh size and avoids explicit reconstruction of non-classical Riemann solvers near the interface. Though it was proposed a numerical scheme using the moving mesh strategy also used in [31], the reconstruction step in such a scheme would not guarantee that it is well-balanced and hence proving convergence would be difficult. On the other hand, using the discretization scheme motivated by the work of [83], the approximate solution by our verifies the well-balanced property of the scheme, monotone and stable in $\mathbf{L}^\infty$.

The properties of the scheme deduced in this thesis, i.e. well-balanced and $\mathbf{L}^\infty$ estimate paves way for a rigorous study of the convergence of the scheme. This would be a topic for future studies. Though the PDE considered in this here is general, it can be adapted to study physical problems in traffic and pedestrian flows.

Appendices

Appendix I: Notations

Throughout this work, we used the following notations:

ρ	the unknown of the scalar conservation law.
∂_t, ∂_x	partial derivative operator with respect to time and space respectively.
F, f	the flux function of the hyperbolic conservation law in this work.
$\mathbb{R}$	the set of real numbers $(-\infty, +\infty)$.
$\mathbb{R}^+$, $\mathbb{R}_0^+$	the set $(0, +\infty)$ and the set $[0, +\infty)$, (i.e. positive real numbers including 0) respectively.
$\mathbb{N}$	the set of natural numbers.
$\mathbb{N}^*$	the set of natural numbers including zero.
Σ	a subset of $\mathbb{R}$.
Ω	the set $\mathbb{R}^+ \times \mathbb{R}$.
Π, Π_x	the bounded set of $\mathbb{R}^+ \times]-1, 1[$ and $]-1, 1[$ respectively.
$\mathbf{C}_c^\infty(\Omega; \mathbb{R})$	a space of infinitely differentiable and continuous functions from Ω to $\mathbb{R}$.
$\mathbf{L}^\infty(\Omega; [0, R])$	the set of bounded and measurable functions from Ω to $[0, R]$.
$\gamma^l\rho(t)$, $\gamma^r\rho(t)$	left and right traces in ρ towards an interface at t.
$\mathrm{TV}\rho(t, \cdot)$	The total variation of a given function $\rho(t, \cdot)$.
$\mathbf{Lip}([0, R]; \mathbb{R}^+)$	the space of Lipschitz continuous function from $[0, R]$ to $\mathbb{R}^+$.
$\mathbb{1}_{x>\xi(t)}$	the indicator function equaling 1 if $x > \xi(t)$ and 0 otherwise.
$\mathbf{BV}(\mathbb{R}^+; \mathbb{R})$	The space of functions of bounded variation from $\mathbb{R}^+$ to $\mathbb{R}$.
$\Delta t > 0$	The numerical time step .
$x_{j+1/2}^n$	The grid point for $j \in \mathbb{Z}$ at $t^n, \forall \in \mathbb{N}$.
$\mathcal{C}_j^n$	A computational cell at $t^n, \forall j \in \mathbb{Z}, n \in \mathbb{N}$.
Δx_j^n	The space step at the cell $\mathcal{C}_j^n$.

Appendix II: The numerical code

The following is the MATLAB code used to show the simulations of the numerical solution proposed in this thesis.

```
%% Description
%A Godunov's scheme for space-time discontinuous CL:
%\rho_t + (K(x,t)f(\rho))_x = 0 on the interval
% [-xa,xa], xa=1 and flux is
% f(U) = \rho*(1-\rho)
% K(x,t) = sign(x-xi(t))
% boundary condtions: \rho(t, -xa)=\rho(t, xa) = 0.
% In the code, U=\rho.
%% Files
%xi.m encodes the information (like its slope) of the turning curve.
%godunov.m has the implementation of the modified flux at xi.
%flux.m is the flux f(\rho)=U*(1-\rho)
%square.m contains the Riemann data
%data2.m contains a general initial data (piecewise constant).
%the function profileU.m may be used to obtain a color map of the ...
    U in the
%x-t plane.

%% The code

clear
close all
clf

%global declarations
global Nx
global Umax
global Ucrit
global xa
global xb
global Dt
global Dx
Umax = 1; %maximum density value
Ucrit = 0.5; % critical density

%Space dicretization
Nx= 2000; %the total number of cell grid point
xa = -1; xb =-xa;
Dx = (xb-xa)/(Nx); % the space step size
I = linspace(xa, xb, Nx+1);

%CFL condition
```

```
42 cfl  = 0.45;
43 Dt = Dx*cfl;
44 mu = Dt/Dx;
45
46 Tmax = 1.1; %the maximum time to run the simulation
47 Tnmax = round(Tmax/Dt);
48 T0 = 0.6;
49 %  T1 = 0.6;
50 % T2 = 1.;
51
52 Tn0 = round(T0/Dt);
53 %Tn1 = round(T1/Dt);
54 %Tn2 = round(T2/Dt);
55 time_t = 0:Dt:Tmax;
56
57 %Pre-location of vectors and matrices
58 rho = zeros(Tnmax, Nx ); %stores the cell density averages
59 Xgrids = zeros(Tnmax, Nx+1); %stores all the grid points
60 Xcenters = zeros(Tnmax, Nx); %holds cell centers.
61 alphas = zeros(1, Tnmax); %store the slope of \xi
62 xi_t = zeros(1, Tnmax);
63 Tcurve = zeros(1,Tnmax); %needed to be able to show \xi as a ...
      vertical line during simulation
64 TV = zeros(1, Tnmax);
65
66 %different slopes of xi apriori
67 %alphas(1,1:end) = -1.2;
68 alphas(1,1:Tn0) = 0.6;
69 %alphas(1,Tn0+1:Tn1) = 0.;
70 %alphas(1,Tn1+1:Tn2)=0;
71 %alphas(1, Tn2+1:Tn2+2000)=.2;
72 xi_t(1,1) = -0.1;
73
74 %initial mesh grid with adaptation
75 m0 = find(xi_t(1,1) ≥ I(1:end-1) & xi_t(1,1) < I(2:end));
76 Xgrids(1, 1:m0-1) = I(1: m0-1);
77 Xgrids(1, m0) = xi_t(1, 1);
78 Xgrids(1, m0+1:end) = I(m0+1:end);
79
80 %initial centers
81 Xcenters(1,:) =  0.5*(Xgrids(1, 2:end)+Xgrids(1,1:end-1));
82
83 %initial data
84 rho(1,:) = square(Xgrids(1, 1:end-1));
85
86 % boundary conditions
87 rho(:, 1) = 0;
88 rho(:, end) = 0;
```

```
89
90  TV(1,1) = sum(abs(rho(1,2:end)-rho(1,1:end-1)))*Dx;
91  Dfdu = @(u)1-2*u;
92
93  tn = 1;
94  while tn < Tnmax && abs(xi_t(tn)) < 1-4*Dx
95      xi_t(tn+1) = xi_t(tn) + Dt*alphas(tn);
96
97      %looks for index likely to contain xi^tn
98       m1 = find(xi_t(tn) ≥ I(1:end-1) & xi_t(tn) < I(2:end)); ...
             %finds m(n)
99       m2 = find(xi_t(tn+1) ≥ I(1:end-1) & xi_t(tn+1) < I(2:end)); ...
             %finds m(n+1)
100
101     if m2 == m1+1
102       %% case B corresponding to dot_xi > 0
103        Xgrids(tn+1, 1:m2-1) = I(1:m2-1);
104        Xgrids(tn+1, m2) = xi_t(tn+1);
105        Xgrids(tn+1, m2+1:end) = I(m2+1:end);
106
107        %update centers and cell lengths
108        Xcenters(tn+1,:) = 0.5*(Xgrids(tn + 1, 2:end) + ...
              Xgrids(tn+1, 1:end-1));
109
110        %marching formulas for x<xi
111        hjLl =  godunov(rho(tn, 1:m1-3), rho(tn, 2:m1-2), -1, ...
              alphas(tn));
112        hjRl =  godunov(rho(tn, 2:m1-2), rho(tn, 3:m1-1), -1, ...
              alphas(tn));
113        rho(tn+1, 2:m2-3) = rho(tn, 2:m1-2) - mu*(hjRl - hjLl);
114
115        %update formulae at x=xi from the left.
116        ha = godunov(rho(tn, m1), rho(tn, m1+1), 0, alphas(tn));
117        hjaL = godunov(rho(tn, m1-2), rho(tn, m1-1), -1, alphas(tn));
118        rho(tn+1,m2-1) = rho(tn, m1-1)*(xi_t(tn) - Xgrids(tn, ...
              m1-1))/(xi_t(tn+1) - Xgrids(tn+1, m2-2)) - ...
119            (Dt/(xi_t(tn+1) - Xgrids(tn+1, m2-2)))*(ha - hjaL);
120
121        rho(tn+1, m2-2) = rho(tn+1, m2-1);
122
123        %from the right
124        hjaR = godunov(rho(tn, m1+1), rho(tn, m1+2), +1, alphas(tn));
125        rho(tn+1,m2) = rho(tn, m1+1)*(Xgrids(tn,m1+1) ...
              -xi_t(tn))/(Xgrids(tn+1,m2+1) - xi_t(tn+1)) - ...
126             (Dt/( Xgrids(tn+1, m2+1) - xi_t(tn+1)))*(hjaR - ha) + ...
                   rho(tn, m1+2)*Dx/(Xgrids(tn+1,m2+1) - xi_t(tn+1));
127        rho(tn+1, m2+1) = rho(tn+1, m2);
128
```

```
129         %marching formulas for x>xi
130         hjLrB =  godunov(rho(tn, m1+2:end-2), rho(tn, m1+3:end-1), ...
                +1, alphas(tn));
131         hjRrB =  godunov(rho(tn, m1+3:end-1), rho(tn, m1+4:end), ...
                +1, alphas(tn));
132         rho(tn+1, m2+2:end-1) = rho(tn, m1+3:end - 1) - mu*(hjRrB ...
                - hjLrB);
133 %
134     elseif m2 == m1-1
135 %% This is a third case corresponding to dot_xi < 0
136         Xgrids(tn+1, 1:m2) = I(1:m2);
137         Xgrids(tn+1, m2+1) = xi_t(tn+1);
138         Xgrids(tn+1, m2+2:end) = I(m2+2:end);
139 %         %update centers and cell lengths
140         Xcenters(tn+1,:) = 0.5*(Xgrids(tn + 1, 2:end) + ...
                Xgrids(tn+1, 1:end-1));
141 %         Dxn(tn+1,:) = Xgrids(tn+1, 2:end)-Xgrids(tn+1, 1:end-1);
142
143         %marching formulas for x<xi
144         hjLl =  godunov(rho(tn, 1:m1-4), rho(tn, 2:m1-3), -1, ...
                alphas(tn));
145         hjRl =  godunov(rho(tn, 2:m1-3), rho(tn, 3:m1-2), -1, ...
                alphas(tn));
146         rho(tn+1, 2:m2-2) = rho(tn, 2:m1-3) - mu*(hjRl - hjLl);
147
148 %         %update formulae at x=xi from the left.
149         ha = godunov(rho(tn, m1-1), rho(tn, m1), 0, alphas(tn));
150         hjaL = godunov(rho(tn, m1-3), rho(tn, m1-2), -1, alphas(tn));
151         rho(tn+1,m2-1) = rho(tn, m1-2)*(xi_t(tn) - Xgrids(tn, ...
                m1-2))/(xi_t(tn+1) - Xgrids(tn+1, m2-1)) - ...
152             (Dt/(xi_t(tn+1) - Xgrids(tn+1,m2-1)))*(ha - hjaL);
153
154         %from the right
155         hjaR = godunov(rho(tn, m1), rho(tn, m1+1), +1, alphas(tn));
156         rho(tn+1,m2) = rho(tn, m1)*(Xgrids(tn,m1+2) - ...
                xi_t(tn))/(Xgrids(tn+1, m2+3) - xi_t(tn+1)) - ...
157             (Dt/(Xgrids(tn+1, m2+3) - xi_t(tn+1)))*(hjaR - ha);
158
159         rho(tn+1, m2+1) = rho(tn+1, m2);
160
161         %marching formulas for x>xi
162         hjLrB =  godunov(rho(tn, m1:end-2), rho(tn, m1+1:end-1), ...
                1, alphas(tn));
163         hjRrB =  godunov(rho(tn, m1+1:end-1), rho(tn, m1+2:end), ...
                1, alphas(tn));
164         rho(tn+1, m2+2:end-1) = rho(tn, m1+1:end-1) - mu*(hjRrB - ...
                hjLrB);
165     else
```

```
166         %% case A: m1 = m2.
167         Xgrids(tn+1, 1:m2-1) = I(1:m2-1);
168         Xgrids(tn+1, m2) = xi_t(tn+1);
169         Xgrids(tn+1, m2+1:end) = I(m2+1:end);
170
171         %update centers and cell lengths
172         Xcenters(tn+1,:) = 0.5*(Xgrids(tn + 1, 2:end)+Xgrids(tn+1, ...
                1:end-1));
173
174         %marching formulas for x<xi
175         hjL =  godunov(rho(tn, 1:m1-3), rho(tn, 2:m1-2), -1, ...
                alphas(tn));
176         hjR =  godunov(rho(tn, 2:m1-2), rho(tn, 3:m1-1), -1, ...
                alphas(tn));
177         rho(tn+1, 2:m2-2) = rho(tn, 2:m1-2) - mu*(hjR - hjL);
178
179         %update formulae at x=xi from the left.
180         ha = godunov(rho(tn, m1-1), rho(tn, m1), 0, alphas(tn));
181         hjaL = godunov(rho(tn, m1-2), rho(tn, m1-1), -1, alphas(tn));
182         rho(tn+1,m2-1) = rho(tn, m1-1)*(xi_t(tn) - Xgrids(tn, ...
                m1-1))/(xi_t(tn+1) - Xgrids(tn+1,m2-1)) ...
183          - (Dt/(xi_t(tn+1) - Xgrids(tn+1,m2-1)))*(ha - hjaL);% ...
                 + (Dx/(xi_t(tn+1) - Xpoints(tn+1,m2-2)))*rho(tn,m1-2);
184
185         %from the right
186         hjaRA = godunov(rho(tn, m1+1), rho(tn, m1+2), +1, alphas(tn));
187         rho(tn+1, m2) = rho(tn, m1)*(Xgrids(tn,m1+2) - ...
                xi_t(tn))/(Xgrids(tn+1, m1+2) - xi_t(tn+1)) - ...
188           (Dt/(Xgrids(tn+1, m1+2) - xi_t(tn+1)))*(hjaRA - ha) ...
                  ;%+ rho(tn, m1+1)*(Dx/(Xpoints(tn+1, m1+2) - ...
                  xi_t(tn+1)));
189         rho(tn+1, m2+1) = rho(tn+1, m2);
190
191         %marching formulas for x>xi
192         hjLrB =  godunov(rho(tn, m1+1:end-2), rho(tn, m1+2:end-1), ...
                1, alphas(tn));
193         hjRrB =  godunov(rho(tn, m1+2:end-1), rho(tn, m1+3:end), ...
                1, alphas(tn));
194         rho(tn+1, m2+2:end-1) = rho(tn, m1+2:end-1) - mu*(hjRrB - ...
                hjLrB);
195
196     end
197
198     Tcurve(1, 1:end) = xi_t(1, tn+1);
199     TV(tn+1,:) = sum(abs(rho(tn+1, 2:end) - rho(tn+1,1:end-1)))*Dx;
200
201     plot(Xcenters(tn+1, :), rho(tn+1,:), '-r', Tcurve(1:Tnmax), ...
            time_t(1:Tnmax),'-.b', 'linewidth',2.0);
```

```
202     hold on
203
204     ylabel('\rho(x,t)');
205     xlabel('x');
206     title('Solution profile');
207     axis([xa-0.1 xb+.1 -0.1 1.1])
208     legend( strcat('Dx=', num2str(Dx, '%4.4f\n'), ', time = ', ...
            num2str(time_t(tn),'%4.3f\n' )),...
209           strcat('turning curve, ','\xi=', num2str(alphas(tn+1)), ...
                '\times t'));
210     grid on
211     hold off
212     pause(0.01)
213     tn = tn + 1;
214 end
```

The following are the pre-defined functions used in the above code: The flux function, $f(\rho)$

```
1  function [f]=flux(U, k)
2
3  global Umax;
4  %global v;
5
6  if U> 0 && U<Umax
7      f=k*U.*(1-U);
8  else
9      f=0;
10 end
```

The numerical flux function,

```
1  function [g] = godunov(ul, ur, k, a)
2  nl = length(ul);
3  % nr = length(ur);
4  g = zeros(1,nl);
5
6  v = @(u)1-u;
7
8  Dfdu = @(uu, kk) kk*(1-2*uu);
9   for i = 1:nl
10     if  k == 0
11         %intermediate state for a>v(ur)
12         umra = 0.5*(1 + a) - sqrt((0.5*(1+a)).^2 + ...
               ur(i)*(1-a-ur(i)));
13         umrb = 0.5*(1 + a) + sqrt((0.5*(1+a)).^2 + ...
               ur(i)*(1-a-ur(i)));
```

```
14          ua = [umra, umrb];
15          umr = ua(ua≥0 & ua < ur(i));
16          %intermdediate state for a<-v(ul)
17          umla = 0.5*(1-a) - sqrt((0.5*(1-a)).^2 + ul(i)*(1+a-ul(i)));
18          umlb = 0.5*(1-a) + sqrt((0.5*(1-a)).^2 + ul(i)*(1+a-ul(i)));
19          ub = [umla, umlb];
20          uml = ub(ub≥0 & ub<ul(i));
21
22          if a>v(ur(i))
23             gg =  flux(umr, -1) - a*umr;
24          elseif a < -v(ul(i))
25             gg =  flux(uml, +1) - a*uml;
26          else
27             gg = 0;
28          end
29      g(i) = gg;
30      else
31          if Dfdu(ul(i),k)<0 && Dfdu(ur(i),k)>0
32              if ul(i) ≥ ur(i)
33                  Uc = fzero(@(u) Dfdu(u,k), [ul(i),ur(i)]);
34              else
35                  Uc = fzero(@(u) Dfdu(u,k), [ur(i),ul(i)]);
36              end
37              g(i) = flux(Uc,k);
38          else
39              s = (flux(ul(i),k)-flux(ur(i),k))/(ul(i) - ur(i));
40              if s ≥ 0
41                  g(i) = flux(ul(i), k);
42              else
43                  g(i) = flux(ur(i),k);
44              end
45          end
46
47      end
48  end
```

The initial data

```
1  function u=square(X)
2  % U=square(X) create a square wave on X
3  global xa;
4  global xb;
5  n = length(X);
6   rhor = 0.9;
7   rhol = 0.6;
8  % rhol = 0.;
9  % rhor = 0.9;
10 x0= 0.3;
```

```
11 for i=1:n
12     if (X(i) > xa)&&(X(i) < x0)
13         u(i) = rhol;
14     elseif (X(i) ≥ x0)&&(X(i) < xb)
15         u(i) = rhor;
16     end
17 end
```

Bibliography

[1] Adimurthi and G. D. Veerappa Gowda. Conservation law with discontinuous flux. *J. Math. Kyoto Univ.*, 43(1):27–70, 2003.

[2] Adimurthi, Jérôme Jaffré, and GD Veerappa Gowda. Godunov-type methods for conservation laws with a flux function discontinuous in space. *SIAM J. Numer. Anal.*, 42(1):179–208, 2004.

[3] Adimurthi, Siddhartha Mishra, and GD Veerappa Gowda. Optimal entropy solutions for conservation laws with discontinuous flux-functions. *J. Hyperbolic Differ. Equ.*, 2(04):783–837, 2005.

[4] Adimurthi, Siddhartha Mishra, and G. D. Veerappa Gowda. Explicit Hopf-Lax type formulas for Hamilton-Jacobi equations and conservation laws with discontinuous coefficients. *J. Differential Equations*, 241(1):1–31, 2007.

[5] D. Amadori and M. Di Francesco. The one-dimensional Hughes model for pedestrian flow: Riemann-type solutions. *Acta Math. Sci. Ser. B (Engl. Ed.)*, 32(1):367–379, 2012.

[6] D. Amadori, C. Donadello, and K. A. Gyamfi. A Godunov type scheme for conservation laws with space-time flux discontinuity. In preparation.

[7] D. Amadori, P. Goatin, and M. D. Rosini. Existence results for Hughes' model for pedestrian flows. *J. Math. Anal. Appl.*, 420(1):387 – 406, 2014.

[8] Boris Andreianov. Dissipative coupling of scalar conservation laws across an interface: theory and applications. In *Hyperbolic problems—theory, numerics and applications. Volume 1*, volume 17 of *Ser. Contemp. Appl. Math. CAM*, pages 123–135. World Sci. Publishing, Singapore, 2012.

[9] Boris Andreianov. New approaches to describing admissibility of solutions of scalar conservation laws with discontinuous flux. *ESAIM Proc.*, 50:40–65, 2015.

[10] Boris Andreianov and Clément Cancès. The Godunov scheme for scalar conservation laws with discontinuous bell-shaped flux functions. *Appl. Math. Lett.*, 25(11):1844–1848, 2012.

[11] Boris Andreianov and Clément Cancès. On interface transmission conditions for conservation laws with discontinuous flux of general shape. *J. Hyperbolic Differ. Equ.*, 12(2):343–384, July 2015.

[12] Boris Andreianov, Giuseppe Maria Coclite, and Carlotta Donadello. Well-posedness for vanishing viscosity solutions of scalar conservation laws on a network. *Discrete Contin. Dyn. Syst.*, 37(11):5913, 2017.

[13] Boris Andreianov, Paola Goatin, and Nicolas Seguin. Finite volume schemes for locally constrained conservation laws. *Num. Math.*, 115(4):609–645, 2010.

[14] Boris Andreianov, Kenneth Hvistendahl Karlsen, and Nils Henrik Risebro. A theory of L^1-dissipative solvers for scalar conservation laws with discontinuous flux. *Arch. Ration. Mech. Anal.*, 201(1):27 – 86, 2011.

[15] Boris Andreianov and Nicolas Seguin. Analysis of a burgers equation with singular resonant source term and convergence of well-balanced schemes [well-posedness of a singular balance law]. *DCDS-A*, 32(6):pp–1939, 2012.

[16] Emmanuel Audusse and Benoît Perthame. Uniqueness for scalar conservation laws with discontinuous flux via adapted entropies. *Proc. Roy. Soc. Edinburgh Sect. A*, 135(2):253–265, 2005.

[17] Patrizia Bagnerini, Rinaldo M Colombo, and Andrea Corli. On the role of source terms in continuum traffic flow models. *Math. Comput. Modelling*, 44(9-10):917–930, 2006.

[18] C. Bardos, A. Y. Leroux, and J. C. Nedelec. First order quasilinear equations with boundary conditions. *Comm. Partial Differential Equations*, 4(9):1017–1034, 1979.

[19] Nicola Bellomo and Christian Dogbe. On the modeling of traffic and crowds: A survey of models, speculations, and perspectives. *SIAM Rev*, 53(3):409–463, 2011.

[20] Sylvie Benzoni-Gavage and Rinaldo M Colombo. An n-populations model for traffic flow. *European J. Appl. Math.*, 14(5):587, 2003.

[21] A. Bressan, G. Guerra, and W. Shen. Vanishing viscosity solutions for conservation laws with regulated flux. *J. Differential Equations*, 266(1):312–351, January 2019.

[22] Martin Burger, Marco Di Francesco, Peter A. Markowich, and Marie-Therese Wolfram. Mean field games with nonlinear mobilities in pedestrian dynamics. *Discrete Contin. Dyn. Syst. Ser. B*, 19(5):1311–1333, 2014.

[23] R. Bürger, K. H. Karlsen, C. Klingenberg, and N. H. Risebro. A front tracking approach to a model of continuous sedimentation in ideal clarifier-thickener units. *Nonlinear Anal. Real World Appl.*, 4(3):457–481, 2003.

[24] Raimund Bürger, Antonio García, Kenneth H Karlsen, and John D Towers. Difference schemes, entropy solutions, and speedup impulse for an inhomogeneous kinematic traffic flow model. *Netw. Heterog. Media*, 3(1):1, 2008.

[25] Raimund Bürger, Kenneth H Karlsen, and John D Towers. A model of continuous sedimentation of flocculated suspensions in clarifier-thickener units. *SIAM J. Appl. Math.*, 65(3):882–940, 2005.

[26] Christophe Chalons and Paola Goatin. Godunov scheme and sampling technique for computing phase transitions in traffic flow modeling. *Interfaces Free Bound.*, 10(2):197–221, 2008.

[27] Giuseppe Maria Coclite and Nils Henrik Risebro. Conservation laws with time dependent discontinuous coefficients. *SIAM J. Math. Anal.*, 36(4):1293–1309, 2005.

[28] Rinaldo M. Colombo, Paola Goatin, and Massimiliano D. Rosini. A macroscopic model for pedestrian flows in panic situations. In *Current advances in nonlinear analysis and related topics*, volume 32 of *GAKUTO Internat. Ser. Math. Sci. Appl.*, pages 255–272. Gakkōtosho, Tokyo, 2010.

[29] Rinaldo M Colombo and Massimiliano D Rosini. Pedestrian flows and non-classical shocks. *Math. Methods Appl. Sci.*, 28(13):1553–1567, 2005.

[30] Carlos F Daganzo. The cell transmission model: A dynamic representation of highway traffic consistent with the hydrodynamic theory. *Transport. Res. Part B*, 28(4):269–287, 1994.

[31] Maria Laura Delle Monache and Paola Goatin. A front tracking method for a strongly coupled PDE-ODE system with moving density constraints in traffic flow. *Discrete Contin. Dyn. Syst. Ser. S*, 7(3):435–447, June 2014.

[32] Maria Laura Delle Monache and Paola Goatin. Scalar conservation laws with moving constraints arising in traffic flow modeling: an existence result. *J. Differential Equations*, 257(11):4015–4029, 2014.

[33] Maria Laura Delle Monache, Benedetto Piccoli, and Francesco Rossi. Traffic regulation via controlled speed limit. *SIAM J. Control Optim.*, 55(5):2936–2958, 2017.

[34] Marco Di Francesco, Peter A. Markowich, Jan-Frederik Pietschmann, and Marie-Therese Wolfram. On the Hughes' model for pedestrian flow: the one-dimensional case. *J. Differential Equations*, 250(3):1334–1362, 2011.

[35] Stefan Diehl. On scalar conservation laws with point source and discontinuous flux function. *SIAM J. Math. Anal.*, 26(6):1425–1451, 1995.

[36] Stefan Diehl. A conservation law with point source and discontinuous flux function modelling continuous sedimentation. *SIAM J. Appl. Math.*, 56(2):388–419, 1996.

[37] Ronald J DiPerna. Measure-valued solutions to conservation laws. *Arch. Ration. Mech. Anal.*, 88(3):223–270, 1985.

[38] Sylvain Dotti and Julien Vovelle. Convergence of the finite volume method for scalar conservation laws with multiplicative noise: an approach by kinetic formulation. *Stochastics and Partial Differential Equations: Analysis and Computations*, pages 1–46, 2019.

[39] Alexander Dressel and Christian Rohde. A finite-volume approach to liquid-vapour fluids with phase transition. In *Finite volumes for complex applications V*, pages 53–68. ISTE, London, 2008.

[40] Nader El-Khatib, Paola Goatin, and Massimiliano D. Rosini. On entropy weak solutions of Hughes' model for pedestrian motion. *Z. Angew. Math. Phys.*, 64(2):223–251, Apr 2013.

[41] Robert Eymard, Thierry Gallouët, and Raphaèle Herbin. Finite volume methods. In *Handbook of numerical analysis, Vol. VII*, Handb. Numer. Anal., VII, pages 713–1020. North-Holland, Amsterdam, 2000.

[42] Takahiro Ezaki, Daichi Yanagisawa, and Katsuhiro Nishinari. Pedestrian flow through multiple bottlenecks. *Physical Review E*, 86(2):026118, 2012.

[43] T. Gallouët and F. Hubert. On the convergence of the parabolic approximation of a conservation law in several space dimensions. *Chinese Ann. Math. Ser. B*, 20(1):7–10, 1999. A Chinese summary appears in Chinese Ann. Math. Ser. A **2**0 (1999), no. 1, 141.

[44] Mauro Garavello and Benedetto Piccoli. *Traffic flow on networks*, volume 1 of *AIMS Series on Applied Mathematics*. American Institute of Mathematical Sciences (AIMS), Springfield, MO, 2006. Conservation laws models.

[45] Tore Gimse and Nils Henrik Risebro. Riemann problems with a discontinuous flux function. In *Proceedings of Third International Conference on Hyperbolic Problems*, volume 1, pages 488–502, 1991.

[46] Tore Gimse and Nils Henrik Risebro. Solution of the cauchy problem for a conservation law with a discontinuous flux function. *SIAM J. Math. Anal.*, 23(3):635–648, 1992.

[47] Paola Goatin, Simone Göttlich, and Oliver Kolb. Speed limit and ramp meter control for traffic flow networks. *Eng. Optim.*, 48(7):1121–1144, 2016.

[48] Paola Goatin and Matthias Mimault. The wave-front tracking algorithm for Hughes' model of pedestrian motion. *SIAM J. Sci. Comput.*, 35(3):606–622, 2013.

[49] Edwige Godlewski and Pierre-Arnaud Raviart. *Hyperbolic systems of conservation laws*, volume 3/4 of *Mathématiques & Applications (Paris) [Mathematics and Applications]*. Ellipses, Paris, 1991.

[50] Godunov S., Bohachevsky I. Finite difference method for numerical computation of discontinuous solutions of the equations of fluid dynamics. *Mat. Sb.*, 47(89)(3):271–306, 1959.

[51] BD Greenshields, JR Bibbins, WS Channing, and HH Miller. A study of traffic capacity. In *Highway research board proceedings*, volume 1935. National Research Council (USA), Highway Research Board, 1935.

[52] Dirk Helbing. Traffic and related self-driven many-particle systems. *Rev. Modern Phys.*, 73(4):1067, 2001.

[53] Dirk Helbing and Pratik Mukerji. Crowd disasters as systemic failures: analysis of the love parade disaster. *EPJ Data Science*, 1(1):1–40, 2012.

[54] Helge Holden and Nils Henrik Risebro. *Front tracking for hyperbolic conservation laws*, volume 152. Springer, 2015.

[55] Thomas Y Hou and Philippe G LeFloch. Why nonconservative schemes converge to wrong solutions: error analysis. *Math. Comp.*, 62(206):497–530, 1994.

[56] Ling Huang, SC Wong, Mengping Zhang, Chi-Wang Shu, and William HK Lam. Revisiting Hughes' dynamic continuum model for pedestrian flow and the development of an efficient solution algorithm. *Transportation Research Part B: Methodological*, 43(1):127–141, 2009.

[57] R. L. Hughes. A continuum theory for the flow of pedestrians. *Transportation Research Part B: Methodological*, 36(6):507 – 535, 2002.

[58] K. H. Karlsen, N. H. Risebro, and J. D. Towers. L^1 stability for entropy solutions of nonlinear degenerate parabolic convection-diffusion equations with discontinuous coefficients. *Skr. K. Nor. Vidensk. Selsk.*, 1(3):1–49, 2003.

[59] K. H. Karlsen and J. D. Towers. Convergence of the Lax-Friedrichs scheme and stability for conservation laws with a discontinuous space-time dependent flux. *Chin. Ann. Math.*, 25(03):287–318, 2004.

[60] K. H. Karlsen and J. D. Towers. Convergence of a Godunov scheme for conservation laws with a discontinuous flux lacking the crossing condition. *J. Hyper. Differential Equations*, 14(04):671–701, 2017.

[61] Runhild Aae Klausen and Nils Henrik Risebro. Stability of conservation laws with discontinuous coefficients. *J. Differential Equations*, 157(1):41–60, 1999.

[62] Christian Klingenberg and Nils Henrik Risebro. Convex conservation laws with discontinuous coefficients. Existence, uniqueness and asymptotic behavior. *Comm. Partial Differential Equations*, 20(11-12):1959–1990, 1995.

[63] S N Kružkov. First Order Quasilinear Equations in Several Independent Variables. *Math. USSR Sb*, 10(2):217–243, Feb 1970.

[64] Peter Lax and Burton Wendroff. Systems of conservation laws. *Comm. Pure Appl. Math.*, 13(2):217–237, 1960.

[65] Philippe G. Le Floch. *Hyperbolic systems of conservation laws*. Lectures in Mathematics ETH Zürich. Birkhäuser Verlag, Basel, 2002. The theory of classical and nonclassical shock waves.

[66] Jean-Patrick Lebacque, Jean-Baptiste Lesort, and Florence Giorgi. Introducing buses into first-order macroscopic traffic flow models. *Transportation Research Record*, 1644(1):70–79, 1998.

[67] Randall J. LeVeque. *Finite volume methods for hyperbolic problems*. Cambridge Texts in Applied Mathematics. Cambridge University Press, Cambridge, 2002.

[68] Thibault Liard and Benedetto Piccoli. Well-posedness for scalar conservation laws with moving flux constraints. *SIAM J. Appl. Math.*, 79(2):641–667, 2019.

[69] M. J. Lighthill and G. B. Whitham. On kinematic waves. II. A theory of traffic flow on long crowded roads. *Proc. Roy. Soc. London Ser. A*, 229:317–345, 1955.

[70] Huiyuan Liu, Lihui Zhang, Daniel Sun, and Dianhai Wang. Optimize the settings of variable speed limit system to improve the performance of freeway traffic. *IEEE Transactions on Intelligent Transportation Systems*, 16(6):3249–3257, 2015.

[71] Bertrand Maury, Aude Roudneff-Chupin, and Filippo Santambrogio. A macroscopic crowd motion model of gradient flow type. *Math. Models Methods Appl. Sci.*, 20(10):1787–1821, 2010.

[72] Bertrand Maury and Juliette Venel. A discrete contact model for crowd motion. *M2AN Math. Model. Numer. Anal*, 45(1):145–168, 2011.

[73] S. Mishra. Numerical methods for conservation laws with discontinuous coefficients. In *Handbook of numerical methods for hyperbolic problems*, volume 18 of *Handb. Numer. Anal.*, pages 479–506. Elsevier/North-Holland, Amsterdam, 2017.

[74] S. Mochon. An analysis of the traffic on highways with changing surface conditions. *Mathematical Modelling*, 9(1):1 – 11, 1987.

[75] Daniel N Ostrov. Solutions of Hamilton–Jacobi equations and scalar conservation laws with discontinuous space–time dependence. *J. Differential Equations*, 182(1):51–77, 2002.

[76] E. Yu. Panov. Existence of strong traces for quasi-solutions of multidimensional conservation laws. *J. Hyperbolic Differ. Equ.*, 4(4):729–770, 2007.

[77] Donald W Peaceman. *Fundamentals of numerical reservoir simulation*. Elsevier, 2000.

[78] Paul I Richards. Shock waves on the highway. *Operations research*, 4(1):42–51, 1956.

[79] Massimiliano Daniele Rosini. *Macroscopic models for vehicular flows and crowd dynamics: theory and applications*. Understanding Complex Systems. Springer, Heidelberg, 2013. Classical and non-classical advanced mathematics for real life applications, With a foreword by Marek Niezgódka.

[80] Nicolas Seguin and Julien Vovelle. Analysis and approximation of a scalar conservation law with a flux function with discontinuous coefficients. *Math. Models Methods Appl. Sci.*, 13(2):221–257, 2003.

[81] Parongama Sen and Bikas K Chakrabarti. *Sociophysics: an introduction*. Oxford University Press, 2014.

[82] Yushi Suma, Daichi Yanagisawa, and Katsuhiro Nishinari. Anticipation effect in pedestrian dynamics: Modeling and experiments. *Phys. A*, 391(1-2):248–263, 2012.

[83] Abraham Sylla. A LWR model with constraints at moving interfaces. working paper or preprint, June 2021.

[84] Luc Tartar. Compensated compactness and applications to partial differential equations. In *Nonlinear analysis and mechanics: Heriot-Watt symposium*, volume 4, pages 136–212, 1979.

[85] Blake Temple. Global solution of the Cauchy problem for a class of $2\times$ 2 nonstrictly hyperbolic conservation laws. *Adv. in Appl. Math.*, 3(3):335–375, 1982.

[86] John D. Towers. Convergence of a difference scheme for conservation laws with a discontinuous flux. *SIAM J. Numer. Anal.*, 38(2):681–698, 2000.

[87] John D. Towers. A difference scheme for conservation laws with a discontinuous flux: The nonconvex case. *SIAM J. Numer. Anal.*, 39(4):1197–1218, 2001.

[88] John D. Towers. Convergence via OSLC of the Godunov scheme for a scalar conservation law with time and space flux discontinuities. *Numer. Math.*, 139(4):939–969, Aug 2018.

[89] Adrien Treuille, Seth Cooper, and Zoran Popović. Continuum crowds. *ACM Transactions on Graphics (TOG)*, 25(3):1160–1168, 2006.

[90] Alexis Vasseur. Strong traces for solutions of multidimensional scalar conservation laws. *Arch. Ration. Mech. Anal.*, 160(3):181–193, 2001.

[91] Roger White, Guy Engelen, and Inge Uljee. *Modeling cities and regions as complex systems: From theory to planning applications*. MIT Press, 2015.

[92] Hongkai Zhao. A fast sweeping method for eikonal equations. *Math. Comp.*, 74(250):603–627, 2005.

[93] Xiaoguang Zhong, Thomas Y. Hou, and Philippe G. LeFloch. Computational methods for propagating phase boundaries. *J. Comput. Phys.*, 124(1):192 – 216, 1996.